BIPOLAR JUNCTION TRANSISTOR STATIC LARGE-SIGNAL COMPACT MATHEMATICAL MODELS

BIPOLAR JUNCTION TRANSISTOR STATIC LARGE-SIGNAL COMPACT MATHEMATICAL MODELS

By

KOK PAN TANG

A Thesis
Submitted to the Faculty of Graduate Studies
in Partial Fulfillment of the Requirements
for the Degree
Master of Engineering

McMaster University

May 1972

MASTER OF ENGINEERING (1972)
(Electrical Engineering)

McMASTER UNIVERSITY
Hamilton, Ontario

TITLE: Bipolar Junction Transistor Static Large-Signal Compact Mathematical Models

AUTHOR: Kok Pan Tang, B.E.Sc. (University of Western Ontario)

SUPERVISOR: Dr. S. H. Chisholm

NUMBER OF PAGES: xvii, 157

SCOPE AND CONTENTS:

Compact mathematical models used to simulate the static V-I characteristics of bipolar junction transistors are investigated. An abbreviated Gummel-Poon model and various modified Ebers-Moll models employed in computer network analysis programs are compared on the basis of their ability to simulate the common-emitter static characteristics of a silicon double-diffused transistor, the ease of the model parameter evaluation, the compromise between simplicity of model and accuracy of simulation and the ability to represent physical processes of transistor.

ACKNOWLEDGEMENTS

The author wishes to extend his sincerest thanks to Dr. S. H. Chisholm, his faculty supervisor, for his invaluable guidance, continuous encouragement and assistance during the course of this investigation.

The author is much obliged to Dr. J. W. Bandler and Mr. C. Charalambous for their stimulating and helpful discussion in computer-aided circuit analysis and optimization theory. Thanks are also due to Mr. E. Johnston for the permission to use his optimization subroutine.

TABLE OF CONTENTS

LIST OF FIGURES

FIGURE		PAGE
3.3	Test Configuration for determination of I_{CS}	55
3.4	Semilog Plot of I_C versus V_{BC} for $V_{BE} = 0$	57
3.5	Test Configuration for determination of α_F	60
3.6	Test Configuration for determination of α_R	60
3.7	Test Configuration for determination of R_E	64
3.8	Test Configuration for determination of R_C	64
3.9	I_B versus $V_{C'E'}$ for $I_C = 0$	65
3.10	I_B versus $V_{E'C'}$ for $I_E = 0$	66
3.11	Curve Tracer Schematic Diagram for Measurement of I_C versus V_{BE} for $V_{BC} = 0$	71
3.12	Semilog Plot of I_C versus V_{BE} for $V_{BC} = 0$	73
3.13	Test Configuration for determination of I_1, N_{E1}, I_2 and N_{E2}	75
3.14	Semilog Plot of I_B versus V_{BE} for $V_{BC} = 0$	77
3.15	Curve Tracer Schematic Diagram for Measurement of I_B versus V_{BC} for $V_{BE} = 0$	80
3.16	Semilog Plot of I_B versus V_{BC} for $V_{BE} = 0$	82
3.17	Measurements of τ_F and τ_R	84
3.18	$C_{BE}(\doteq C_E)$ versus V_{BE} for $I_C = 0$	89
3.19	C_{CB} and C_C versus V_{CB} for $I_E = 0$	90
3.20	Flow Chart for Automated Model Parameters Determination	93
4.1	Comparison of the Measured with the Simulated Output Characteristics by Model EMM 1	106
4.2	Comparison of the Measured with the Simulated Output Characteristics by Model EMM 2	107

LIST OF TABLES

TABLE		PAGE

LIST OF SYMBOLS

A_0	coefficient of the third order polynomial for α_F
A_1	coefficient of the third order polynomial for α_F
A_2	coefficient of the third order polynomial for α_F
A_3	coefficient of the third order polynomial for α_F
A_B	base cross-sectional area of the device
A_J	device junction cross-sectional area, either A_{JC} or A_{JE} ; whichever is smaller
A_{JC}	collector-base junction cross-sectional area of the device
A_{JE}	emitter-base junction cross-sectional area of the device
B_0	coefficient of the third order polynomial for α_R
B_1	coefficient of the third order polynomial for α_R
B_2	coefficient of the third order polynomial for α_R
B_3	coefficient of the third order polynomial for α_R
BP	base "push-out" factor
C_{BE}	base-emitter junction capacitance
C_C	total collector capacitance
C_{CB}	collector-base junction capacitance
C_E	total emitter capacitance
d_{JE}	diameter of the circular emitter region
d_{JB}	diameter of the circular base region
D	diffusion constant of the carrier

D_e diffusion constant of electron

D_{eo} diffusion constant of electron corresponding to the low field mobility of electron

$E(x)$ electric field at position x

E_1 error function as defined by equation (3.17)

E_2 error function as defined by equation (3.18)

h_{FE} common-emitter d. c. current gain

h_{FEM} measured common-emitter d. c. current gain

h_{FES} simulated common-emitter d. c. current gain

I_1 intercept current associated with base current component 1

I_2 intercept current associated with base current component 2

I_3 intercept current associated with base current component 3

I_B terminal base current

I_{B1} terminal base current component 1

I_{B2} terminal base current component 2

I_{B3} terminal base current component 3

I_{BC} terminal base current component flowing through the base-collector junction

I_{BD} intercept current associated with I_{BDIF}

I_{BDIF} diffusion current of terminal base current component 1

I_{BE} terminal base current component flowing through the base-emitter junction

I_{BM} measured terminal base current

I_{BR} intercept current associated with I_{BREC}

I_{BREC} recombination current of terminal base current component 1

I_C terminal collector current

I_{CC} principal current

I_{CM} measured terminal collector current

I_{CF}	forward component of the collector current
I_{CR}	reverse component of the collector current
I_{CS}	collector-junction short-circuit reverse-saturation current
I_{CSS}	simulated terminal collector current
I_E	terminal emitter current
I_{EF}	forward component of the emitter current
I_{ER}	reverse component of the emitter current
I_{ES}	emitter-junction short-circuit reverse-saturation current
I_F	forward component of the principal current
I_R	reverse component of the principal current
I_S	intercept current associated with the principal current
J_{BC}	base-collector diode current of ECAP II Ebers-Moll model
J_{BE}	base-emitter diode current of ECAP II Ebers-Moll model
J_C	base-collector diode current of SCEPTRE Ebers-Moll model
J_{CC}	principal current density
$Je(x)$	electron current density at position x
J_E	base-emitter diode current of SCEPTRE Ebers-Moll model
J_F	forward current source of SCEPTRE Ebers-Moll model
J_{FWD}	forward current source of ECAP II Ebers-Moll model
J_R	reverse current source of SCEPTRE Ebers-Moll model
J_{REV}	reverse current source of ECAP II Ebers-Moll model
K	Boltzmann constant
M_C	collector-junction emission constant
M_E	emitter-junction emission constant
$n(x)$	electron density at position x
n_i	intrinsic carrier density

n_{0B} equilibrium electron density in the base

n_{pB} electron density in the p-type base region

n_{pB}' excess electron density in the p-type base region

$N(x)$ impurity density at position x

N_B impurity density of the base

N_C collector emission coefficient

N_{E1} emitter emission coefficient associated with I_{B1}

N_{E2} emitter emission coefficient associated with I_{B2}

N_t density of bulk recombination centres

$p(x)$ hole density at position x

$p_B(x)$ hole density of the base at position x

q electronic charge

q_1 normalized partial base charge as defined by equation (2.81)

q_2 normalized partial base charge as defined by equation (2.82)

q_b normalized base charge density

q_B base charge density

q_c normalized excess stored charges associated with the base-collector junction capacitance

q_e normalized excess stored charges associated with the base-emitter junction capacitance

$(q/KT)_{exp.}$ experimental value of (q/KT)

Q partial base charge as defined by equation (2.85)

Q_{B0} zero-bias base charge

Q_B total base charge

Q_C total excess stored charges associated with the base-collector junction capacitance

Q_E	total excess stored charges associated with the base-emitter junction capacitance
$R(x)$	ratio of electron current density to principal current density at position x
$(R)_{ave}$	average value of R(x)
R_B	series resistance of the base
R_{BA}	active base resistance
R_{BAO}	active base resistance at zero-bias condition
R_{BI}	inactive base resistance
R_{BT}	total base resistance
R_C	series resistance of the collector
R_E	series resistance of the emitter
R_m	maximum value of R(x) occuring at x_m
T	junction operating temperature of the device
U	objective function
V_{BE}	base-emitter voltage
$V_{B'E'}$	terminal base-emitter voltage
$V_{BE\ centre}$	base-emitter voltage at the centre of the emitter
$V_{BE\ edge}$	base-emitter voltage at the edge of the emitter
V_{BEM}	measured terminal base-emitter voltage
V_{BES}	simulated terminal base-emitter voltage
V_{BC}	base-collector voltage
$V_{B'C'}$	terminal base-collector voltage
V_{CE}	collector-emitter voltage
$V_{C'E'}$	terminal collector-emitter voltage
V_{CEM}	measured terminal collector-emitter voltage
V_{CES}	simulated terminal collector-emitter voltage
v_s	signal level of the pulse generator

V_s	scattering limited velocity
v_{th}	thermal velocity of carrier
W_B	base width, difference between x_C and x_E
W_{EB}	width of space-charge region of the base-emitter junction
W_H	weighting factor
W_I	weighting factor
x	device structural dimension (Figure 2.6)
x_1, x_2	arbitrary position along x-direction
x_C	boundary between base-collector space-charge region and the base
x_E	boundary between base-emitter space-charge region and the base
x_m	a position, inside the base region where maximum potential occurs
α_F	d. c. forward short-circuit common-base current gain
α_R	d. c. reverse short-circuit common-base current gain
Δ	a change but not necessarily a small change
θ_C	collector-junction exponential factor used in SCEPTRE Ebers-Moll model
θ_E	emitter-junction exponential factor used in SCEPTRE Ebers-Moll model
λ	"ideal" junction exponential factor
λ_C	collector-junction exponential factor used in ECAP II Ebers-Moll model
λ_E	emitter-junction exponential factor used in ECAP II Ebers-Moll model
μ	mobility of carrier
μ_e	mobility of electron
μ_{eo}	low field mobility of electron

σ_n capture cross-sectional area for electron

σ_p capture cross-sectional area for hole

τ_B lifetime of the base

τ_F forward transit time

τ_n lifetime of electron

τ_p lifetime of hole

τ_R reverse transit time

$\phi(x)$ potential in units of Boltzmann voltage corresponding to the intrinsic Fermi-level at position x

ϕ_m maximum potential in units of Boltzmann voltage occuring at x_m

$\phi_n(x)$ potential in units of Boltzmann voltage corresponding to the quasi-Fermi-level of electron at position x

ϕ_{pB} potential in units of Boltzmann voltage corresponding to the quasi-Fermi-level of hole in the base

CHAPTER I

INTRODUCTION

A large-signal model is a mathematical model used to simulate the electrical behaviour of a transistor over a wide range of operating conditions. Such a model should be in a compact form which will approximate the internal electrical behaviour of a transistor at its terminals. Its main usefulness is in transistor circuit design and analysis, especially in integrated-circuits where tolerance calculations are often of interest. Thus an accurate and efficient compact mathematical model is desired.

Over the past twenty years, a number of models have been proposed. In 1954, the first bipolar junction transistor large-signal model, the Ebers-Moll model, was developed and later became widely used. It is based on device physics and covers all operating regimes, that is, active, saturated and cutoff operations. But, various approximations limit the accuracy of the model. Hence, over the past few years, a number of modified Ebers-Moll models have been proposed; those which have received the most attention are the ones employed in ECAP II(1), SCEPTRE(2) and NET-1(3) circuit analysis computer programs and the one recently proposed by John Logan(4) in 1972. Basically, the common approach in these modified Ebers-Moll models consists of retaining the form of the equations of the basic

Ebers-Moll model but increasing the accuracy by allowing certain model parameters to vary with voltages and currents. The functional dependence of these parameters is determined by curve-fitting and by using measurements made at the device terminals. The characterization thus consists of tabulations or empirically defined mathematical functions describing the dependence of such parameters as current gains on revelant voltages and currents.

In 1957, Beaufoy and Sparkes(5) analysed the bipolar junction transistor from a charge control point of view. Their charge control model or the equivalent charge control form of the Ebers-Moll model is directly useful for transient analysis.

In 1970, Gummel and Poon(6) proposed an integral charge control model described by twenty-one parameters (excluding the parasitic resistances) which offers significant advantages in static analysis and does not depend for its validity on many of the approximation upon which the basic Ebers-Moll model is based. Moreover, their model enables trading simplicity for accuracy thereby generating a progression of simpler models; in its simplest form, the Gummel-Poon model can reduce to the basic Ebers-Moll model.

A considerable volume of literature exists dealing with the above-mentioned models, yet very few comprehensive studies comparing the models are available in the literature(7), (8). Hence, it is the purpose of this thesis to present the detailed studies of each of the models; those which will be investigated are the basic Ebers-Moll model and the modified ones used in ECAP II, SCEPTRE and NET-1, and an abbreviated Gummel-Poon model (an abbreviated form of the integral charge control model originally proposed by Gummel and Poon). The models are compared on the bases of (i) their ability to simulate the common-emitter static characteristics of a silicon double-diffused transistor, (ii) the ease of model parameter evaluation, (iii) the compromise between simplicity of the model and accuracy of simulation and (iv) the ability to represent the physical processes of transistor.

The thesis is divided into four main parts. In Chapter II, the development of the large-signal models under investigation is described. In Chapter III, measuring techniques for determining the parameters of the models described in Chapter II are presented. In Chapter IV, computer simulations of the common-emitter static characteristics of a silicon double-diffused transistor by means of different models, are compared with the corresponding characteristics obtained experimentally. In Chapter V, results of the thesis are summarized and discussed, and further studies are suggested.

CHAPTER II

BIPLOAR JUNCTION TRANSISTOR LARGE-SIGNAL STATIC MODELS

2.1 THE EBERS-MOLL MODEL

The Ebers-Moll model is based on the idea of superimposing a "normal" and an "inverse" transistor to which the direct solution of the simplified transport equations for carriers of a p-n junction diode can be applied. The Ebers-Moll's approach is based on device physics but has little direct contact with all of the physical processes, (e.g. the effect of base-width modulation(9), the effects of generation and recombination of carriers in space-charge regions(10), the effect of conductivity modulation in the base(11) and in the collector (12) and the effect of emitter crowding(13), (14)).

Contrary to usual practice, the defining equations of the Ebers-Moll model are formulated here for the n-p-n rather than for the p-n-p transistor with voltage and current reference conditions based on the usual two-port network practice. However, the results apply equally well to p-n-p transistors.

The development of the model begins with some important assumptions (or approximations) which are as follows:

(a) The resistivities of the semiconductor neutral regions are low enough to be negligible.

(b) Low-level injection of carriers holds true. This implies that the injected current densities are low.

(Assumptions (a) and (b) insure that there are no voltage drops within the semiconductor neutral regions other than those across the junctions, and that the emitter efficiency is not a function of emitter current).

(c) The electric field in the neutral regions is independent of currents(15), (16).

(d) Space-charge region widening effects(17) are neglected.

(e) Generation and recombination effects in the space-charge regions(10) are neglected.

(f) Conductivity modulation in the base(11) and in the collector(12) is negligible.

(g) There is a uniform injection of carriers across the emitter area, that is, the emitter crowding(13), (14) is negligible.

(h) The emitter-base and collector-base junctions, respectively, have voltage-current relations of the form given by $(I=I_S(e^{qV/KT}-1))$, (18) i.e. the V-I characteristics of "ideal" p-n junction diodes.

(i) The transistor is a one-dimensional structure in the direction of major current flow.

2.1.1 The Basic Ebers-Moll Model

The development of the basic Ebers-Moll model(19) is based on the fact that one can consider two separate excitations to stand for the result of a general excitation (a given emitter-base voltage and a given collector-base voltage) of the transistor when they are applied in combination. Emitter-base and collector-base voltages determine the minority carrier densities at the edges of the space-charge regions and thus prescribe the boundary conditions for carrier densities in the base region. The same total carrier currents described by the carrier transport equations can be found by the application first of the prescribed emitter-base voltage and zero collector-base voltage and second of the prescribed collector-base voltage and zero emitter-base voltage as by both voltages applied simultaneously. This results in the validity of the use of "superposition" of the carrier current densities. By the principle of "superposition", the emitter and collector currents, I_E and I_C in terms of their components under forward and reverse voltage conditions can be written as follows:

$$I_E = I_{EF} + I_{ER} \tag{2.1}$$

$$I_C = I_{CF} + I_{CR} \tag{2.2}$$

Where the subscripts F and R denote the forward and reverse components respectively.

The definition of terminal currents and their current components are shown in Figure 2.1.

Making use of "ideal" p-n junction theory(18), one can write for the forward component of the emitter current, under the condition that the emitter-base junction is forward-biased with zero collector-base junction voltage,

$$(-I_{EF}) = I_{ES}(e^{q(-V_{EB})/KT} - 1) \tag{2.3}$$

Where I_{ES} is the magnitude of the emitter-base junction short-circuit reverse-saturation current with zero collector-base junction voltage. The forward component of the collector current denoted by I_{CF} is smaller than I_{EF} because not all of the minority carriers that are injected into the base from the emitter can reach the collector. If the fraction of the minority carriers that reach the collector is denoted by α_F, termed the d. c. forward short-circuit common-base current gain, then the forward component of the collector current is,

$$I_{CF} = -\alpha_F I_{EF} = \alpha_F I_{ES}(e^{q(-V_{EB})/KT} - 1) \qquad (2.4)$$

Similarly, one can write for the reverse components of the collector and the emitter currents under the condition that the collector-base junction is forward-biased with zero emitter-base junction voltage

$$(-I_{CR}) = I_{CS}(e^{q(-V_{CB})/KT} - 1) \qquad (2.5)$$

$$I_{ER} = -\alpha_R I_{CR} = \alpha_R I_{CS}(e^{q(-V_{CB})/KT} - 1) \qquad (2.6)$$

where I_{CS} is the magnitude of the collector-base junction short-circuit reverse-saturation current with zero emitter-base junction voltage and α_R is termed the d. c. reverse short-circuit common-base current gain.

The negative signs wherever they appear in equations (2.1) to (2.6) inclusive denote that the directions of the quantities (either voltage or current) are opposite to those defined on the basis of two-port active network convention.

Substitution of equations (2.3) to (2.6) inclusive into equations (2.1) and (2.2), yields

$$I_E = -I_{ES}(e^{q(-V_{EB})/KT} - 1) + \alpha_R I_{CS}(e^{q(-V_{CB})/KT} - 1) \qquad (2.7)$$

$$I_C = -I_{CS}(e^{q(-V_{CB})/KT} - 1) + \alpha_F I_{ES}(e^{q(-V_{EB})/KT} - 1) \qquad (2.8)$$

If the transistor structure is symmetrical, which however is not usually the case in a planar-diffused type, $\alpha_F = \alpha_R$. But, even for a non-symmetrical structure, it is usually assumed that $\alpha_F I_{ES} = \alpha_R I_{CS}$ as proposed by Ebers-Moll(19). By use of this reciprocity relationship, equations (2.7) and (2.8) can be rewritten as,

$$I_E = -I_{ES}(e^{q(-V_{EB})/KT} - 1) + \alpha_F I_{ES}(e^{q(-V_{CB})/KT} - 1) \qquad (2.9)$$

$$I_C = -I_{CS}(e^{q(-V_{CB})/KT} - 1) + \alpha_F I_{ES}(e^{q(-V_{EB})/KT} - 1) \qquad (2.10)$$

The form of equations (2.9) and (2.10), except for the n-p-n formulation and choice of reference conditions for voltages and currents, is the one most commonly referred to as the Ebers-Moll equations and used to define the Ebers-Moll model. A circuit representation of the Ebers-Moll model is shown in Figure 2.2.

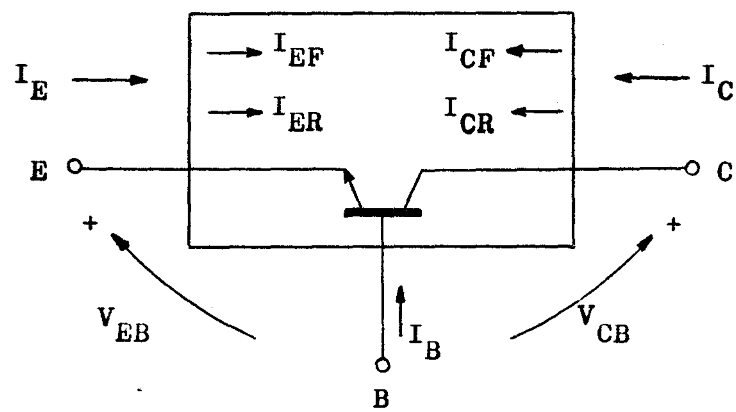

Figure 2.1 Definition of Terminal Currents and Their Forward and Reverse Components, Based on the Two-Port Network Configuration.

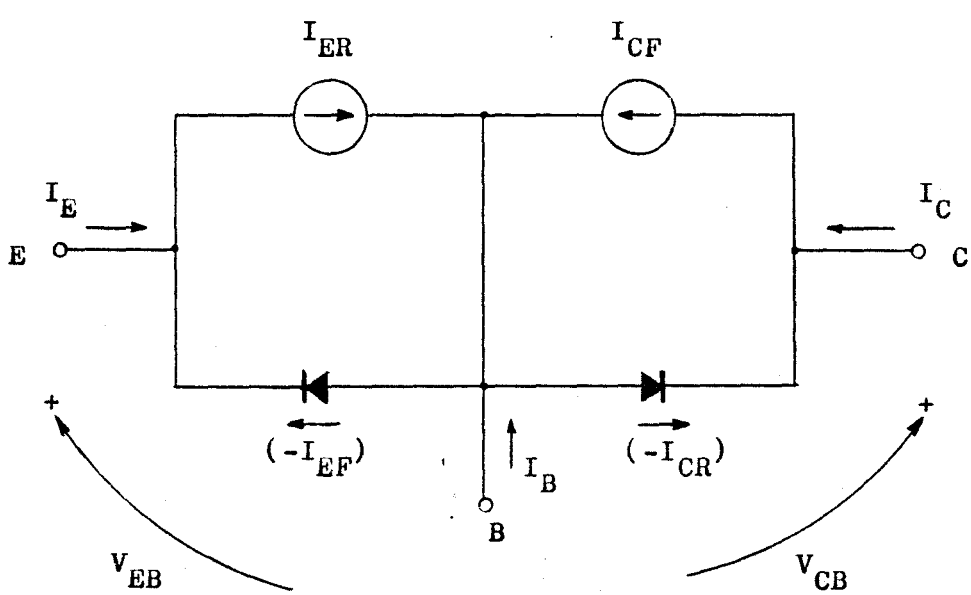

Figure 2.2 The Basic Ebers-Moll Model

2.1.2 The Modified Ebers-Moll Models

The basic Ebers-Moll model just developed in Section 2.1.1, is known to involve considerable errors if the parameters α_F and α_R are considered to be constant and the reciprocity relationship (i.e. $\alpha_F I_{ES} = \alpha_R I_{CS}$) is assumed. Because the model is based on the low-level injection theories introduced by Shockley(18), the greatest error for modern diffused silicon transistors is in the normal active (or quasi-linear) region where processes not accounted for, such as high-level injection of minority carriers, carrier generation and recombination in the space-charge regions, base-width modulation as a function of collector-base junction voltage, conductivity modulation in the base and in the collector at high current levels, surface leakage across the collector-base junction and ohmic resistances of the neutral regions, can contribute substantially to the overall characteristics. For example, without consideration of these processes, variation of d. c. common-emitter current gain will not appear in the model. Modification of the basic Ebers-Moll model is therefore necessary in order to improve the model accuracy. Three common modified Ebers-Moll models are chosen for investigation.

2.1.2(a) The Modified Ebers-Moll Model used in ECAP II

This model is basically the same as the basic Ebers-Moll model. Constant d. c. short-circuit common-base current gains, α_F and α_R are still assumed, but reciprocity is not assumed. The model includes junction space-charge region and diffusion capacitances, but since the investigation of the model here has been restricted to the static case, these capacitances are deleted.

The modifications made to the model can be described as follows:

(i) A base resistance used to account for the finite resistivity of the semiconductor of the base region is simulated by a fixed resistor in series with the base lead in the model.

(ii) Two current generators have been modified by replacing the "ideal" junction exponential factors, q/KT with empirical collector and emitter junction exponential factors, λ_C and λ_E respectively, which take into account the fact that practical transistors do not have "ideal" p-n junction diode exponential factors but some value between q/KT and q/2KT. Non-ideality is considered to be due to surface recombination, recombination in the interfaces between the substrate and the epitaxial layers as well as in the space-charge regions and the enhanced recombination due to the lattice imperfection in the heavily doped emitter region.

The basic Ebers-Moll's equations (2.7) and (2.8) are then written in the form of,

$$I_E = -I_{ES}(e^{\lambda_E V_{BE}} - 1) + \alpha_R I_{CS}(e^{\lambda_C V_{BC}} - 1) \qquad (2.11)$$

$$I_C = -I_{CS}(e^{\lambda_C V_{BC}} - 1) + \alpha_F I_{ES}(e^{\lambda_E V_{BE}} - 1) \qquad (2.12)$$

Transformation of equations (2.11) and (2.12) into the form as appeared in the ECAP II program, gives

the diode currents
$$J_{BE} = I_{ES}(e^{\lambda_E V_{BE}} - 1) \tag{2.13}$$

$$J_{BC} = I_{CS}(e^{\lambda_C V_{BC}} - 1) \tag{2.14}$$

the current generators
$$J_{FWD} = \alpha_F J_{BE} \tag{2.15}$$

$$J_{REV} = \alpha_R J_{BC} \tag{2.16}$$

the terminal currents
$$I_E = -J_{BE} + J_{REV} \tag{2.17}$$

$$I_C = -J_{BC} + J_{FWD} \tag{2.18}$$

A circuit representation of the model is shown in Figure 2.3.

This modified Ebers-Moll model has a total of seven model parameters, viz. I_{CS}, I_{ES}, α_F, α_R, λ_C, λ_E and R_B .

2.1.2(b) The Modified Ebers-Moll Model used in SCEPTRE

The modifications made to this model are essentially the same as those to the model in ECAPII. The reciprocity is also not assumed. The junction exponential factors are denoted by θ_C and θ_E, respectively, which are identical to λ_C and λ_E in the model of ECAPII. The junction capacitances are included in this model but do not feature in the static case.

The main features of this model can be stated below:

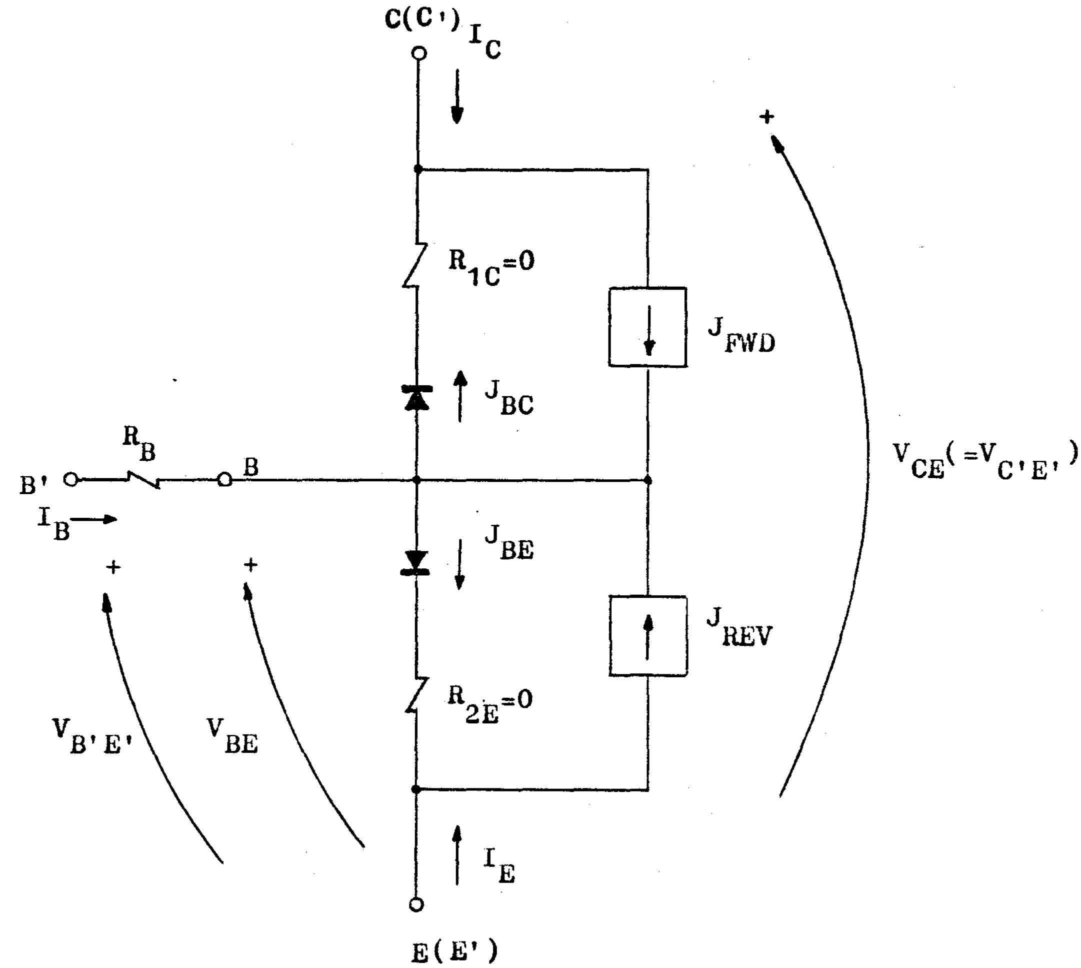

Figure 2.3 The Modified Ebers-Moll Model Used in ECAP II with Omission of Junction Capacitances and Dummy Resistors R_{1C} and R_{2E} equal to zero

(i) The d. c. forward and reverse short-circuit common-base current gains, α_F and α_R are not considered to be constant but allowed to vary with both junction voltages and currents. The functional dependence of these parameters is determined by measurements made at the transistor terminals. The characterization thus consists of tabulations of the dependence of these parameters on the relevant voltages and currents. The accuracy of the model can be increased by increasing the number of data points obtained from the terminal -measurements in constructing the tables for such parameters.

(ii) In addition to the base resistance, R_B, a series collector resistance, R_C is included in this model to account for the finite resistivity of the semiconductor of the neutral collector region. This R_C is significant while the transistor is operating at high current levels.

The model defining equations are written in the form of,

$$I_E = -I_{ES}(e^{\theta_E V_{BE}} - 1) + \alpha_R I_{CS}(e^{\theta_C V_{BC}} - 1) \tag{2.19}$$

$$I_C = -I_{CS}(e^{\theta_C V_{BC}} - 1) + \alpha_F I_{ES}(e^{\theta_E V_{BE}} - 1) \tag{2.20}$$

Transformation of equations (2.19) and (2.20) into the form as appeared in the SCEPTRE program yields,

The diode currents $$J_E = I_{ES}(e^{\theta_E V_{BE}} - 1) \tag{2.21}$$

$$J_C = I_{CS}(e^{\theta_C V_{BC}} - 1) \qquad (2.22)$$

The current generators $$J_F = \alpha_F J_E \qquad (2.23)$$

$$J_R = \alpha_R J_C \qquad (2.24)$$

Where α_F and α_R are functions of junction operating conditions and their values are determined experimentally.

The terminal currents $$I_E = -J_E + J_R \qquad (2.25)$$

$$I_C = -J_C + J_F \qquad (2.26)$$

This model contains eight model parameters. They are I_{CS}, I_{ES}, α_F, α_R (their values entered in a tabulated form), θ_C, θ_E, R_B and R_C.

The circuit representation of the model is shown in Figure 2.4.

2.1.2(c) The Modified Ebers-Moll Model used in NET-1

This model is essentially the same as the first two modified Ebers-Moll models. The reciprocity and constant current gains are also not assumed. The junction capacitances are also deleted in the static case. The features different from that of the previous two modified Ebers-Moll model can be described as follows:

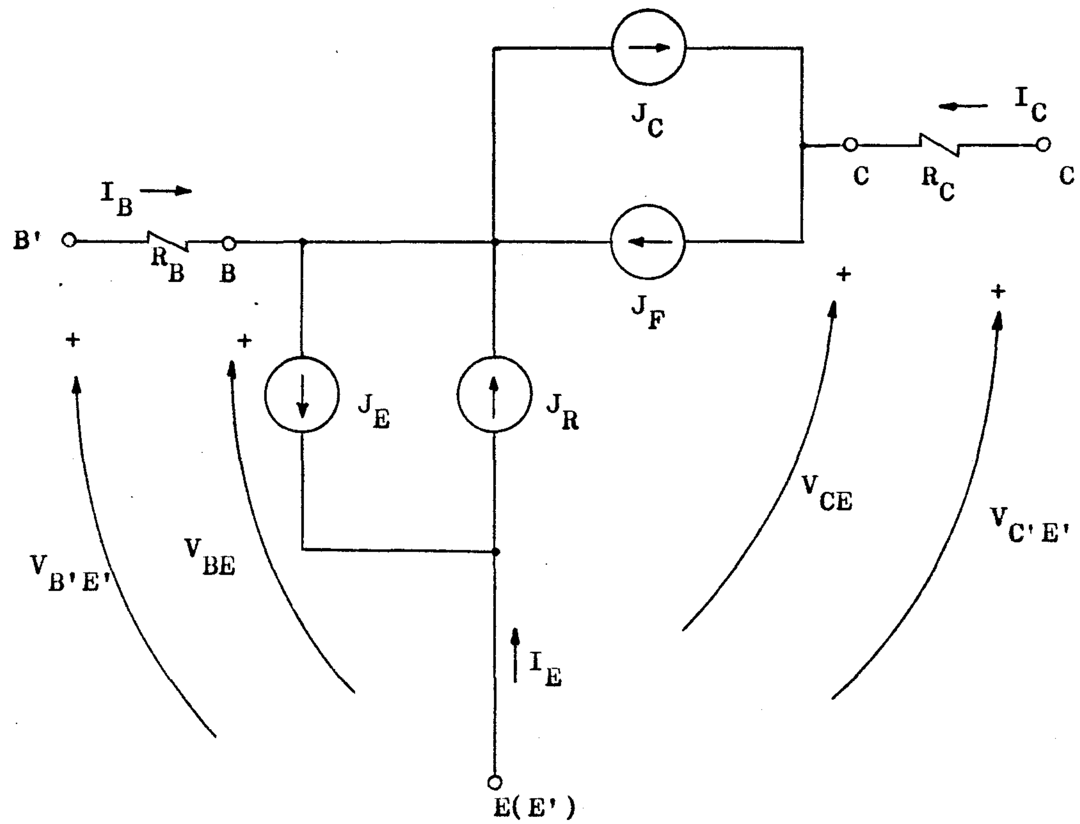

Figure 2.4 The Modified Ebers-Moll Model Used in SCEPTRE Program with Omission of Junction Capacitances and Junction Leakage Resistances

(i) The expressions for d. c. forward and reverse short-circuit common-base current gains, α_F and α_R are modelled by means of two third order polynomials, shown below:

$$\alpha_F = A_0 + A_1(V_{BE}) + A_2(V_{BE})^2 + A_3(V_{BE})^3 \tag{2.27}$$

$$\alpha_R = B_0 + B_1(V_{BC}) + B_2(V_{BC})^2 + B_3(V_{BC})^3 \tag{2.28}$$

(ii) The expressions for the two current generators are also modelled by means of empirical expressions which are the same as those in the models of ECAPII and SCEPTRE, but different notations for the junction exponential factors are used. The junction exponential factors which are denoted by θ_C and θ_E in the model of SCEPTRE are expressed here in the forms of q/KTM_C and q/KTM_E respectively. Hence, two model parameters, M_C and M_E termed the junction emission constants for the collector-base junction and the emitter-base junction are introduced.

(iii) Besides R_B and R_C, R_E is also included in this model to account for the finite resistivity of the semiconductor of the emitter neutral region.

Based on the above-mentioned modifications, equations (2.7) and (2.8) can be rewritten as follows:

$$I_E = -I_{ES}(e^{qV_{BE}/KTM_E} - 1) + \alpha_R I_{CS}(e^{qV_{BC}/KTM_C} - 1) \tag{2.29}$$

$$I_C = -I_{CS}(e^{qV_{BC}/KTM_C} - 1) + \alpha_F I_{ES}(e^{qV_{BE}/KTM_E} - 1) \qquad (2.30)$$

Where α_F and α_R are given by equations (2.27) and (2.28).

This model consists of fifteen model parameters. That is, I_{CS}, I_{ES}, M_C, M_E, R_C, R_B, R_E and two sets of coefficients of the third order polynomials (i.e. A_0, A_1, A_2, A_3 and B_0, B_1, B_2, B_3).

The circuit representation is shown in Figure 2.5.

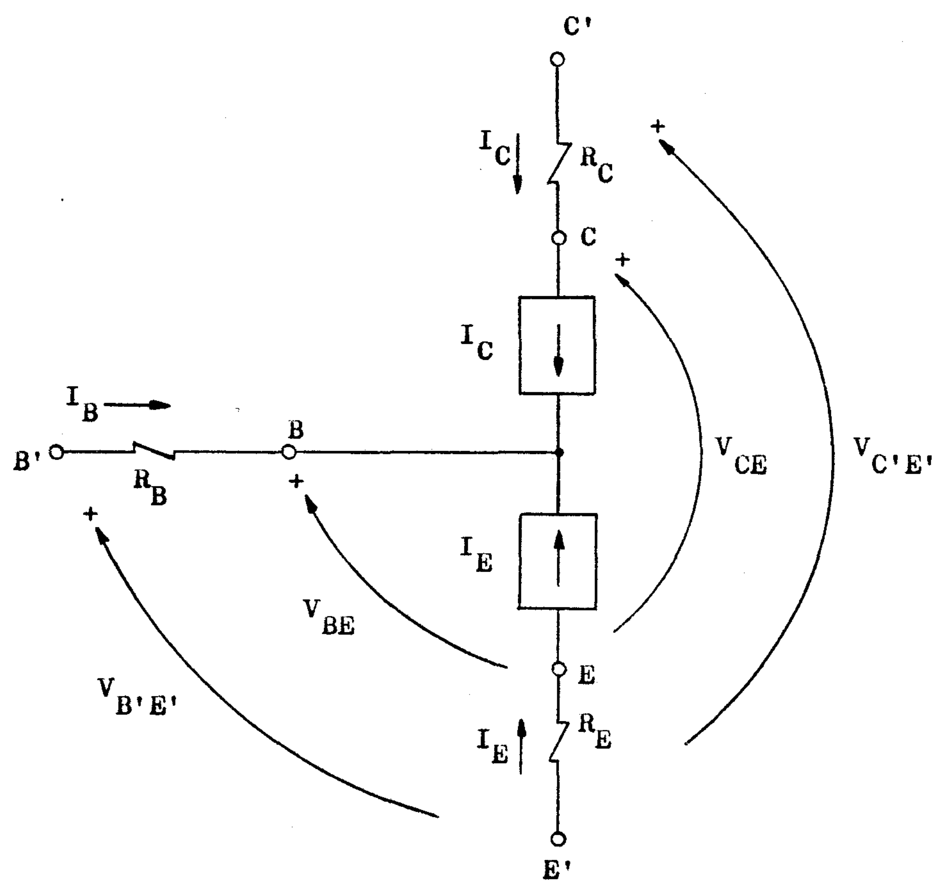

Figure 2.5 The Modified Ebers-Moll Model Used in NET-1 program with Omission of Junction Capacitances and Junction Leakage Resistances

2.2 THE ABBREVIATED GUMMEL-POON MODEL

As noted in Section 2.1, the static behaviour of a bipolar junction transistor is characterized in terms of the flow of minority carrier currents in the various parts of the device structure. The currents flow in response to excess carrier concentrations established by the individual actions of the emitter-base and collector-base junctions. On the other hand, the device characterization may be visualized in terms of the charge in the base region for the various operating regimes. This leads to the basic idea behind the development of the Gummel-Poon model (or the integral charge-control model) which is based on the charge-control concept(20) and Gummel's new charge-control relation for the bipolar junction transistor(21). The original Gummel-Poon model(22) describes the static and low-frequency behaviour of the transistor and in its most general form contains twenty-one parameters excluding the extrinsic parameters. The model presented here is an abbreviated form of the original model and contains only thirteen parameters excluding the extrinsic parameters, such as the series resistances of the semiconductors.

2.2.1 Consideration of Various Current Components in Transistor Operation

Figure 2.6 illustrates the various current components involved in an n-p-n transistor operating in the normal active mode. The current carried by electrons, called the principal current and denoted by I_{CC} is shown schematically as a function of distance from the emitter through the base to the collector regions. This

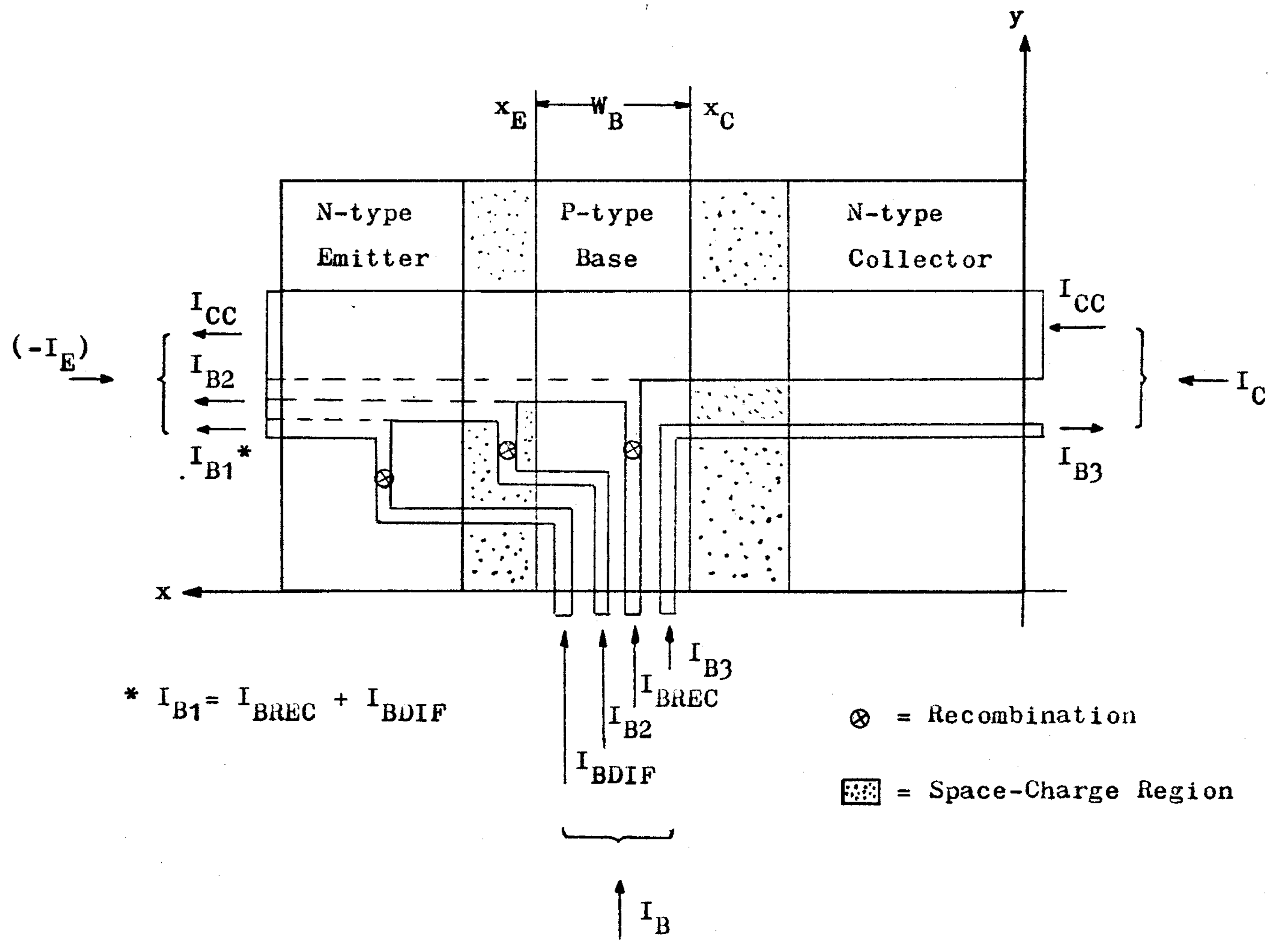

Figure 2.6 Illustration of the Terminal Currents and Their Current Components of an N-P-N Transistor assumed one-dimensional structure for Active Mode Operation

principal current is caused by the injection of minority carriers from the emitter to the base because of the action of the forward-biased emitter-base junction. Most of the carriers (electrons) can travel across the narrow base region, through the collector-base junction to the collector. A small fraction of these carriers recombine with the majority carriers (holes) in the base. This fraction contributes to the recombination current, in the base, which is a component of the total base current and denoted by I_{BREC}. Moreover, this recombination current can be minimized by making the base as thin as possible and by using, for the base, semiconductor material which has a relatively large lifetime. On the other hand, at the boundary between the emitter-base space-charge region and the p-type base, designated by plane x_E (referred to Figure 2.6), it can be shown that as a consequence of the forward-biased emitter-base junction, the majority carriers (holes) of the base are back-injected into the emitter through the emitter-base junction. The current carried by the holes due to the back-injection into the emitter yields another component of the base current. This current component can be separated into two parts: part 1, denoted by I_{BDIF}, is the diffusion current due to holes which are back-injected into the emitter then diminished by recombination there, while part 2, symbolized by I_{B2},* is a recombination current representing recombination in the emitter-base space-charge region. In addition,

* The symbol, I_{B1} is reserved for later use in equation (2.31).

because the collector-base junction is reverse-biased, holes are extracted from the collector into the base which yields one more component of the base current, denoted by I_{B3}. The recombination in the space-charge region of the collector-base junction is negligible. This occurs because the electric field in the space-charge region is directed from the collector to the base (in the n-p-n case) so that all the minority carriers (electrons) that reach the edge of the space-charge region are swept out of the base into the collector where they are collected. The generation in the space-charge region is also negligible because of the suppression resulting from the presence of mobile carriers injected from the emitter.

The terminal emitter current is the flow of the total charge carriers across the boundary plane, x_E per unit time, that is, the principal current, I_{CC} plus the sum of the base current components, I_{BREC}, I_{BDIF} and I_{B2}. Likewise, the collector current is given by the sum of the principal current and base current component I_{B3}. The base current is obviously the sum of I_{BREC}, I_{BDIF}, I_{B2} and I_{B3}. Both the currents I_{BREC} and I_{BDIF} are typically "ideal" currents, that is, they are proportional to ($e^{qV_{BE}/KT}$) respectively and can therefore be combined in the form of,

$$I_{B1} = I_{BREC} + I_{BDIF} \tag{2.31}$$

Furthermore, since the components I_{B1} and I_{B2} are emitter contributions while component I_{B3} is collector contribution, it can be written that,

$$I_{BE} = I_{B1} + I_{B2} \tag{2.32}$$

$$I_{BC} = I_{B3} \tag{2.33}$$

To facilitate the development of the transistor model, using the assumed current conventions shown in Figure 2.6, the terminal currents can be expressed in explicit forms as follows:

$$I_B = I_{BE} + I_{BC} \tag{2.34}$$

$$I_C = I_{CC} - I_{BC} \tag{2.35}$$

$$(-I_E) = I_{CC} + I_{BE} \tag{2.36}$$

2.2.2 <u>Modelling the Base Current</u>

Having understood the base current components in transistor operation with reference to Figure 2.6, one can model the base current components first, thence the sum of them gives the total base current I_B.

(a) <u>The Base Current Component</u> I_{B1}

As defined by equation (2.31), this current component is the sum of I_{BREC} and I_{BDIF}. I_{BDIF}, the hole current back-injected into the n-type emitter can be determined by means of the static p-n junction theory(18) by considering the emitter-base junction as an isolated p-n junction, under forward-biased condition. Since the emitter is more heavily doped than the base, this implies that the low-level injection of carriers from the base can be achieved. As a result, this current is dominated by the "ideal" current which follows the "ideal" p-n junction theory. If the emitter is several diffusion length wide, this current is given by,

$$I_{BDIF} = I_{BD}(e^{qV_{BE}/KT} - 1) \tag{2.37}$$

I_{BREC}, the hole current which supports recombination in the base can be evaluated provided the approximate form of the minority carrier distribution and the doping profile in the base is known. For low recombination rate in the base, the per unit volume recombination rate is n_{pB}'/τ_B where $n_{pB}' = n_{pB} - n_{0B}$ is the excess minority carrier (electron) concentration and τ_B is the lifetime of the base. The total number of electrons which recombine in the base per unit time is the integral of n_{pB}'/τ_B over the volume of the neutral base region. Inasmuch as a hole is required for each electron which vanishes in the base, the current I_{BREC} is given by,

$$I_{BREC} = qA_{JE}\int (n_{pB}'(x)/\tau_B)\mathbf{dx} \tag{2.38}$$

However, in practical diffused transistors, the recombination properties in the base are not known to the detail required for the evaluation of the integral in equation (2.38). The assumption of the linear minority carrier distribution in the base is a gross simplification. But the detailed studies have confirmed that the base recombination current can be given by

$$I_{BREC} = I_{BR}(e^{qV_{BE}/KT} - 1) \qquad (2.39)$$

Where I_{BR} is a constant of proportionality.
The combination of equations (2.37) and (2.39) gives I_{B1} as defined by equation(2.31), viz.

$$I_{B1} = (I_{BD} + I_{BR})\ (e^{qV_{BE}/KT} - 1) \qquad (2.40)$$

or $$I_{B1} = I_1(e^{qV_{BE}/KT} - 1) \qquad (2.41)$$

Where I_1 can be considered as a physical parameter of the model and its value can be determined experimentally.

In a real transistor, the lack of lattice perfection in the semiconductor causes enhanced local recombination as well as surface recombination in the p- and n- regions. This current and the junction voltage, V_{BE} are therefore not exactly related through the "ideal" junction exponential factor, q/KT but some value which may vary between q/KT and q/2KT. From the practical point of view, equation (2.41) is thus replaced by a more general function of V_{BE}

which is characterized by an emitter emission coefficient, N_{E1} associated with the emitter-base junction. Equation (2.41) then becomes,

$$I_{B1} = I_1(e^{qV_{BE}/KTN_{E1}} - 1) \tag{2.42}$$

For a typical transistor of good quality, the emitter emission coefficient, N_{E1} should have a value very close to unity. In general, its value lies between 1.0 and 1.5.

(b) The Base Current Component I_{B2}

The hole current which supports recombination in the space-charge region of the emitter-base junction is typically "non-ideal" current. Since the space-charge region is the volume well-defined by the width of the space-charge layer (for a given junction cross-sectional area) which is a function of the junction voltage, for single-level recombination centres in the space-charge region, this recombination current can be expressed(23), (24), (25), (26), (27), as

$$I_{B2} = \frac{qn_i W_{EB} A_{JE}}{\sqrt{\tau_n \tau_p}} (e^{qV_{BE}/2KT} - 1) \tag{2.43}$$

with

$$\tau_n = (\sigma_n v_{th} N_t)^{-1} \tag{2.43a}$$

$$\tau_p = (\sigma_p v_{th} N_t)^{-1} \tag{2.43b}$$

For practical purposes, the junction exponential factor, $(q/2KT)$ appearing in equation (2.43) is modified in a way similar to that for I_{B1}, by introducing one more emitter emission coefficient, denoted by N_{E2} having a value typically between 1.5 and 2.0. If the quantity $((qn_i W_{EB} A_{JE})/(\tau_n \tau_p)^{1/2})$ is interpreted as an intercept current, symbolized by I_2, equation (2.43) then becomes

$$I_{B2} = I_2(e^{qV_{BE}/KTN_{E2}} - 1) \tag{2.44}$$

(c) <u>The Base Current Component</u> I_{B3}

Likewise, the current carried by holes extracted from the collector region can be evaluated by means of the static p-n junction theory. For the practical transistors, the reverse-biased collector-base junction does not obey the "ideal" p-n junction theory. It is for this reason that a collector emission coefficient, N_C is introduced in a way similar to that for I_{B1} to account for the effects of surface recombination, recombination in the interfaces between substrate and epitaxial layers.

If the collector region is several diffusion length wide, this component is given by

$$I_{B3} = I_3(e^{qV_{BC}/KTN_C} - 1) \tag{2.45}$$

Where I_3 is considered as a model parameter and its value can be determined experimentally.

In addition, it can be shown that I_{B3}, in the active mode of transistor operation, is a negative quantity which agrees with the assumed direction of the carrier flow shown in Figure 2.6. Since the collector-base junction is reverse-biased, for large reverse-bias voltage, the exponential term (e^{qV_{BC}/KTN_C}) is sufficiently small compared with the unity in equation (2.45). This automatically implies that I_{B3} is a negative quantity. Nevertheless, without the loss of generality, I_{B3} is expressed in the form appearing in equation (2.45).

The base current components having been formulated, the base current can now be expressed in an explicit form as follows:

$$I_{BE} = I_1(e^{qV_{BE}/KTN_{E1}} - 1) + I_2(e^{qV_{BE}/KTN_{E2}} - 1) \tag{2.46}$$

$$I_{BC} = I_3(e^{qV_{BC}/KTN_C} - 1) \tag{2.47}$$

$$I_B = I_1(e^{qV_{BE}/KTN_{E1}} - 1) + I_2(e^{qV_{BE}/KTN_{E2}} - 1) + I_3(e^{qV_{BC}/KTN_C} - 1) \tag{2.48}$$

2.2.3 Modelling the Collector Current

In this section, the collector current will be developed on the basis of a charge-control concept in conjunction with the mathematical theory of the p-n junction.

(a) The Principal Current I_{CC}

In order to implement the derivation of I_{CC} in a simple fashion, the following important assumptions are made:

(i) The diffusion constant, D and the mobility, μ of the carriers are related through Einstein relationship, that is,

$$D = \frac{KT}{q} \mu \qquad (2.49)$$

(ii) The built-in field E, and the built-in potential ϕ (in units of Boltzmann voltage), being functions of distance from the collector, are related by

$$E(x) = - \frac{KT}{q} \cdot \frac{d\phi(x)}{dx} \qquad (2.50)$$

(iii) The velocity-field relation is idealized by the field dependent mobility expression, that is,

$$\mu = \frac{\mu o}{1 + \frac{\mu o \left| E(x) \right|}{Vs}} \qquad (2.51)$$

By assumption (i), the low field mobility, μo is equal to qDo/KT in which Do is the corresponding diffusion constant. $|E|$ is the magnitude of the built-in field and Vs is the scattering-limited velocity approximately equal to 10^7 cm/sec.

(iv) The low-field mobility, μo is independent of doping of the background material.

(v) The electric fields are low enough for avalanche multiplication of carriers to be negligible.

As a starting point, the carrier transport equation(28) describing the electron current density Je(x) carried by the injected carriers (electrons) from the emitter through the base to the collector is

$$Je(x) = q\mu eE(x)n(x) + qDe \frac{dn(x)}{dx} \tag{2.52}$$

Since the electron current density Je(x) is a function of distance, a quantity R(x), which is a ratio of the current density at position x to the principal current density Jcc entering the collector terminal, is defined by

$$R(x) = \frac{Je(x)}{Jcc} \tag{2.53}$$

Application of appropriate subscript "e" representing electron to the parameters D, μ, Do and μo in equations (2.49), (2.50) and (2.51) and substitution of those equations into equation (2.52) yield

$$\frac{dn(x)}{dx} - n(x)\frac{d\phi(x)}{dx} - \frac{JccR(x)}{KT\left[\dfrac{\mu eo}{1 + \dfrac{\mu eo\,|E(x)|}{Vs}}\right]} = 0 \qquad (2.54)$$

Further simplification of equation (2.54) leads to,

$$\frac{dn(x)}{dx} - n(x)\frac{d\phi(x)}{dx} - \frac{Jcc}{qDeo}\,R(x) - \frac{Jcc}{qVs}\left|\frac{d\phi(x)}{dx}\right|R(x) = 0 \qquad (2.55)$$

In order to solve the differential equation (2.55), the specified upper and lower limits for the integral are required. They are x_1 and x_2 which are arbitrary but confined in a feasible region of integration. Multiplication of both sides of equation (2.55) by $e^{-\phi(x)}$ and integration from x_1 to x_2 with respect to x, give

$$\int_{x_1}^{x_2} \frac{dn(x)}{dx}\,(e^{-\phi(x)})\,dx - \int_{x_1}^{x_2} n(x)\,\frac{d\phi(x)}{dx}\,(e^{-\phi(x)})\,dx$$

$$- \frac{Jcc}{qDeo}\int_{x_1}^{x_2} R(x)(e^{-\phi(x)})\,dx - \frac{Jcc}{qVs}\int_{x_1}^{x_2} R(x)\left|\frac{d\phi(x)}{dx}\right|(e^{-\phi(x)})\,dx = 0$$

(2.56)

Application of integral calculus technique to first two terms of equation (2.56), yields

$$\int_{x_1}^{x_2} \frac{dn(x)}{dx} \left(e^{-\phi(x)}\right) dx + \left[n(x)\left(e^{-\phi(x)}\right)\Big|_{x_1}^{x_2} - \int_{x_1}^{x_2} \frac{dn(x)}{dx} \left(e^{-\phi(x)}\right) dx \right]$$

$$- \frac{Jcc}{qDeo}\int_{x_1}^{x_2} R(x)\left(e^{-\phi(x)}\right) dx - \frac{Jcc}{qVs}\int_{x_1}^{x_2} R(x)\left|\frac{d\phi(x)}{dx}\right|\left(e^{-\phi(x)}\right) dx = 0 \tag{2.57}$$

or

$$n(x_2)\left(e^{-\phi(x_2)}\right) - n(x_1)\left(e^{-\phi(x_1)}\right) =$$

$$\frac{Jcc}{qDeo}\int_{x_1}^{x_2} R(x)\left(e^{-\phi(x)}\right) dx + \frac{Jcc}{qVs}\int_{x_1}^{x_2} R(x)\left|\frac{d\phi(x)}{dx}\right|\left(e^{-\phi(x)}\right) dx \tag{2.57a}$$

Since equation (2.57a) is valid for any region defined by x_1 and x_2, x_1 and x_2 can be chosen to be x_C and x_E respectively, where x_C and x_E are the outside edges of space-charge regions of collector-base and emitter-base junctions respectively. This is done in agreement with the assumed convention of current flow in Figure 2.6, i.e. the direction of flow of the principal current, I_{CC} is positive while flowing from the collector to the emitter and its direction is opposite to that of the flow of its carriers (electrons).

Hence,

$$n(x_E)\left(e^{-\phi(x_E)}\right) - n(x_C)\left(e^{-\phi(x_C)}\right) =$$

$$\frac{Jcc}{qDeo}\int_{x_C}^{x_E} R(x)\left(e^{-\phi(x)}\right) dx + \frac{Jcc}{qVs}\int_{x_C}^{x_E} R(x)\left|\frac{d\phi(x)}{dx}\right|\left(e^{-\phi(x)}\right) dx \tag{2.57b}$$

The Boltzmann relation gives,

$$n(x) = n_i(e^{\phi(x) - \phi_n(x)}) \tag{2.58 }$$

At the outside edges of the space-charge regions of the emitter-base and the collector-base junctions, equation (2.58) becomes

$$n(x_C) = n_i(e^{\phi(x_C) - \phi_n(x_C)}) \tag{2.58a}$$

$$n(x_E) = n_i(e^{\phi(x_E) - \phi_n(x_E)}) \tag{2.58b}$$

Substitution of equations (2.58a) and (2.58b) into equation (2.57b) and simplification of the resulting equation gives,

$$J_{CC} = \frac{qD_{eo}n_i^2(e^{-\phi_n(x_E)} - e^{-\phi_n(x_C)})}{\int_{x_C}^{x_E} R(x)n_i(e^{-\phi(x)})dx + \frac{n_iD_{eo}}{V_s}\int_{x_C}^{x_E} R(x)\left|\frac{d\phi(x)}{dx}\right|(e^{-\phi(x)})dx} \tag{2.59 }$$

Owing to lack of details in the function behaviour of $\phi(x)$ appearing in both terms of the denominator of equation (2.59), the assessment of the relative magnitude of these terms is necessary so as to show that the second term is much less than the first term and hence the second term is negligible. With reference to Figure 2.7, it can be realized that, inside the base region, there exists a

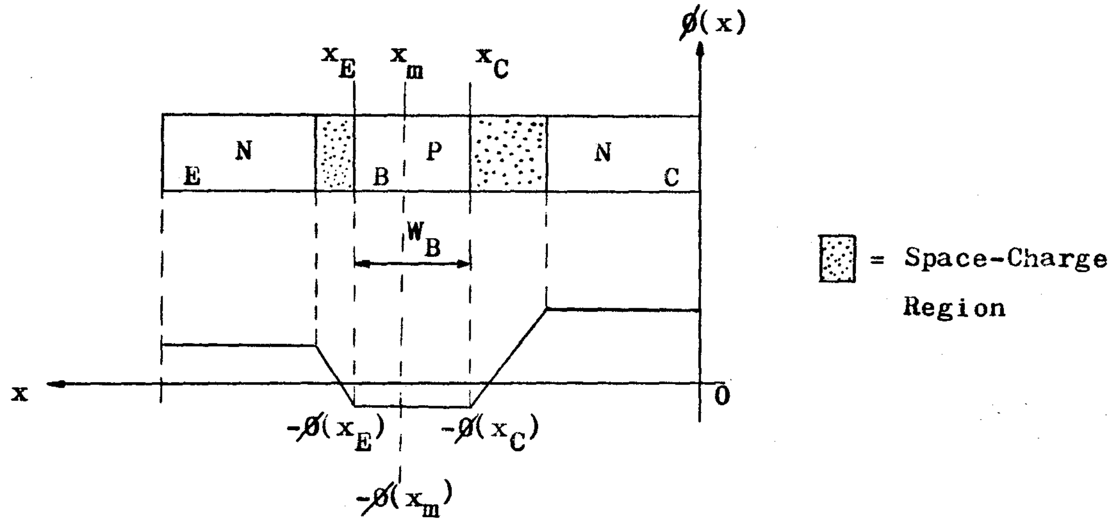

Figure 2.7 The Distribution of the Internal Potentials Corresponding to the Intrinsic Fermi-level of an N-P-N Transistor

maximum built-in potential, ϕ_m at x_m. $\phi_m (= \phi(x_m))$ can have a finite value. Similarly, R(x) can have a value $R_m (= R(x_m))$, corresponding to ϕ_m, which is also a finite value. Furthermore, in the base region, $\phi(x)$ and R(x) do not differ markedly from ϕ_m and R_m respectively, the first integral then becomes,

$$\int_{x_C}^{x_E} R(x) n_i (e^{-\phi(x)}) \, dx \doteq R_m n_i (e^{-\phi_m}) \int_{x_C}^{x_E} dx$$

$$\doteq W_B R_m n_i (e^{-\phi_m}) \qquad (2.60)$$

and the second integral becomes,

$$\frac{n_i D_{eo}}{V_s} \int_{x_C}^{x_E} R(x) \left| \frac{d\phi(x)}{dx} \right| (e^{-\phi(x)}) \, dx \doteq \frac{D_{eo} n_i R_m}{V_s} (e^{-\phi_m}) \int_{x_C}^{x_E} d|\phi(x)|$$

$$\doteq \frac{D_{eo}}{V_s}\left[|\phi(x_E)| - |\phi(x_C)|\right] R_m n_i (e^{-\phi_m})$$

$$\doteq \frac{D_{eo}}{V_s} \Delta|\phi| R_m n_i (e^{-\phi_m}) \tag{2.61}$$

Also, in the base region between x_E and x_C, the potential $|\phi(x_E)|$ does not differ markedly from $|\phi(x_C)|$ but they are close to each other in magnitude. $\Delta|\phi|$ is approaching to an infinitesimal value. The value of (D_{eo}/V_s) is approximately equal to 100 Å which is small compared with the base width W_B of the most advanced transistors at the present time. Hence, the second integral in the rest of the derivation can be neglected. Equation (2.59) then becomes,

$$J_{CC} = \frac{qD_{eo} n_i^2 (e^{-\phi_n(x_E)} - e^{-\phi_n(x_C)})}{\int_{x_C}^{x_E} R(x) n_i (e^{-\phi(x)}) dx} \tag{2.62}$$

If the quasi-Fermi-level of holes in the base region is assumed to be constant, the corresponding electrostatic potential of holes, ϕ_{pB} will be constant. The emitter-base and collector-base junction voltages can be defined by the differences of the electrostatic potentials across the junctions. That is,

$$V_{BE} = \frac{KT}{q} (\phi_{pB} - \phi_n(x_E)) \tag{2.63}$$

$$V_{BC} = \frac{KT}{q} (\phi_{pB} - \phi_n(x_C)) \qquad (2.64)$$

or

$$-\phi_n(x_E) = \frac{q}{KT} V_{BE} - \phi_{pB} \qquad (2.63a)$$

$$-\phi_n(x_C) = \frac{q}{KT} V_{BC} - \phi_{pB} \qquad (2.64a)$$

The junction voltages, V_{BE} and V_{BC} are positive quantities differing from the terminal junction voltages by ohmic drops.

Substitution of equations (2.63a) and (2.64a) in equation (6.62) gives,

$$J_{CC} = \frac{qD_{eo}n_i^2(e^{qV_{BE}/KT} - e^{qV_{BC}/KT})}{\int_{x_C}^{x_E} R(x)n_i(e^{\phi_{pB} - \phi(x)})dx} \qquad (2.65)$$

Again, substitution of equation (2.66), the Boltzmann relation

$$p_B(x) = n_i(e^{\phi_{pB} - \phi(x)}) \qquad (2.66)$$

in equation (2.65) gives,

$$J_{CC} = \frac{qD_{eo}n_i^2(e^{qV_{BE}/KT} - e^{qV_{BC}/KT})}{\int_{x_C}^{x_E} R(x)p_B(x)dx} \qquad (2.67)$$

If an average value of R(x) is defined by,

$$(R)_{ave} = \frac{\int_{x_C}^{x_E} R(x)p_B(x)dx}{\int_{x_C}^{x_E} p_B(x)dx} \tag{2.68}$$

then the expression in the denominator of equation (2.67) becomes,

$$\int_{x_C}^{x_E} R(x)p_B(x)dx = (R)_{ave}\int_{x_C}^{x_E} p_B(x)dx$$

$$= (R)_{ave}\left(\frac{q_B}{q}\right) \tag{2.69}$$

with q_B termed the base charge density (i.e. the base charge per unit area) in units of electric charge q, defined by the integration of hole density (in units of per volume) over the region from x_C to x_E with respect to x.

If the base charge and current densities are changed to the total base charges and current in accordance with the sign convention in Figure 2.6, then

$$I_{CC} = J_{CC}A_J \qquad (2.70)$$

$$Q_B = q_B A_J \qquad (2.71)$$

where A_J is the device junction cross-sectional area, either A_{JE} or A_{JC} whichever is smaller.

Substitution of equations (2.69) to (2.71) inclusive into equation (2.67) yields,

$$I_{CC} = \frac{(qA_J n_i)^2 D_{eo}(e^{qV_{BE}/KT} - e^{qV_{BC}/KT})}{Q_B(R)_{ave}} \qquad (2.72)$$

For large current gain (i.e. $h_{FE} \gg 1$), $(R)_{ave}$ is nearly unity and varies little with bias. Equation (2.72) then reduces to

$$I_{CC} = \frac{(qA_J n_i)^2 D_{eo}}{Q_B}(e^{qV_{BE}/KT} - e^{qV_{BC}/KT}) \qquad (2.72a)$$

At zero-bias condition, the total amount of base charges, denoted by Q_{BO} is approximately given by

$$Q_{BO} \doteq qA_J N_B \qquad (2.73)$$

Where the sign of Q_{BO} is in agreement with that of the total number of impurities (excess acceptor for p-type base region), N_B per unit area in the base.

Substitution of equation (2.73) in equation (2.72a) gives,

$$I_{CC} = \frac{qA_J n_i^2 D_{eo}}{N_B} \left(e^{qV_{BE}/KT} - e^{qV_{BC}/KT}\right) \frac{Q_{BO}}{Q_B} \qquad (2.74)$$

If the quantity $((qA_J n_i^2 D_{eo})/N_B)$ is interpreted as an intercept current, denoted by I_S, equation (2.74) can be written as,

$$I_{CC} = I_S\left(e^{qV_{BE}/KT} - e^{qV_{BC}/KT}\right) \frac{Q_{BO}}{Q_B} \qquad (2.75)$$

Equation (2.75) defines the principal current in which the intercept current can be determined experimentally.

(b) <u>The Base Charge</u> Q_B

The principal current, I_{CC} can be separated into an emitter and a collector component or a forward and a reverse component, I_F and I_R, as follows:

$$I_{CC} = \frac{I_S Q_{BO}}{Q_B} \left(e^{qV_{BE}/KT} - 1\right) - \frac{I_S Q_{BO}}{Q_B} \left(e^{qV_{BC}/KT} - 1\right)$$

$$= I_F - I_R \qquad (2.76)$$

thence

$$I_F = \frac{I_S Q_{BO}}{Q_B} \left(e^{qV_{BE}/KT} - 1\right) \qquad (2.76a)$$

$$(-I_R) = \frac{I_S Q_{BO}}{Q_B}\left(e^{qV_{BC}/KT} - 1\right) \qquad (2.76b)$$

The total base charge, Q_B represents the sum of the zero-bias base charge, $Q_{BO,}$ the excess stored charges Q_E and Q_C associated with the emitter-base and collector-base junction space-charge capacitances, and the negative charges, $\tau_F I_F$ (due to the injected electrons from the emitter while the transistor is in normal operation) and $\tau_R(-I_R)$ (due to the injected electrons from the collector while the transistor operates in an reverse mode). That is,

$$Q_B = Q_{BO} + Q_E + Q_C + (BP)\,I_F\tau_F + (-I_R)(-\tau_R) \qquad (2.77)$$

It should be noted, in equation (2.77) that at low-level injection condition, the base "push-out" factor, BP can be taken as unity since the base-width is approximately equal to the metallurgical base-width. At high levels, when base "push-out" occurs, BP is greater than unity. For details, reference(22) can be referred to.

In the modelling of the base charge, accuracy and simplicity may be traded. For a simple representation, the base "push-out" factor may be assumed to be unity, and the emitter-base and collector-base space-charge region capacitances C_E and C_C, and the forward and the reverse transit times τ_F and τ_R, are assumed to be constant in equation (2.77). The assumed value of BP equal to unity leads to the rapid falloff of the d.c. common-emitter current gain, h_{FE} at high collector current levels due to the rapid increase of Q_B. The assumption of constant emitter-base and collector-base space-charge region capacitances means that the modelling equations for Q_E and Q_C are linear functions of the emitter-base and collector-base junction voltages respectively. That is,

$$C_E = \frac{dQ_E}{dV_{BE}} \tag{2.78 }$$

$$Q_E = \int C_E \, dV_{BE} = C_E V_{BE} \tag{2.78a}$$

$$C_C = \frac{dQ_C}{dV_{BC}} \tag{2.79 }$$

$$Q_C = \int C_C \, dV_{BC} = C_C V_{BC} \tag{2.79a}$$

The above assumptions afford significant simplification in modelling the base charge. If the properly averaged values of τ_F, τ_R, C_E and C_C are obtained, the errors due to these assumptions are not expected to exceed a few percent for typical situations.

The minus sign before τ_R appearing in equation (2.77) arises because the total base charge contains holes neutralizing the negative charges, $\tau_F I_F$ and $\tau_R I_R$.

For modelling Q_B, it is convenient to normalize all charges in equation (2.77) with respect to the zero-bias base charge, Q_{BO} and replace I_F and $(-I_R)$ in accordance with equations (2.76a) and (2.76b), thence

$$q_b = 1 + q_e + q_c + \frac{I_S}{q_b Q_{BO}} \left(\tau_F (e^{qV_{BE}/KT} - 1) + \tau_R (e^{qV_{BC}/KT} - 1) \right) \tag{2.80}$$

For convenience, let

$$q_1 = 1 + q_e + q_c \tag{2.81}$$

$$q_2 = \frac{I_S}{Q_{BO}} \left(\tau_F (e^{qV_{BE}/KT} - 1) + \tau_R (e^{qV_{BC}/KT} - 1) \right) \tag{2.82}$$

Solution to equation (2.80) for q_b, gives

$$q_b = \tfrac{1}{2}(q_1) + \left((q_1/2)^2 + q_2 \right)^{\frac{1}{2}} \tag{2.83}$$

Multiplication of equation (2.83) by Q_{BO}, yields

$$Q_B = Q + \sqrt{Q^2 + \frac{I_S}{Q_{BO}^{-1}} \left(\tau_F (e^{qV_{BE}/KT} - 1) + \tau_R (e^{qV_{BC}/KT} - 1) \right)} \tag{2.84}$$

Where $Q = \tfrac{1}{2}(q_1 Q_{BO})$ (2.85)

Substitution of equations (2.78a), (2.79a) and (2.81) into equation (2.85) yields,

$$Q = \frac{Q_{BO} + V_{BE}C_E + V_{BC}C_C}{2} \qquad (2.86)$$

The principal current, I_{CC} is therefore defined by equations (2.75), (2.84) and (2.86). According to equation (2.35), the collector terminal current can be expressed as,

$$I_C = I_S(e^{qV_{BE}/KT} - e^{qV_{BC}/KT})\frac{Q_{BO}}{Q_B} - I_3(e^{qV_{BC}/KTN_C} - 1) \qquad (2.87)$$

with Q_B defined by equations (2.84) and (2.86).

Eventually, the defining equation for the terminal emitter current is unnecessary, since it is not independent and can be obtained by Kirchhoff's current law, i.e. $I_E = -(I_B + I_C)$ on the basis of the assumed current directions in Figure 2.6.

Equations (2.48) and (2.87) are used to define the abbreviated Gummel-Poon model of the intrinsic portion of the transistor.

2.2.4 <u>The Emitter, Collector and Base Resistances</u>

(a) <u>The Emitter and Collector Resistances</u> R_E and R_C

To the intrinsic transistor model described, the series resistances of the emitter and collector should be included to account for the finite resistivities of the semiconductor materials of those regions. In a way similar to that in the modified Ebers-Moll models, the series resistances can be modelled to a first order approximation by the lumped resistors having constant values in series with the emitter and collector leads respectively. The values of these series resistances can be determined experimentally.

(b) The Base Resistance R_{BT}

In view of the lateral current flows in the base region, the base region can be divided into two regions of interest: (i) the inactive base region, under the base contact, through which the total base current must flow and (ii) the active base region, under the emitter, through which the minority carrier current flows longitudinally. Hence, the base resistance should be the combination of two resistances which account for the effect of the voltage drops in the inactive and active base regions respectively.

The inactive base resistance, R_{BI} can be simulated by a fixed resistor in series with the base lead since the total base current must flow through the inactive base region and the current path is through the material of finite conductivity.

The active base resistance, R_{BA} is a variable because of conductivity modulation of the active base region. From the charge-control concept, the active base resistance can be modelled as a function of the base charge. For circular geometry and non-uniform base layer of the device, R_{BA} is given(29) by

$$R_{BA} = \frac{1}{8 \pi q \mu_h \int_{x_C}^{x_E} N(x) dx} \tag{2.88}$$

Where N(x) is the excess acceptor density in the base region as a function of distance x.

If $N(x) \gg n_i$, it is true that $p(x) \doteq N(x)$. Hence,

$$R_{BA} = \frac{1}{8 \pi q \mu_h \int_{x_C}^{x_E} p(x) dx} \tag{2.89}$$

As stated in the previous section, the $\int_{x_C}^{x_E} p(x)dx$ gives the total base charge, q_B per unit area in units of electric charge, q. Therefore,

$$R_{BA} = \frac{1}{8 \pi q \mu_h (q_B/q)} = \frac{1}{8\pi \mu_h q_B} \tag{2.90}$$

Multiplication of q_B by A_J gives

$$R_{BA} = \frac{A_J}{8 \pi \mu_h Q_B} \tag{2.91}$$

At zero-bias condition, equation (2.91) becomes,

$$R_{BAO} = \frac{A_J}{8\pi \mu_h Q_{BO}} \tag{2.92}$$

Where R_{BAO} is the inactive base resistance at zero-bias condition.

Combination of equations (2.91) and (2.92) yields,

$$R_{BA} = R_{BAO} \frac{Q_{BO}}{Q_B} \tag{2.93}$$

with R_{BAO} defined by equation (2.92) which is considered as one of the intrinsic model parameters because it accounts for the effect in the active base region.

The total base resistance, R_{BT} is therefore given by,

$$R_{BT} = R_{BI} + R_{BAO} \frac{Q_{BO}}{Q_B} \tag{2.94}$$

The total number of parameters of the abbreviated Gummel-Poon model is sixteen which are I_1, I_2, I_3, I_S, N_C, N_{E1}, N_{E2}, τ_F, τ_R, C_C, C_E, Q_{BO}, R_{BAO}, R_{BI}, R_E and R_C. The circuit representation of the model is shown in Figure 2.8.

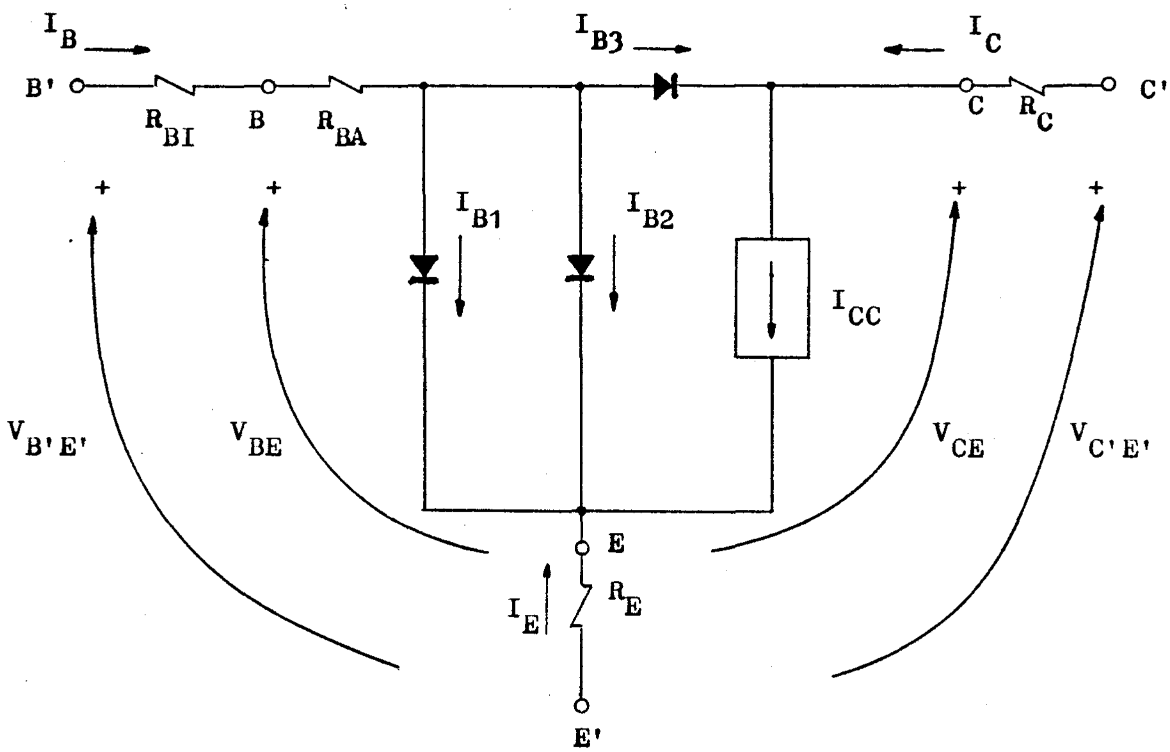

Figure 2.8 Circuit Representation of the Abbreviated Gummel-Poon Model

CHAPTER III

DETERMINATION OF MODEL PARAMETERS

Transistor models have been presented in Chapter II. The detailed methods for determination of both intrinsic (including static and transient charge-control parameters) and extrinsic (including series resistances of the emitter, collector and inactive base regions) model parameters are presented in this chapter. The sample transistor chosen for measurements is a type 2N1613, n-p-n silicon, double-diffused, annular structural configuration, for high-speed switching and d. c. to U.H.F. amplifier applications.

Some of the geometric dimensions of the transistor structure are obtained microscopically.

All electrical measurements are carried out at room temperature of 25^{o} C (or 298^{o} K) and measured values are expressed in M.K.S. units.

3.1 THE PARAMETERS OF THE MODIFIED EBERS-MOLL MODELS

Since the model parameters of the three modified Ebers-Moll models are basically the same, the separate evaluation of parameters of each model will not be presented. All the model parameters are determined experimentally.

3.1.1 The Intrinsic Model Parameters

There are six intrinsic model parameters, viz. I_{ES}, I_{CS}, λ_E or θ_E ($\Rightarrow M_E$), λ_C or θ_C ($\Rightarrow M_C$), α_F and α_R to be determined.

(a) Emitter-Junction Short-Circuit Reverse-Saturation Current, I_{ES}, Emitter-Junction Exponential Factor, λ_E, Emitter-Junction Constant, θ_E and Emitter-Junction Emission Constant, M_E

In view of equation (2.11) or (2.19) or (2.29), I_{ES} can be determined from the active region measurements of the emitter-base terminal junction voltage as a function of emitter current with zero collector-base terminal junction voltage. The equation on which this measurement is based is,

$$\left| I_E \right| = I_{ES}\left(e^{\lambda_E V_{BE}} - 1\right) \tag{3.1}$$

The test configuration used in obtaining this measurement is shown in Figure 3.1. The measured data are listed in Table 3-1.

Figure 3.2 shows a semi-log plot of $\left| I_E \right|$ versus V_{BE} in which the intercept current obtained by extrapolation from the high current region of this plot gives the value of I_{ES}. Besides the graphical extrapolation, analytical manipulation is also available, hence the graphically obtained value of I_{ES} is not shown in Figure 3.2. The slope of the straight line portion yields the value of λ_E (or θ_E) from which M_E can be obtained.

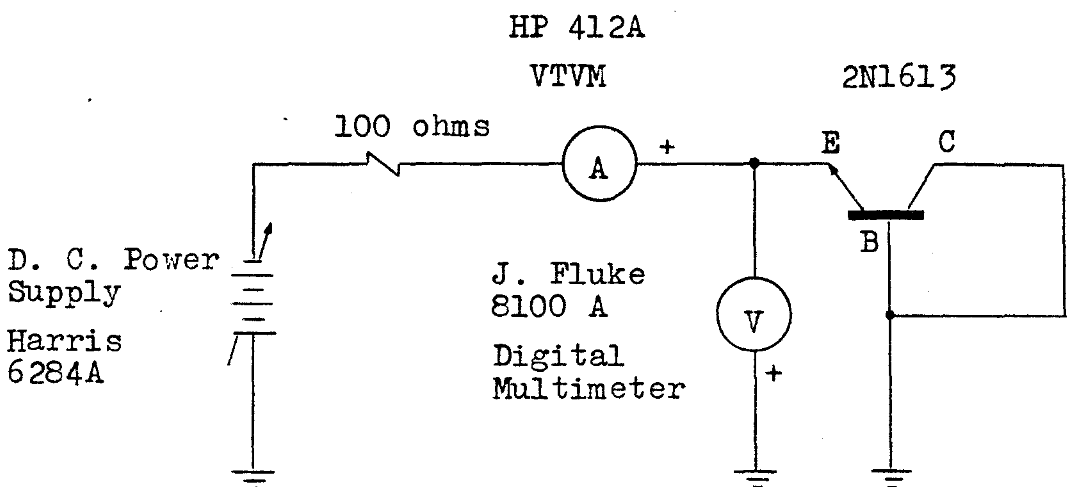

Figure 3.1 Test Configuration for determination of I_{ES}

$I_E(A)$	$V_{BE}(V)$	$I_B(A)^*$
1.00×10^{-6}	0.4284	--
2.00×10^{-6}	0.4448	--
5.00×10^{-6}	0.4696	--
8.00×10^{-6}	0.4825	--
1.00×10^{-5}	0.4881	--
2.00×10^{-5}	0.5079	--
5.00×10^{-5}	0.5345	--
8.00×10^{-5}	0.5475	--
1.00×10^{-4}	0.5538	--
2.00×10^{-4}	0.5731	--
5.00×10^{-4}	0.5975	--
8.00×10^{-4}	0.6098	--
1.00×10^{-3}	0.6157	--
2.00×10^{-3}	0.6350	--
5.00×10^{-3}	0.6618	--
8.00×10^{-3}	0.6766	--
1.00×10^{-2}	0.6829	--
2.00×10^{-2}	0.7025	--
3.00×10^{-2}	0.7176	--
4.00×10^{-2}	0.7290	--
8.00×10^{-2}	0.7650	--
1.00×10^{-1}	0.7881	2.05×10^{-3}

Table 3-1 I_E versus V_{BE} for $V_{BC} = 0$ volt

* For use in determining the inactive base resistance, R_B

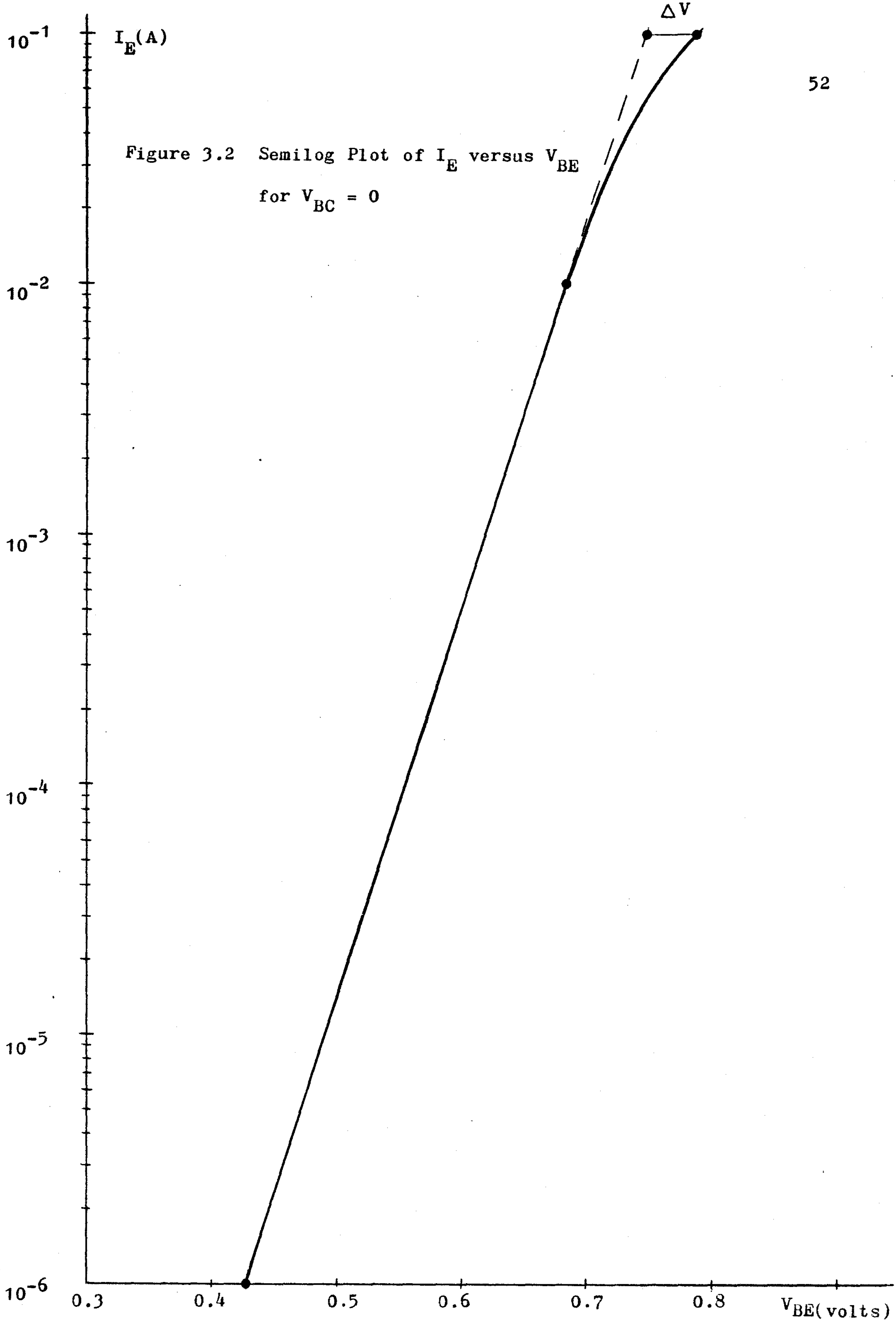

Figure 3.2 Semilog Plot of I_E versus V_{BE} for $V_{BC} = 0$

<u>Calculations of</u> I_{ES}, λ_E, θ_E <u>and</u> M_E

$$\lambda = \frac{q}{KT} = \underline{38.9} \text{ volts}^{-1} \tag{3.2}$$

Choose two data points shown below from Figure 3.2 (or Table 3-1). These points should be chosen in the microampere region to avoid the effect of ohmic drops due to the resistances of the transistor neutral regions.

$$|I_{E2}| = 10^{-2} \text{ A.} \qquad V_{BE2} = 0.6829 \text{ volt}$$

$$|I_{E1}| = 10^{-6} \text{ A.} \qquad V_{BE1} = 0.4284 \text{ volt}$$

Use of equation (3.1) gives,

$$\lambda_E = \frac{\ln(\ |I_{E2}| \,/\, |I_{E1}|\ )}{V_{BE2} - V_{BE1}} = \underline{36.2} \text{ volts}^{-1}$$

Likewise,

$$\theta_E = \underline{36.2} \text{ volts}^{-1}$$

The value of M_E is given by

$$M_E = \frac{KT}{q}\lambda_E = \underline{1.075}$$

The value of I_{ES} is given by

$$I_{ES} = \frac{|I_{E2}|}{e^{\lambda_E V_{BE2}} - 1} = \underline{1.6\text{x}10^{-13}} \ \text{A}.$$

(b) <u>Collector-Junction Short-Circuit Reverse-Saturation Current</u>, I_{CS}, <u>Collector-Junction Exponential Factor</u>, λ_C, <u>Collector-Junction Constant</u>, θ_C <u>and Collector-Junction Emission Constant</u>, M_C

By using equation (2.12) or (2.20) or (2.30), I_{CS} can be determined from the measurement of the collector-base terminal junction voltage as a function of collector current under the condition that the transistor operates in the reverse mode with zero base-emitter terminal junction voltage. The equation on which this measurement is based is,

$$I_C = I_{CS}(e^{\lambda_C V_{BC}} - 1) \tag{3.3}$$

By means of the same measurement techniques employed in Section (a) with test configuration shown in Figure 3.3, the measured data are obtained and listed in Table 3-2. The semi-log plot of I_C versus V_{BC} is shown in Figure 3.4.

Similarly, the analytical manipulation for obtaining the values of I_{CS}, λ_C, θ_C and M_C, on the basis of two data points from Table 3-2 are given as follows:

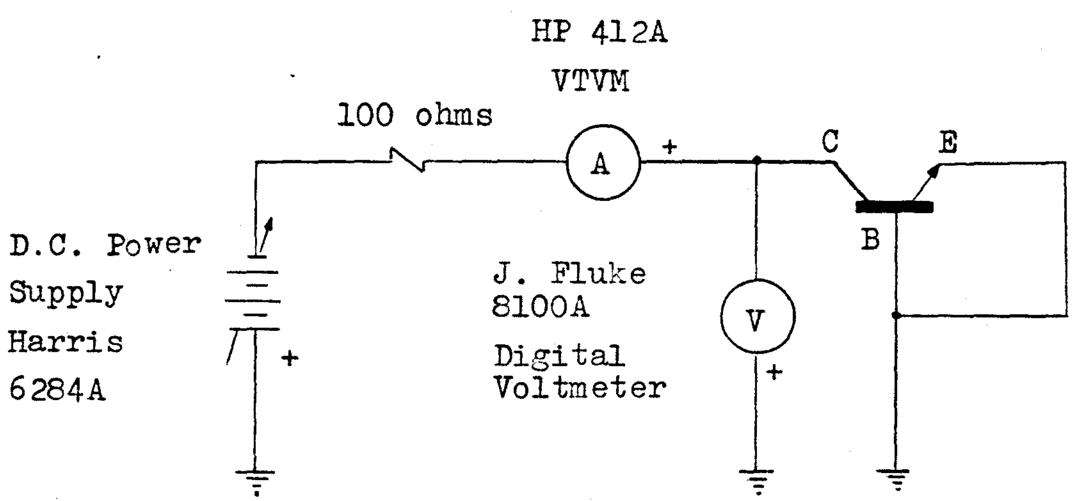

Figure 3.3 Test Configuration for determination of I_{CS}

I_C(A)	V_{BC}(V)
1.00×10^{-6}	0.4033
2.00×10^{-6}	0.4237
5.00×10^{-6}	0.4507
8.00×10^{-6}	0.4653
1.00×10^{-5}	0.4715
2.00×10^{-5}	0.4922
5.00×10^{-5}	0.5195
8.00×10^{-5}	0.5335
1.00×10^{-4}	0.5399
2.00×10^{-4}	0.5600
5.00×10^{-4}	0.5874
8.00×10^{-4}	0.6029
1.00×10^{-3}	0.6105
2.00×10^{-3}	0.6360
5.00×10^{-3}	0.6776
8.00×10^{-3}	0.7052
1.00×10^{-2}	0.7166

Table 3-2 I_C versus V_{BC} for V_{BE} = 0 volt

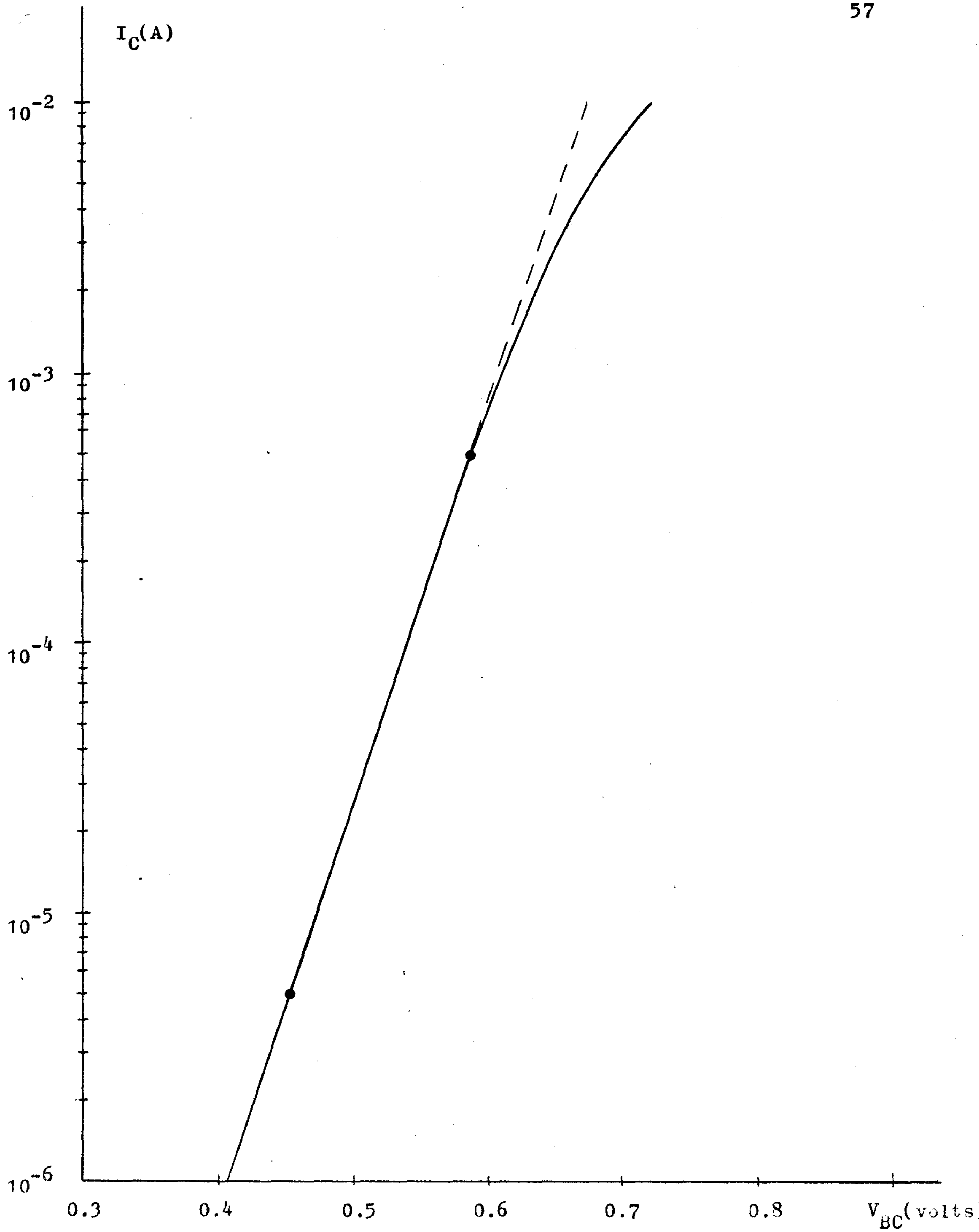

Figure 3.4 Semilog Plot of I_C versus V_{BC} for $V_{BE} = 0$

Two data points chosen for calculation are:

$I_{C2} = 5\text{x}10^{-4}$ A. $\quad V_{BC2} = 0.5874$ volt

$I_{C1} = 5\text{x}10^{-6}$ A. $\quad V_{BC1} = 0.4507$ volt

The calculation results are:

$\lambda_C = \underline{33.75}$ volt^{-1}

$\theta_C = \underline{33.75}$ volt^{-1}

$M_C = \underline{1.155}$

$I_{CS} = \underline{1.18\text{x}10}^{-12}$ A.

(c) <u>D. C. Forward Short-Circuit Common-Base Current Gain</u>, α_F

α_F can be determined as a function of emitter current for different values of base current, I_B. To obtain α_F, the test configuration of Figure 3.5 is utilized. The base current varies over a wide range from 50 nA to 500 μA. The collector current corresponding to each value of I_B for fixed collector-emitter voltage is recorded. Knowing the collector and base currents, the emitter current is then calculated from $I_E = -(I_C + I_B)$. α_F is given by,

$$\alpha_F = - \frac{I_C}{I_E} \tag{3.4}$$

Values of I_B, I_C, I_E and α_F are tabulated in Table 3-3. An averaged value of α_F's equal to 0.9857, over the base current ranging from 10 μA to 500 μA will be used as the constant parameter value in the ECAP II Ebers-Moll model to approximate the static characteristics over a wide range of base current of the transistor operation.

All the calculated values of α_F are listed in Table 3-3, to be used later in the SCEPTRE Ebers-Moll model.

The reason for utilizing the low collector-emitter voltage is to insure that the transistor is operating in the active mode so as to obtain the best possible fit of the Ebers-Moll models.

(d) D. C. Reverse Short-Circuit Common-Base Current Gain, α_R

α_R can be determined in a way similar to that employed in Section (c). The test configuration for use in determining α_R is shown in Figure 3.6. Table 3-4 shows the measured data and the values of α_R calculated by means of

$$\alpha_R = -\frac{I_E}{I_C} \qquad (3.5)$$

All those calculated values of α_R are useful for the SCEPTRE Ebers-Moll model and will be entered in a tabular form to the computer analysis program.

An averaged value of α_R's equal to 0.5112, over the base current ranging from 10 μA to 500 μA will be used as the constant parameter value in the ECAP II Ebers-Moll model to approximate the

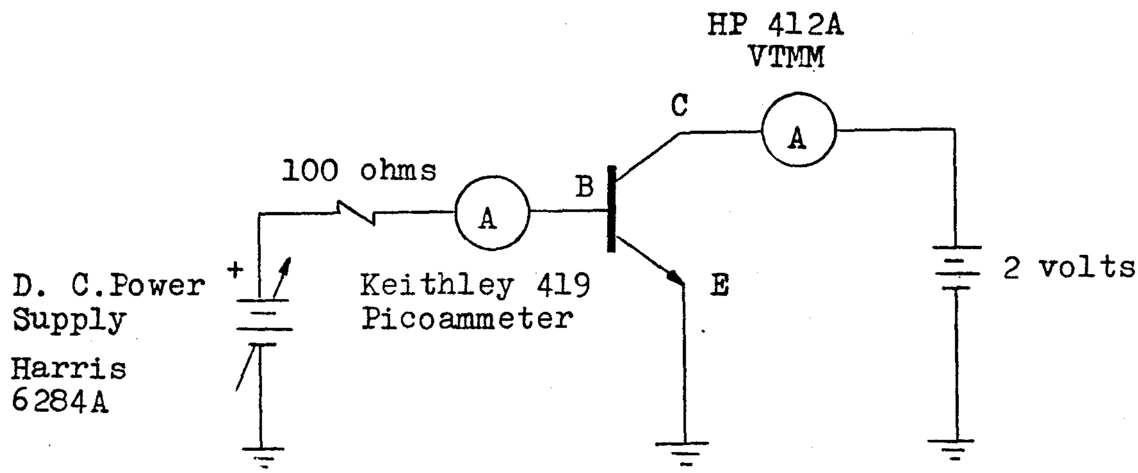

Figure 3.5 Test Configuration for determination of α_F

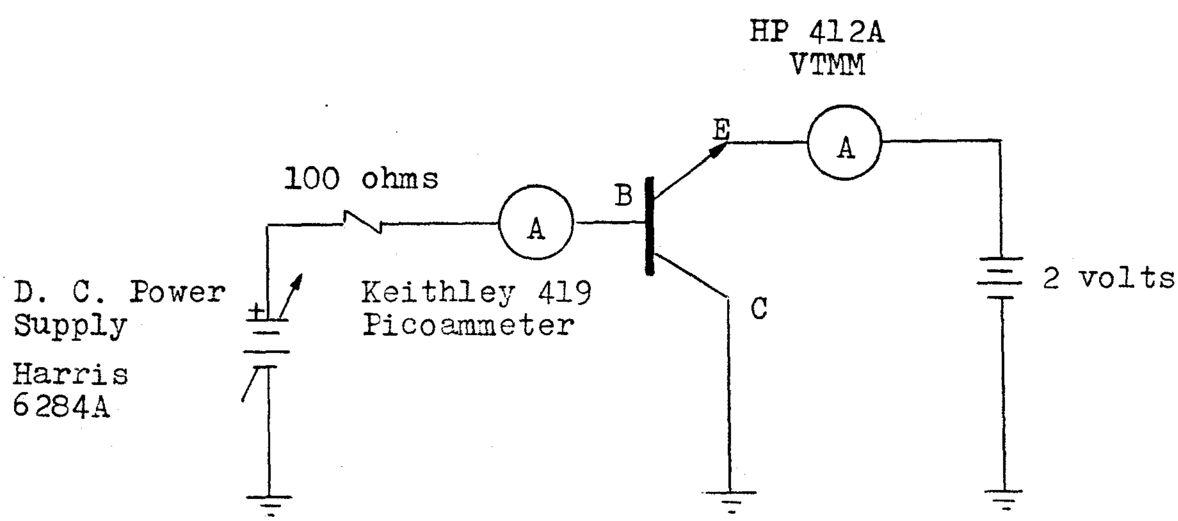

Figure 3.6 Test Configuration for determination of α_R

I_B(A)	I_C(A)	$-I_E=I_B+I_C$ (A)	$\alpha_F=-(I_C/I_E)$
5.00×10^{-8}	4.95×10^{-7}	5.45×10^{-7}	0.9082
1.00×10^{-7}	1.36×10^{-6}	1.46×10^{-6}	0.9315
2.00×10^{-7}	3.75×10^{-6}	3.95×10^{-6}	0.9494
5.00×10^{-7}	1.36×10^{-5}	1.41×10^{-5}	0.9645
1.00×10^{-6}	3.42×10^{-5}	3.52×10^{-5}	0.9716
2.00×10^{-6}	8.23×10^{-5}	8.43×10^{-5}	0.9763
5.00×10^{-6}	2.52×10^{-4}	2.57×10^{-4}	0.9805
1.00×10^{-5}	5.74×10^{-4}	5.84×10^{-4}	0.9828
4.00×10^{-5}	2.70×10^{-3}	2.74×10^{-3}	0.9854
6.00×10^{-5}	4.15×10^{-3}	4.21×10^{-3}	0.9857
1.20×10^{-4}	8.65×10^{-3}	8.77×10^{-3}	0.9863
5.00×10^{-4}	3.58×10^{-2}	3.63×10^{-2}	0.9862

Table 3-3 Measurement of I_B & I_C for use in determination of α_F at constant V_{CE} = 2 volts

I_B(A)	I_E(A)	$-I_C=I_B+I_E$ (A)	$\alpha_R=-(I_E/I_C)$
5.00×10^{-8}	1.00×10^{-8}	6.00×10^{-8}	0.1667
1.00×10^{-7}	3.00×10^{-8}	1.30×10^{-7}	0.2308
2.00×10^{-7}	7.00×10^{-8}	2.70×10^{-7}	0.2593
5.00×10^{-7}	2.40×10^{-7}	7.40×10^{-7}	0.3243
1.00×10^{-6}	5.70×10^{-7}	1.57×10^{-6}	0.3631
2.00×10^{-6}	1.34×10^{-6}	3.34×10^{-6}	0.4012
5.00×10^{-6}	3.95×10^{-6}	8.95×10^{-6}	0.4413
1.00×10^{-5}	8.90×10^{-6}	1.89×10^{-5}	0.4709
4.00×10^{-5}	4.19×10^{-5}	8.19×10^{-5}	0.5116
6.00×10^{-5}	6.40×10^{-5}	1.24×10^{-4}	0.5161
1.20×10^{-4}	1.33×10^{-4}	2.53×10^{-4}	0.5257
5.00×10^{-4}	5.02×10^{-4}	1.00×10^{-4}	0.5010

Table 3-4 Measurement of I_B & I_E for use in determination of α_R at constant V_{EC} = 2 volts

static characteristics over a wide range of base current of the transistor operation.

(e) <u>The Coefficients of the Third Order Polynomials used to determine the D. C. Forward and Reverse Short-Circuit Common-Base Current Gains</u>

The coefficients A_0, A_1, A_2, A_3, B_0, B_1, B_2 and B_3 can only be determined theoretically by means of curve-fitting techniques. The values of those coefficients are to be adjusted such that the shape of the curves described by the third order polynomials can best fit the shape of the curves of α_F versus I_B and α_R versus I_B defined by Tables 3-3 and 3-4 respectively. For curve-fitting technique, Section 3.2.2 can be referred to. The initial values of A_0, A_1, A_2, A_3, B_0, B_1, B_2, and B_3 are equal to unity. The error criteria for α_F and α_R are given by $\sum_{j=1}^{12}(\alpha_{FSj}-\alpha_{Fj})^2$ and $\sum_{j=1}^{12}(\alpha_{RSj}-\alpha_{Rj})^2$ respectively, where α_{FS} and α_{RS} are the simulated α_F and α_R calculated by using equations (2.27) and (2.28), and the modified Ebers-Moll model used in NET-1. Pattern Search is used to minimize the deviation (described by the error criteria) between the measured and the simulated current gains. The simulated current gains based on the optimal values of coefficients of two third order polynomials shown in Table 3-5 are given in Appendix C.

	For α_F		For α_R
A_0	0.839760	B_0	0.318899
A_1	0.268489	B_1	0.312386
A_2	0.143319	B_2	0.186316
A_3	-0.324963	B_3	-0.266397

TABLE 3-5 Values of Coefficients of two Third Order Polynomials used to determine α_F and α_R

3.1.2 The Extrinsic Model Parameters

There are three extrinsic parameters (i.e. R_E, R_C and R_B). In the modified Ebers-Moll model employed in ECAP II, only R_B is included while the one in SCEPTRE, both R_B and R_C are included. All three are included in the modified Ebers-Moll model in NET-1.

(a) The Series Resistances of the Emitter and Collector Regions, R_E and R_C

A static method is used to determine these resistances. It is based on a model of the transistor consisting of an ideal device whose paths have no resistances with additional path resistances shown in Figures 3.7 and 3.8.

The basic principal used to develop this measuring technique is that when a base current is supplied to the base terminal and one of the other two terminals is left open-circuited, then with reference to Figure 3.7, the terminal collector-emitter voltage is given by,

$$\text{for } I_C = 0 , \qquad V_{C'E'} = V_{CE} + I_B R_E \tag{3.6}$$

and a plot of $V_{C'E'}$ versus I_B in Figure 3.9 yields the value of R_E, the slope of the linear portion of this plot.

Similarly, with reference to Figure 3.8, the terminal emitter-collector voltage is given by,

$$\text{for } I_E = 0 , \qquad V_{E'C'} = V_{EC} + I_B R_C \tag{3.7}$$

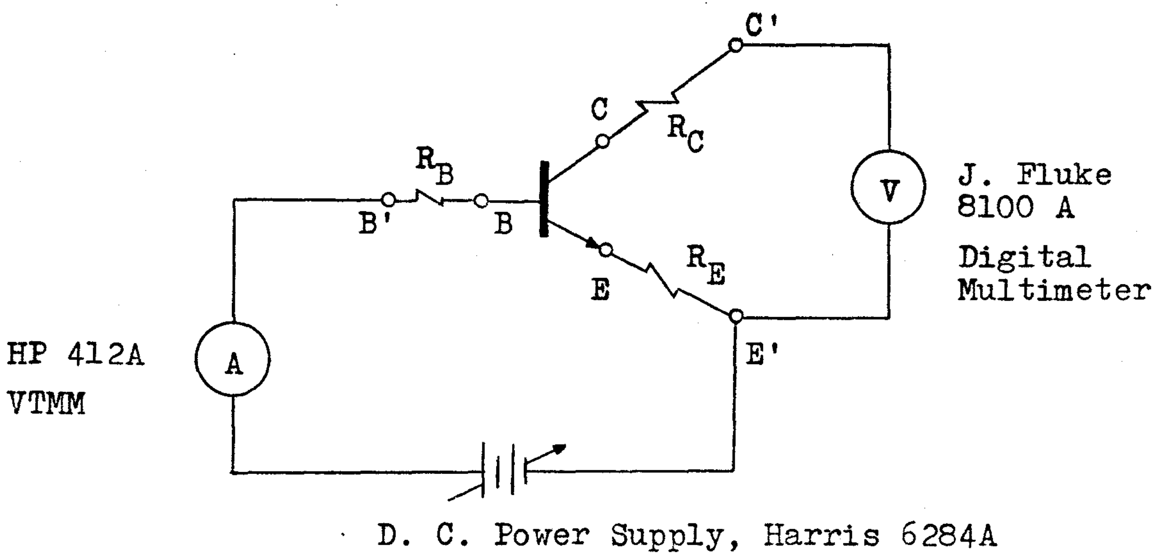

Figure 3.7 Test Configuration for determination of R_E

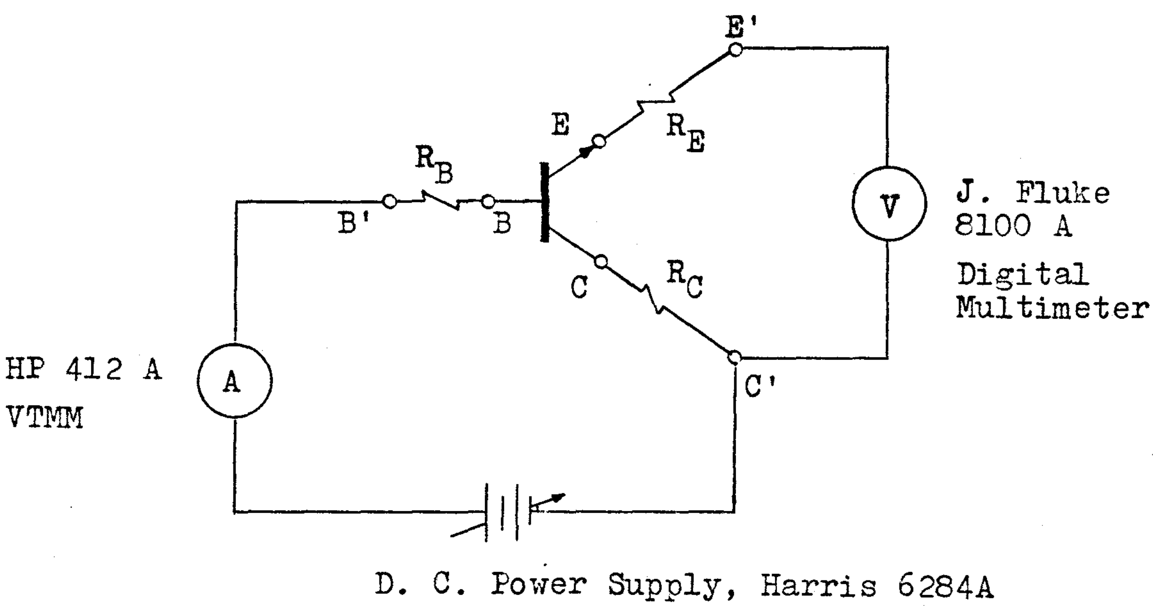

Figure 3.8 Test Configuration for determination of R_C

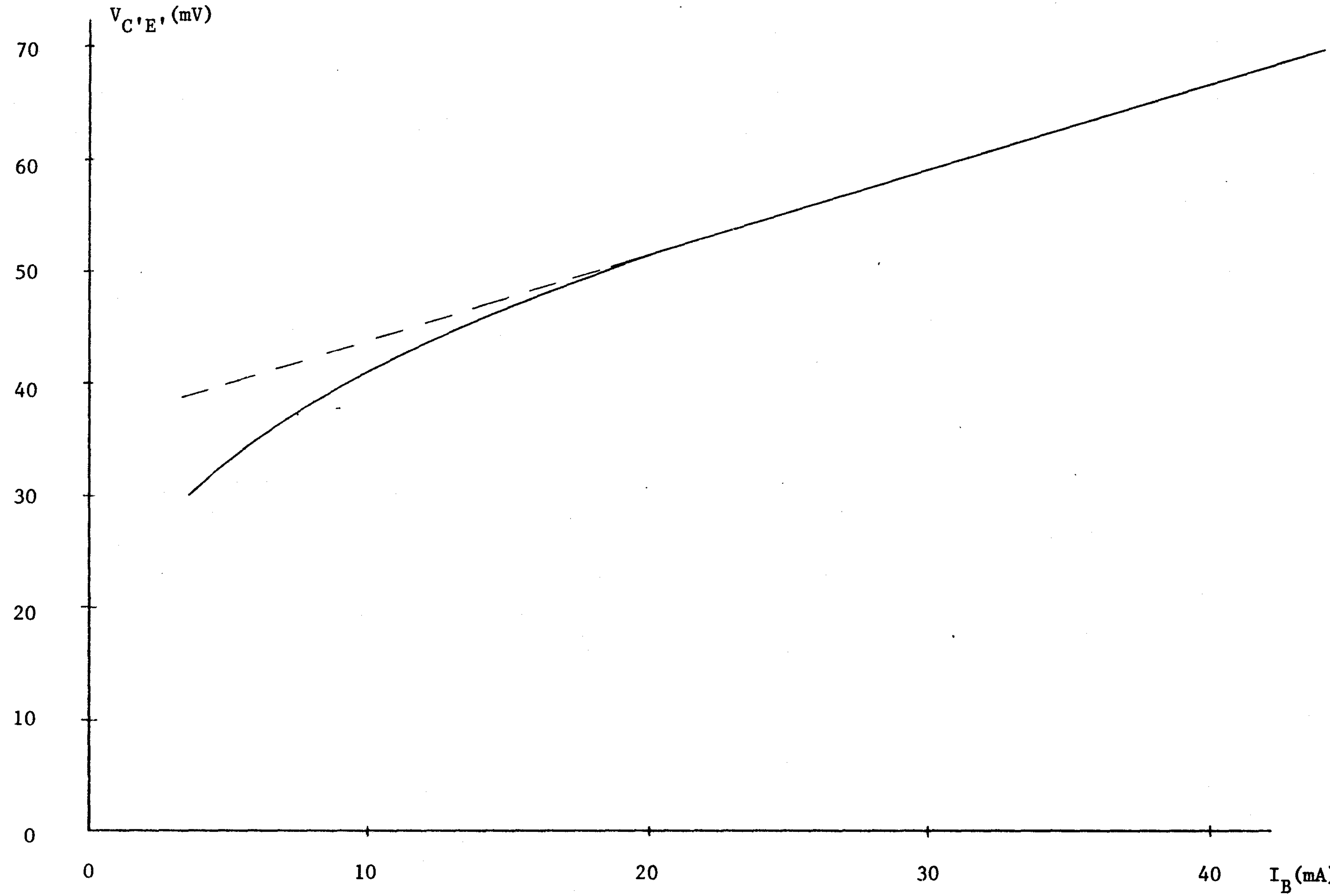

Figure 3.9 I_B versus $V_{C'E'}$ for $I_C = 0$

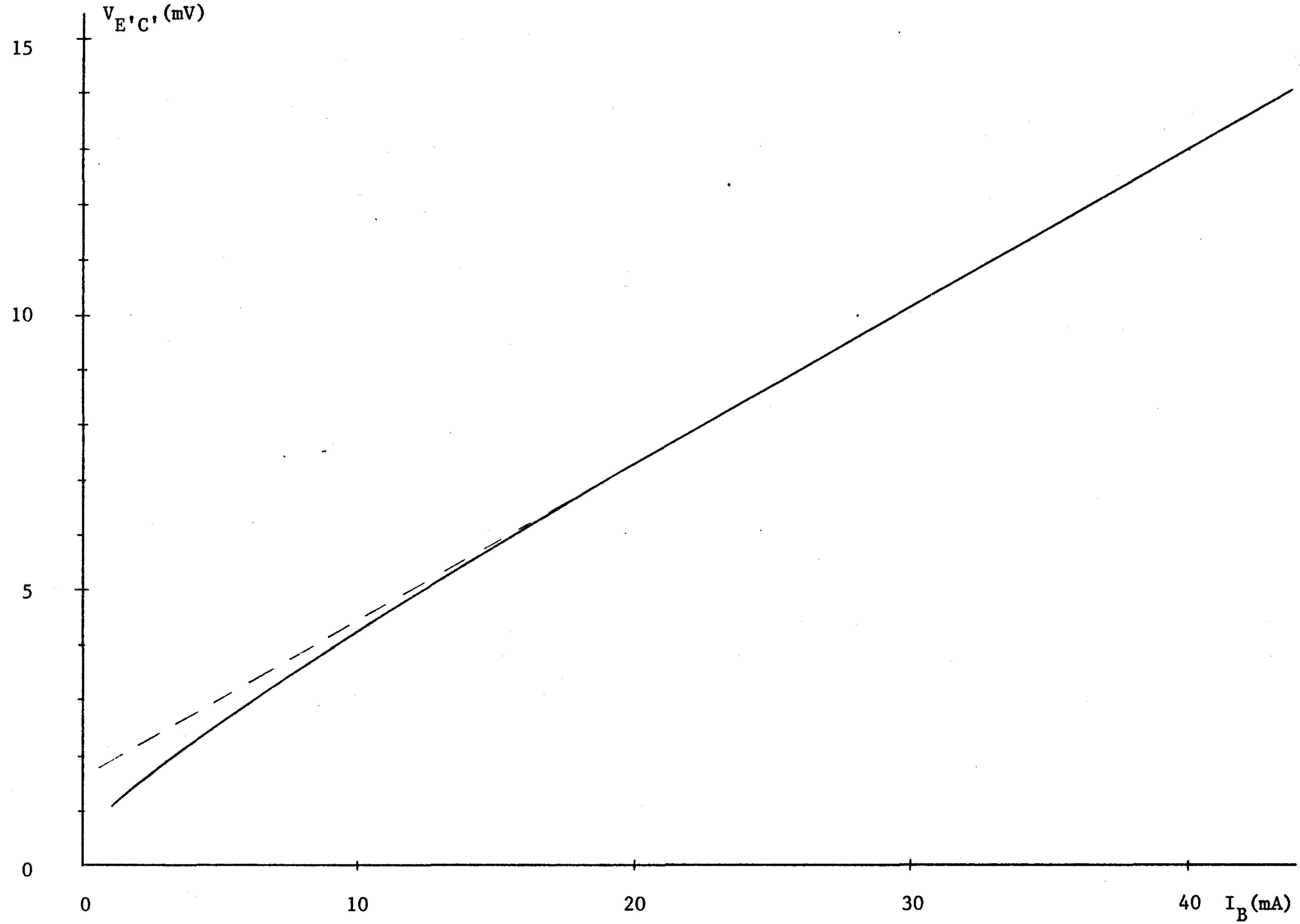

Figure 3.10 I_B versus $V_{E'C'}$ for $I_E = 0$

The value of R_C is given by the slope of the linear portion of the $V_{E'C'}$ versus I_B plot in Figure 3.10.

The measured data are shown in Tables 3-6 and 3-7 respectively. The estimated value of R_E and R_C are equal to 0.0724 ohm and 0.291 ohm respectively.

(b) The Series Resistance of the Base Region, R_B

Based on the assumption that R_E is small enough to be negligible (actually, R_E = 0.0724 ohm is sufficiently small compared with R_B), R_B can be determined from the V_{BE} versus $\log I_E$ plot in Figure 3.2. At high emitter current levels, this curve deviates from the straight line portion of the curve valid at lower current levels. The deviation at high current levels can be ascribed to the effect of R_B. Hence, R_B can be calculated from,

$$R_B = \frac{\Delta V}{I_B} \tag{3.8}$$

where ΔV is the difference between the measured emitter-base drop and the value extrapolated from the straight line portion of the plot at low current levels.

The calculation of R_B based on the data obtained from Figure 3.2 and Table 3-1, is as follows:

At I_B = 2.05 mA, while I_E = 100 mA

ΔV = 0.788 - 0.746 = 0.042 volt

Hence, R_B = 20.49 ohms

I_B(mA)	$V_{C'E'}$(mV)
3.5	30.0
4.0	31.2
4.5	32.2
5.0	33.2
6.0	35.0
7.0	36.8
8.0	38.6
9.0	39.8
10.0	41.2
12.0	43.6
14.0	46.0
16.0	48.1
18.0	50.0
20.0	51.6
25.0	55.8
30.0	59.5
35.0	63.3
38.0	65.2
40.0	66.6

Table 3-6 Measured Data for Determination of R_E

I_B(mA)	$V_{E'C'}$(mV)
1.0	1.1
2.0	1.5
3.0	1.9
4.0	2.2
5.0	2.6
6.0	2.9
7.0	3.3
8.0	3.6
9.0	3.9
10.0	4.2
12.0	4.9
14.0	5.5
16.0	6.1
18.0	6.7
20.0	7.3
25.0	8.7
30.0	10.1
35.0	11.6
40.0	13.0

Table 3-7 Measured Data for Determination of R_C

3.2 THE PARAMETERS OF THE ABBREVIATED GUMMEL-POON MODEL

There is a total of thirteen intrinsic model parameters. In this section, the intrinsic model parameters will be determined by two methods, that is: (I) Conventional (Experimental) method, (II) Method of automated model parameter determination. The latter method is used since the experimental method involves some uncertainties such as the exact nature of the impurity doping profiles in the transistor regions, the minority-carrier diffusion constant (actually it is not a constant but depends to some extent on the impurity concentration of the semiconductor), the variation of charge-control parameters with the operating conditions and so forth. Method II is, therefore, employed to obtain more precise values of the parameters in order to get the best possible fit to the static characteristics of the transistor.

The extrinsic model parameters, R_E, R_C and R_B described in Section 3.1.2 are used to account for the finite resistivities of the semiconductor materials of the emitter, collector and base regions respectively, therefore they can be applied equally well to the abbreviated Gummel-Poon model without any necessary modifications. In addition, R_B of the modified Ebers-Moll models is identical to R_{BI} of the abbreviated Gummel-Poon model but they are different only in notation. By taking the experimental results directly from Section 3.1.2, the values of R_E, R_C and R_{BI} are 0.0724 ohm, 0.291 ohm and 20.49 ohms respectively.

3.2.1 <u>Conventional Method</u> (Method I)

(a) <u>The Intercept Current</u>, I_S

By viewing equation (2.87), the following approximations and condition are assumed so as to determine I_S.

(i) Short-circuit base-collector terminals.

(ii) Measure I_C-V_{BE} characteristics of transistor under low-bias condition.

(iii) Approximate the ratio of Q_{BO}/Q_B to unity. Subject to condition (ii), this approximation is reasonable.

Based on the above, equation (2.87) reduces to,

$$I_C = I_S(e^{qV_{BE}/KT} - 1) \qquad (3.9)$$

From equation (3.9), a measurement of I_C versus V_{BE} would be sufficient to determine I_S. The schematic diagram of Curve Tracer for this measurement is shown in Figure 3.11. The measured data are shown in Table 3-8.

A semi-log plot of I_C versus V_{BE} shown in Figure 3.12 results in a straight line whose intercept on the I_C-ordinate gives the value of I_S. Analytical manipulation for determining I_S is given as follows:

Verify the slope of the plot, first, by choosing two points within the microampere region from Table 3-8.

$$I_{C2} = 1 \text{ mA} \qquad V_{BE2} = 0.6189 \text{ V.}$$

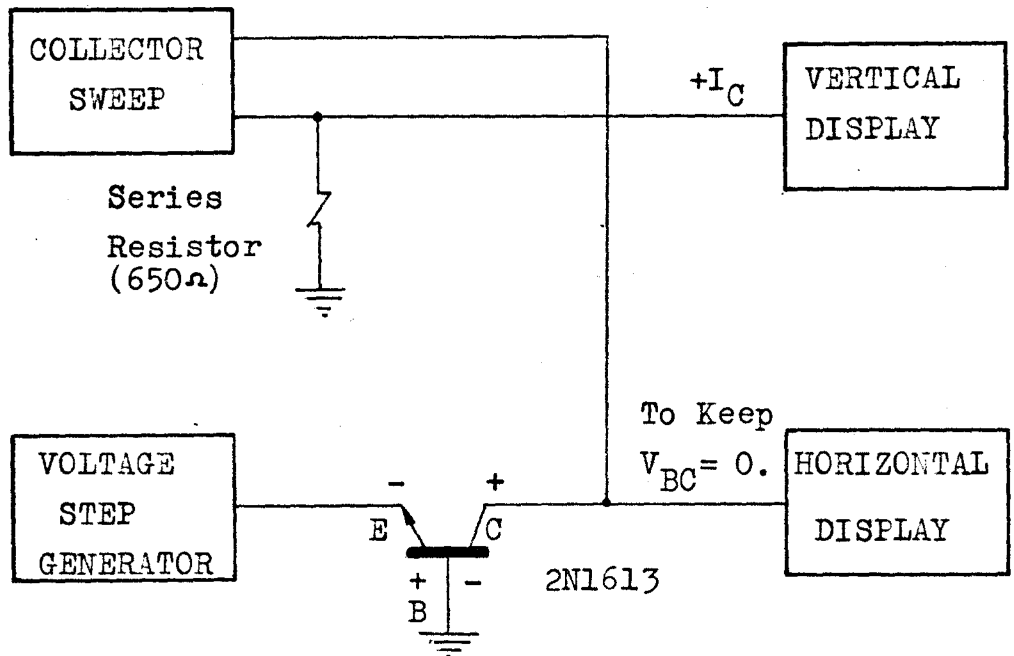

Figure 3-11 Curve Tracer (Tektronix 576) Schematic Diagram for Measurement of I_C versus V_{BE} for V_{BC} = 0. (Using Common-Base Configuration on Curve Tracer)

I_C(A)	V_{BE}(V)
1.0×10^{-6}	0.4360
2.0×10^{-6}	0.4529
5.0×10^{-6}	0.4759
8.0×10^{-6}	0.4877
1.0×10^{-5}	0.4933
2.0×10^{-5}	0.5112
5.0×10^{-5}	0.5348
8.0×10^{-5}	0.5468
1.0×10^{-4}	0.5525
2.0×10^{-4}	0.5706
5.0×10^{-4}	0.5942
8.0×10^{-4}	0.6068
1.0×10^{-3}	0.6189
2.0×10^{-3}	0.6376
5.0×10^{-3}	0.6651
8.0×10^{-3}	0.6795

Table 3-8 I_C versus V_{BE} for V_{BC} = 0 volt

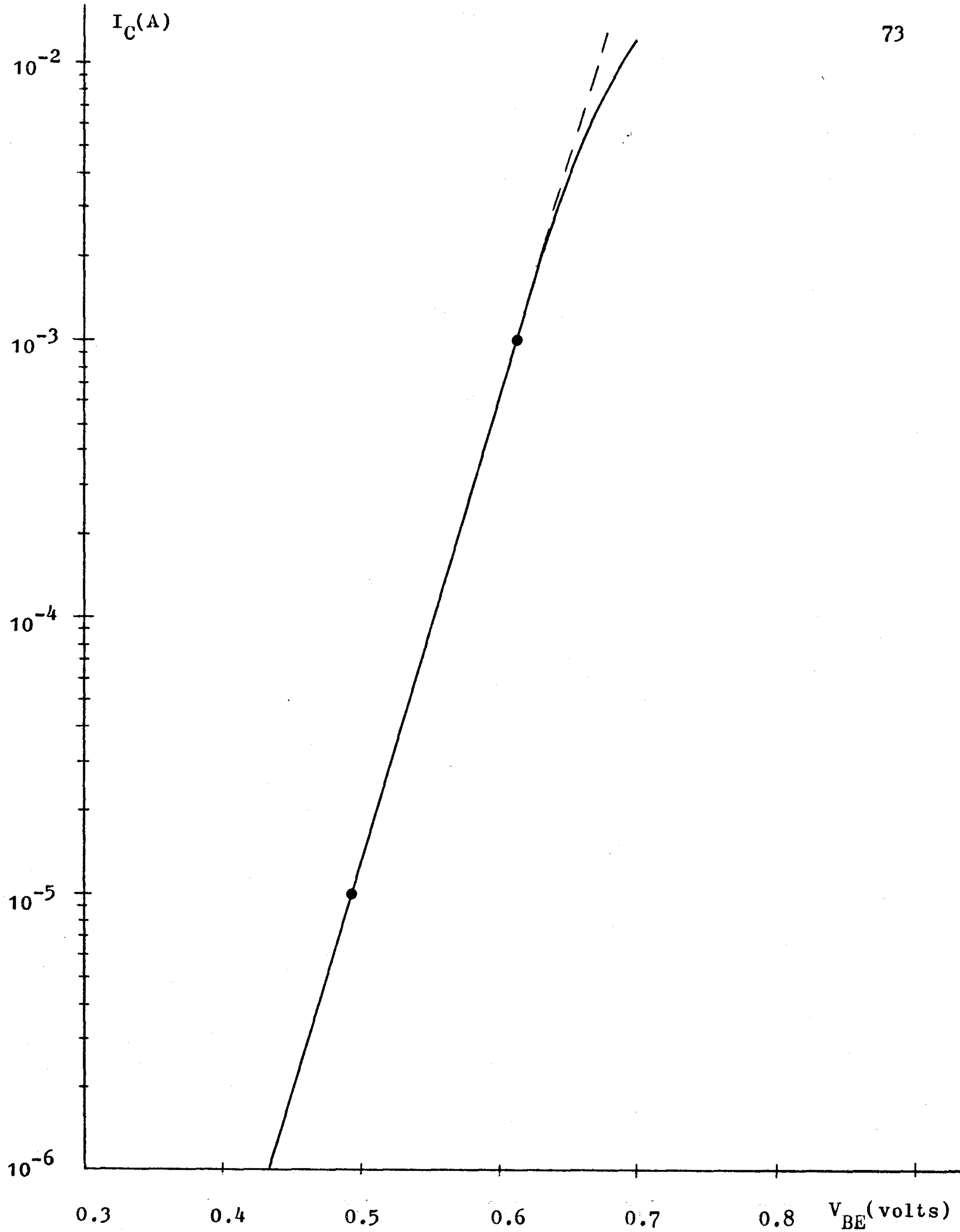

Figure 3.12 Semilog Plot of I_C versus V_{BE} for $V_{BC} = 0$

$$I_{C1} = 10\ \mu A \qquad\qquad V_{BE1} = 0.4933\ V.$$

then using equation (3.9),

$$(q/KT)_{exp.} = \frac{\ln(I_{C2}/I_{C1})}{V_{BE2} - V_{BE1}} = \underline{36.67}\ \text{volt}^{-1}\ \text{vs.}\ (q/KT) = 38.9\ \text{volt}^{-1}$$

Calculate I_S by means of equation (3.9),

$$I_S = \frac{I_{C2}}{e^{(q/KT)_{exp.}V_{BE2}} - 1} = \underline{1.396\text{x}10^{-13}}\ \text{A}.$$

(b) <u>The Intercept Currents</u>, I_1 <u>and</u> I_2 <u>and the Emitter Emission Coefficients</u>, N_{E1} <u>and</u> N_{E2}

In view of equation (2.48), by short-circuiting the collector-base terminals, the equation reduces to the form of,

$$I_B = I_1(e^{qV_{BE}/KTN_{E1}} - 1) + I_2(e^{qV_{BE}/KTN_{E2}} - 1) \qquad (3.10)$$

Hence, a measurement of I_B as a function of V_{BE} is required. The schematic diagram for this measurement is shown in Figure 3.13. The measured data are tabulated in Table 3-9.

A semi-log plot of I_B versus V_{BE} is shown in Figure 3.14 from which two straight line sections marked 1 and 2 respectively can be observed. The intercept current, I_1 can be obtained by

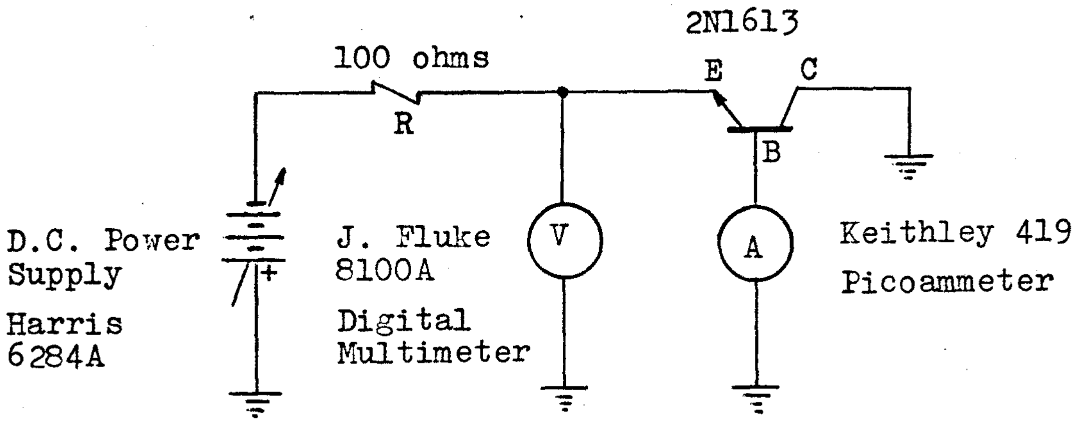

(a) Test Configuration for low base current levels (below 1 μA)

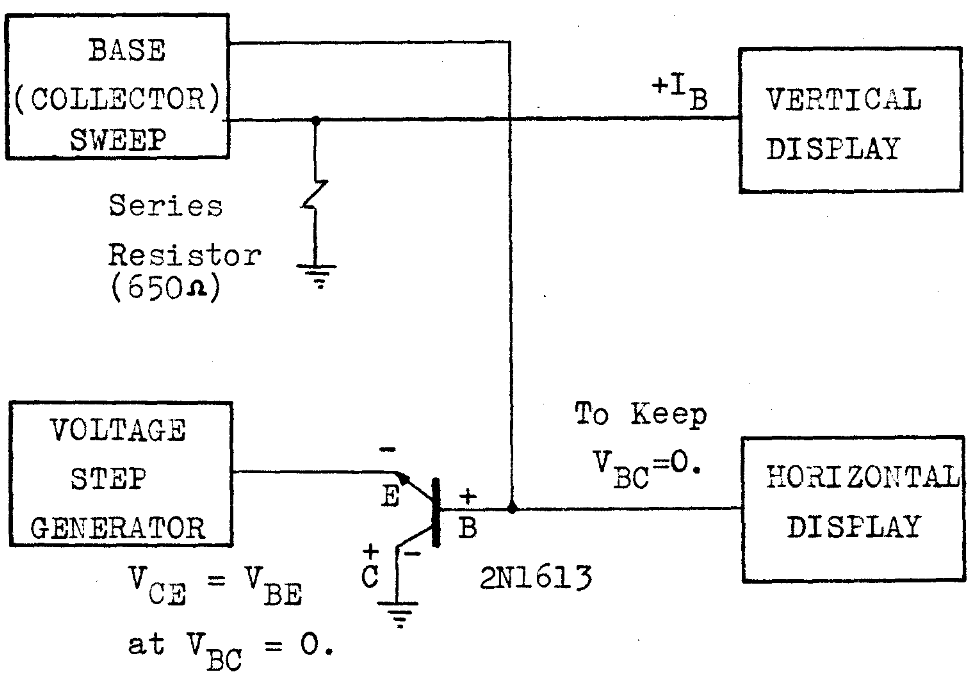

(b) Test Configuration* for high base current levels (above 1 μA), using Curve Tracer, Tektronix type 576

* - (1) Use Common-Base Configuration on Curve Tracer.
(2) Interchange 'B' and 'C' leads of the tested transistor.

Figure 3.13 Test Configuration for determination of I_1, N_{E1}, I_2 and N_{E2}

I_B(A)	V_{BE}(V)
6.000×10^{-13}	0.0100
7.500×10^{-13}	0.0179
1.300×10^{-12}	0.0200
2.300×10^{-12}	0.0300
5.200×10^{-12}	0.0500
8.950×10^{-12}	0.0700
2.140×10^{-11}	0.1000
7.640×10^{-11}	0.1500
2.674×10^{-10}	0.2000
8.724×10^{-10}	0.2500
2.857×10^{-9}	0.3000
9.510×10^{-9}	0.3500
3.100×10^{-8}	0.4000
1.150×10^{-7}	0.4500
4.400×10^{-7}	0.5000
2.050×10^{-6}	0.5500
1.010×10^{-6}	0.5250
1.000×10^{-6}	0.5240
1.500×10^{-6}	0.5380
2.000×10^{-6}	0.5470
3.000×10^{-6}	0.5595
4.000×10^{-6}	0.5685
6.000×10^{-6}	0.5815

I_B(A)	V_{BE}(V)
8.0×10^{-6}	0.5915
1.0×10^{-5}	0.5970
1.5×10^{-5}	0.6100
2.0×10^{-5}	0.6180
2.5×10^{-5}	0.6240
3.0×10^{-5}	0.6300
3.5×10^{-5}	0.6340
4.0×10^{-5}	0.6393
4.5×10^{-5}	0.6425
5.0×10^{-5}	0.6458
5.5×10^{-5}	0.6475
6.0×10^{-5}	0.6505
6.5×10^{-5}	0.6545
7.0×10^{-5}	0.6555
8.0×10^{-5}	0.6595
9.0×10^{-5}	0.6630
1.0×10^{-4}	0.6665
1.5×10^{-4}	0.6810
2.0×10^{-4}	0.6900
2.5×10^{-4}	0.6980
3.0×10^{-4}	0.7050
3.5×10^{-4}	0.7140
4.0×10^{-4}	0.7200

Table 3-9 I_B versus V_{BE} for V_{BC} = 0 volt

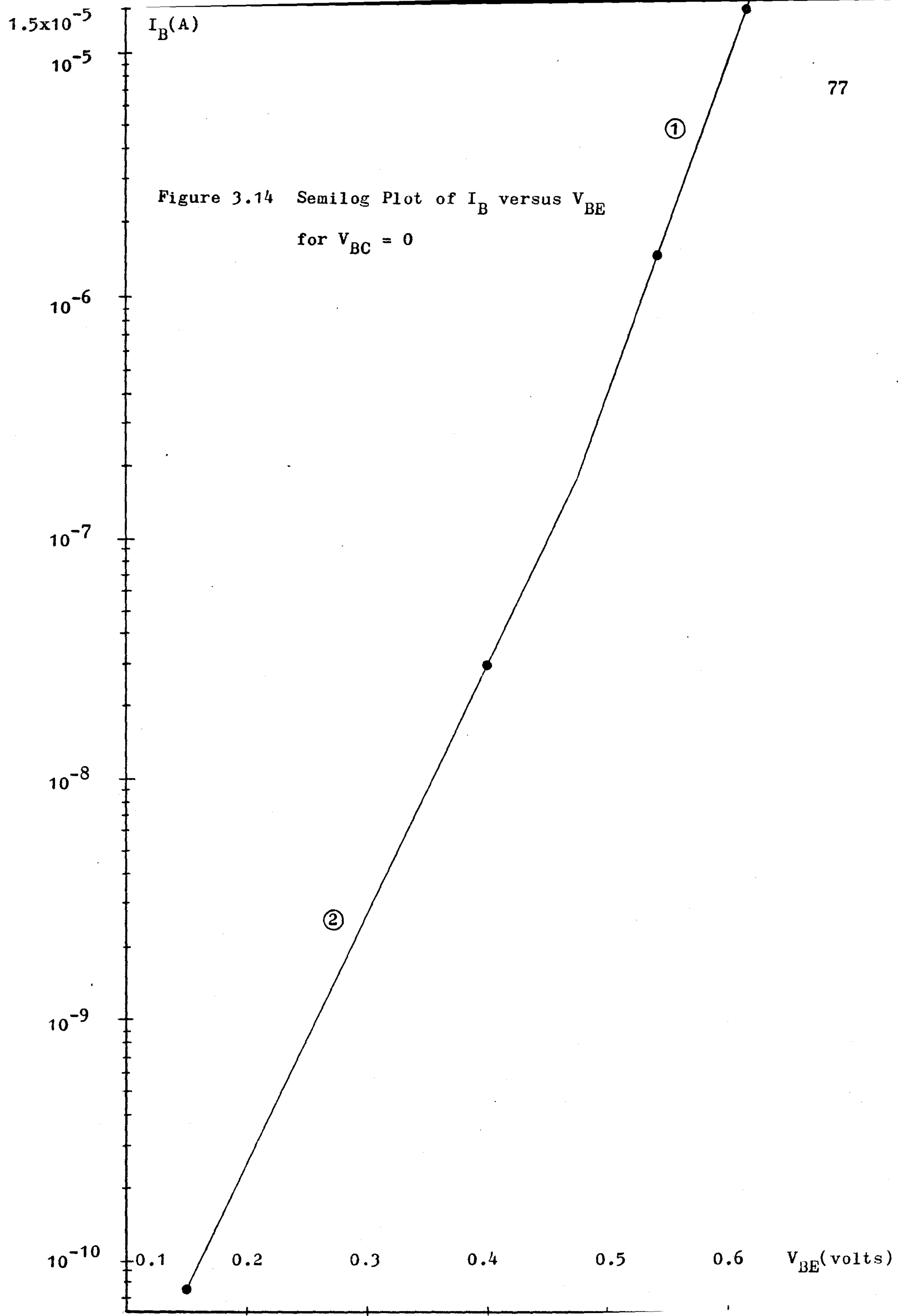

Figure 3.14 Semilog Plot of I_B versus V_{BE} for $V_{BC} = 0$

extrapolation of straight line section ① back to $V_{BE} = 0$ and the slope of this straight line section yields the value of (q/KTN_{E1}) from which the value of N_{E1} can be computed. The intercept current, I_2 can be determined by extrapolation of straight line section ② back to $V_{BE} = 0$ and the slope of this straight line section gives the value of (q/KTN_{E2}) from which the second emitter emission coefficient, N_{E2} can be calculated.

Calculation of I_1, N_{E1}, I_2 and N_{E2} is shown below:

(i) To find I_1 and N_{E1}

Pick two points from the straight line section ① in Figure 3.8.

$$I_{B①2} = 1.5\text{x}10^{-5} \text{ A.} \qquad V_{BE①2} = 0.610 \text{ volt}$$

$$I_{B①1} = 1.5\text{x}10^{-6} \text{ A.} \qquad V_{BE①1} = 0.538 \text{ volt}$$

Use equation (3.10) with second term dropped out,

$$(q/KTN_{E1}) = \frac{\ln(I_{B①2}/I_{B①1})}{V_{BE①2} - V_{BE①1}} = \underline{31.98} \text{ volt}^{-1}$$

$$I_1 = \frac{I_{B①2}}{e^{V_{BE①2}(q/KTN_{E1})} - 1} = \underline{5.0567\text{x}10^{-14}} \text{ A.}$$

$$N_{E1} = \frac{\lambda}{q/KTN_{E1}} = \underline{1.217} \qquad \text{for } \lambda = \underline{38.9} \text{ volt}^{-1}$$

(ii) To find I_2 and N_{E2}

Pick two points from the straight line section ② in Figure 3.8.

$$I_{B②2} = 3.10\times10^{-8} \text{ A.} \qquad V_{BE②2} = 0.4 \text{ volt}$$

$$I_{B②1} = 7.64\times10^{-11} \text{ A.} \qquad V_{BE②1} = 0.15 \text{ volt}$$

Use equation (3.10) with the first term dropped out and compute I_2 and N_{E2} in the way shown in part (i), thence

$$I_2 = \underline{2.065\times10}^{-12} \text{ A.}$$

$$N_{E2} = \underline{1.618}$$

(c) <u>Intercept Current</u>, I_3 <u>and Collector Emission Coefficient</u>, N_C

By specifying the condition that the base-emitter terminals are short-circuited, equation (2.48) reduces to,

$$I_B = I_3(e^{qV_{BC}/KTN_C} - 1) \qquad (3.11)$$

To obtain I_3, a measurement of I_B versus V_{BC} is required. The schematic diagram for this measurement is shown in Figure 3.15. The measured data are tabulated in Table 3-10.

A semi-log plot of I_B versus V_{BC} is shown in Figure 3.16

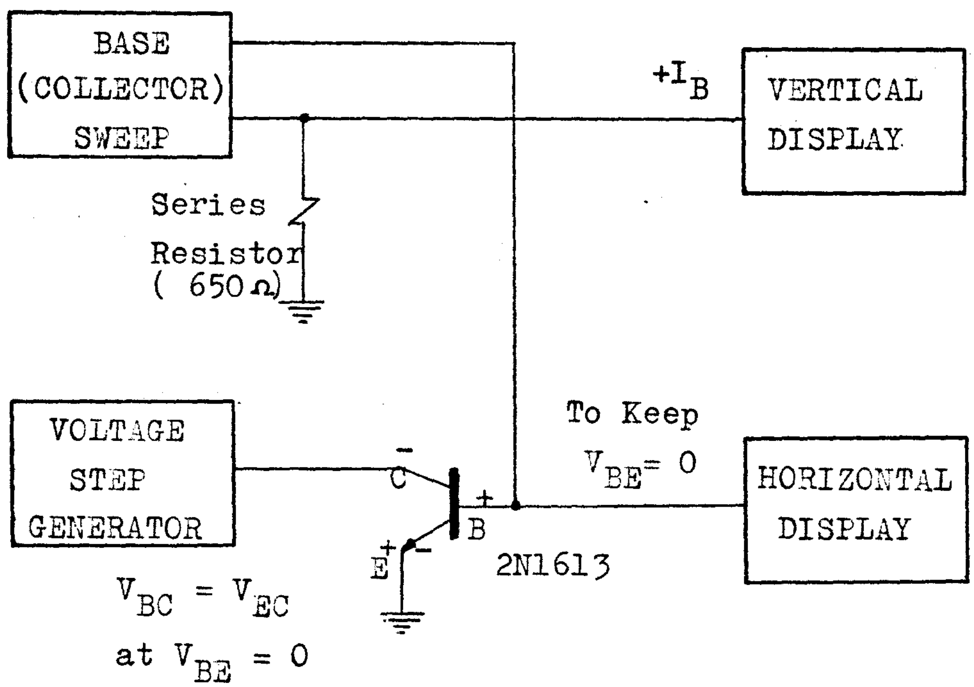

Figure 3.15 Curve Tracer (Tektronix type 576) Schematic Diagram for Measurements* of I_B versus V_{BC} for $V_{BE} = 0$.

* - (1) Use Common-Base Configuration on Curve Tracer.

(2) Modify the normal terminal-connections of the transistor to the socket of the Curve Tracer, by connecting 'E' of the socket to 'C'-lead of the transistor; 'B' to 'E' and 'C' to 'B'.

I_B(A)	V_{BC}(V)
$1.0x10^{-6}$	0.4210
$2.0x10^{-6}$	0.4425
$4.0x10^{-6}$	0.4630
$6.0x10^{-6}$	0.4755
$1.0x10^{-5}$	0.4920
$2.0x10^{-5}$	0.5120
$4.0x10^{-5}$	0.5320
$6.0x10^{-5}$	0.5425
$1.0x10^{-4}$	0.5590
$2.0x10^{4}$	0.5790
$4.0x10^{-4}$	0.5990
$6.0x10^{-4}$	0.6105
$1.0x10^{-3}$	0.6290
$2.0x10^{-3}$	0.6540
$4.0x10^{-3}$	0.6810
$6.0x10^{-3}$	0.6980
$1.0x10^{-2}$	0.7250

Table 3-10 I_B versus V_{BC} for V_{BE} = 0 volt

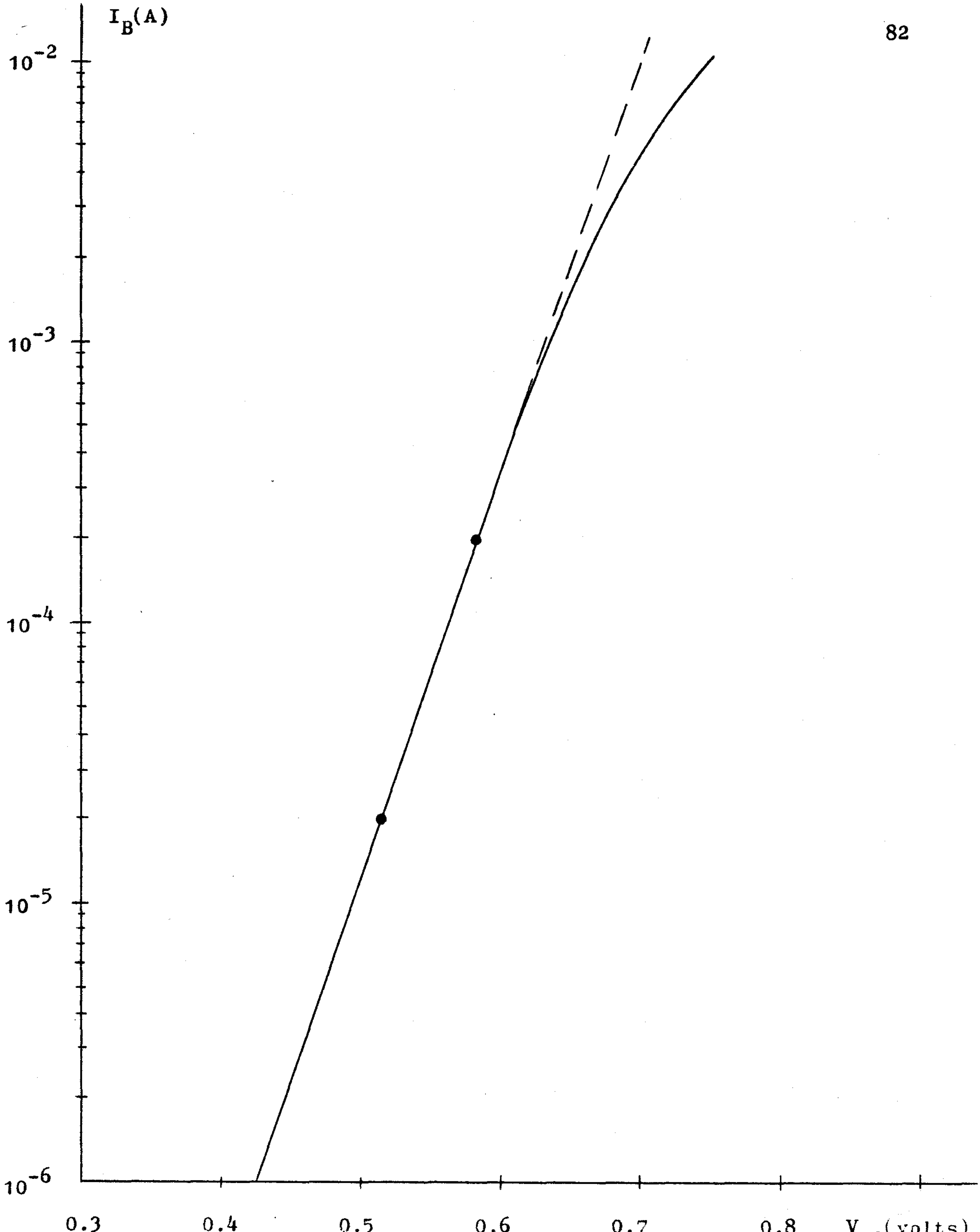

Figure 3.16 Semilog Plot of I_B versus V_{BC} for $V_{BE} = 0$

in which the intercept on I_B-axis extrapolated from the straight line portion of the plot gives the value of I_3. The slope of this straight line gives the value of (q/KTN_C) from which the collector emission coefficient, N_C can be evaluated.

A similar analytical manipulation to that shown in Section 3.1.1(a) is used to calculate I_3 and N_C.

Two data points chosen for calculation are:

$I_{B2} = 200\ \mu A$ $\qquad V_{BC2} = 0.579$ volt

$I_{B1} = 20\ \mu A$ $\qquad V_{BC1} = 0.512$ volt

The calculated results are:

$I_3 = \underline{4.563 \times 10^{-13}}$ A.

$N_C = \underline{1.133}$

(d) The Forward and Reverse Transit Times, τ_F and τ_R

The basic measurement technique for τ_F and τ_R is indicated in Figure 3.17(a). The schematic diagram shown is principally for the measurement of forward transit time when switching the base current through a step change Δi_B. The magnitude of the input voltage step is made much larger than the change in v_{BE} so that the step change in base current is given by,

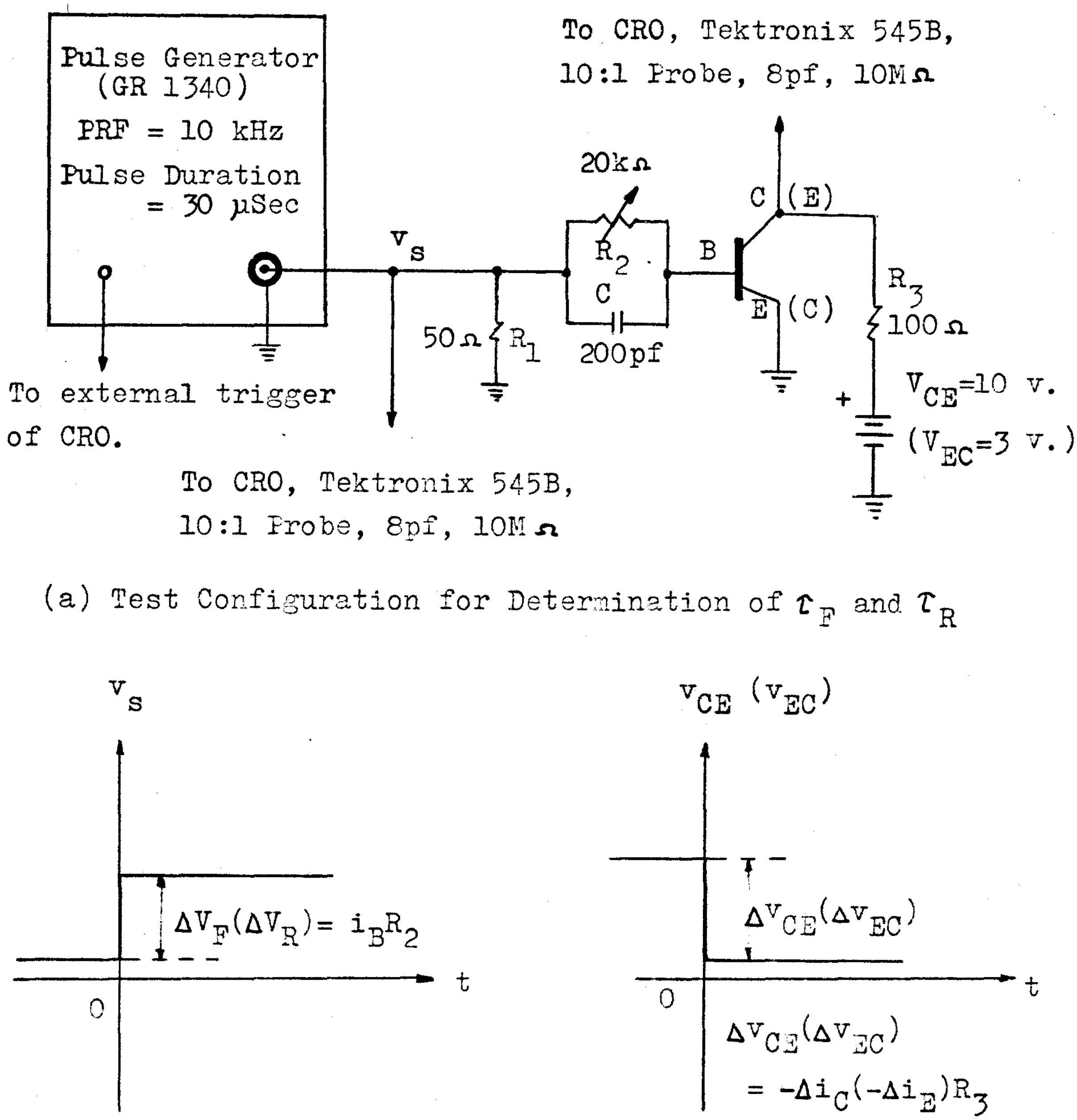

(a) Test Configuration for Determination of τ_F and τ_R

(b) Waveform of v_s as a function of time

(c) Waveform of $V_{CE}(V_{EC})$ as a function of time

Figure 3-17 Measurements of τ_F and τ_R (Symbols and quantities inside the brackets are for τ_R)

$$\Delta i_B = \frac{\Delta V_F}{R_2} \tag{3.12}$$

During measurement, R_2 and C should be appropriately adjusted such that v_{CE} and i_C undergo step changes. Figure 3.17(c) shows the step v_{CE} response at the condition that R_2 and C are appropriately adjusted.

The transit time is approximately given(30) by,

$$\tau_F = R_3 C \left| \frac{\Delta V_F}{\Delta v_{CE}} \right| \tag{3.13}$$

In order to insure the best possible accuracy, the transistor should operate in the forward active mode since τ_F is associated with the forward injection of the charges across the emitter-base junction.

The reverse transit time, τ_R can be measured by using the same technique described. Minor changes in the schematic diagram shown in Figure 3.17(a) are: (i) Interchange the collector and emitter leads of the transistor; (ii) Reducing the magnitude of the collector-emitter voltage $|V_{CE}|$ to 3 volts with the polarities remaining unchanged, to avoid base-emitter junction breakdown since the base-emitter junction, in this case, is reverse-biased.

The measured data and calculations of the forward and reverse transit times are as follows:

$R_3C = 2\text{x}10^{-8}$ ohm-farads

For forward transit time:

$$\Delta V_F = 0.60 \quad \text{volt}$$

$$\Delta v_{CE} = 4.53 \quad \text{volt}$$

Use of equation (3.13) gives,

$$\tau_F = \underline{2.65 \times 10^{-9}} \quad \text{sec.}$$

For reverse transit time:

$$\Delta V_R = 3.600 \quad \text{volt}$$

$$\Delta v_{EC} = 0.025 \quad \text{volt}$$

Use of equation (3.13) with modifications that subscript F is changed to R; and Δv_{CE} to Δv_{EC}, gives,

$$\tau_R = \underline{2.88 \times 10^{-6}} \quad \text{sec.}$$

(e) <u>The Emitter and Collector Capacitances</u>, C_E <u>and</u> C_C

According to equation (2.77), the charges Q_E and Q_C are the excess stored charges associated with the emitter-base and collector-base junction capacitances respectively. These are space-charge region capacitances as defined by Chawla and Gummel(31) and depend only on doping profile of the impurities and applied junction voltages and are independent of frequency.

The space-charge region capacitance measurements were done by means of a Boonton model 71A capacitance meter, at a reference frequency 1 MHz for different applied junction voltages. The measured emitter-base junction capacitance, C_{BE} is the emitter-base input capacitance with emitter-base junction forward-biased and the output open (i.e. $I_C = 0$). The measured collector-base capacitance, C_{CB} is the collector-base output capacitance with collector-base junction reverse-biased and the input open (i.e. $I_E = 0$). The measured data are shown in Tables 3-11 and 3-12 and Figures 3.18 and 3.19.

In the abbreviated Gummel-Poon model, the collector capacitance, C_C refers only to the capacitance between collector and the active base region under the emitter. The measured C_{CB} is larger by approximately the ratio of the base to the emitter area. The reduction of C_{CB} by the ratio of the base to the emitter area gives the measured collector capacitance, C_C shown in Figure 3.19 and Table 3-13. The emitter capacitance, C_E is approximately equal to C_{BE} without involving considerable error as one can realize from the device geometry of the planar-diffused transistor. For the geometry of the sample transistor, 2N1613, one can refer to Appendix A.

As mentioned previously, C_E and C_C are assumed to be constant. For a silicon transistor, conduction commences when V_{BE} reaches approximately 0.5 volt and reaches perhaps a peak of 0.7 volt during conduction. Hence, V_{BE} will average very closely to 0.6 volt.

Therefore, it will be assumed that the capacitance of emitter at V_{BE} = 0.6 volt is a reasonable approximation to use in the model. From Table 3-11, $C_E(\doteq C_{BE})$ is 387 pf at V_{BE} = 0.6 volt. The value of $C_C(= (A_{JE}/A_B)xC_{CB})$ equal to 3.67 pf at V_{CB} = 16.0 volts from Table 3-13 is chosen to approximate the overall average capacitance over the range of collector-base junction voltage from 0 volt to 30 volts.

V_{BE}(V)	0.00	0.10	0.20	0.30	0.40	0.50	0.55	0.58	0.60	0.65
C_{BE}(pf)	74.2	77.9	82.9	89.5	99.0	120.0	180.0	300.0	387.0	830.0

Table 3-11 Measured $C_{BE}(\doteq C_E)$ versus V_{BE} for I_C = 0.

V_{CB}(V)	0.00	0.50	1.00	2.00	4.00	6.00	8.00	10.0	12.0	14.0	16.0	18.0
C_{CB}(pf)	35.0	27.7	24.4	20.6	17.0	15.0	13.7	12.7	12.0	11.4	10.9	10.5

Table 3-12 Measured C_{CB} versus V_{CB} for I_E = 0.

V_{CB}(V)	0.00	0.50	1.00	2.00	4.00	6.00	8.00	10.0	12.0	14.0	16.0	18.0
C_C (pf)	11.8	9.34	8.23	6.95	5.73	5.06	4.62	4.28	4.05	3.84	3.67	3.54

Table 3-13 Reduced $C_{CB}(=C_C)$ versus V_{CB} for I_E = 0.

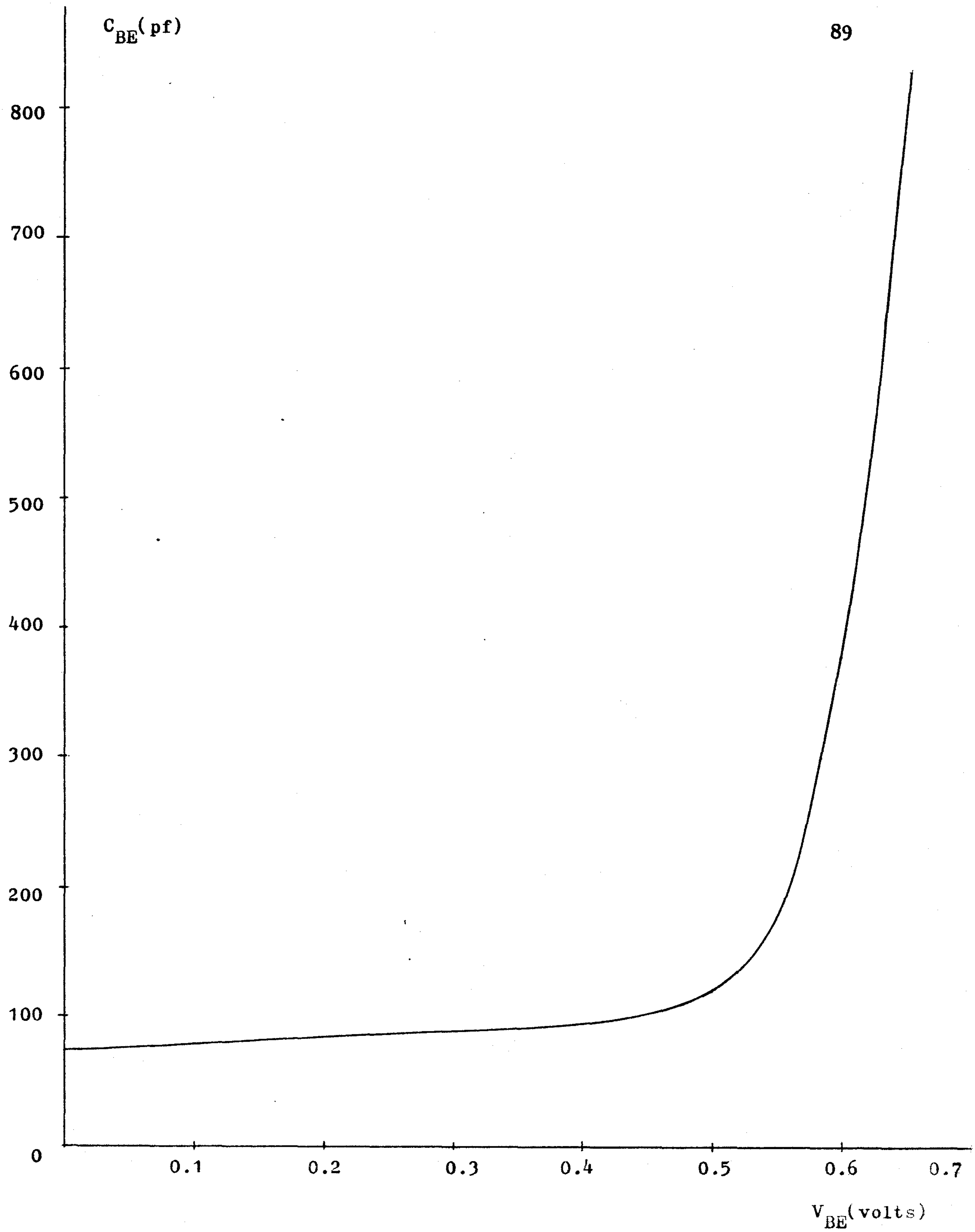

Figure 3.18 $C_{BE}(\doteq C_E)$ versus V_{BE} for $I_C = 0$

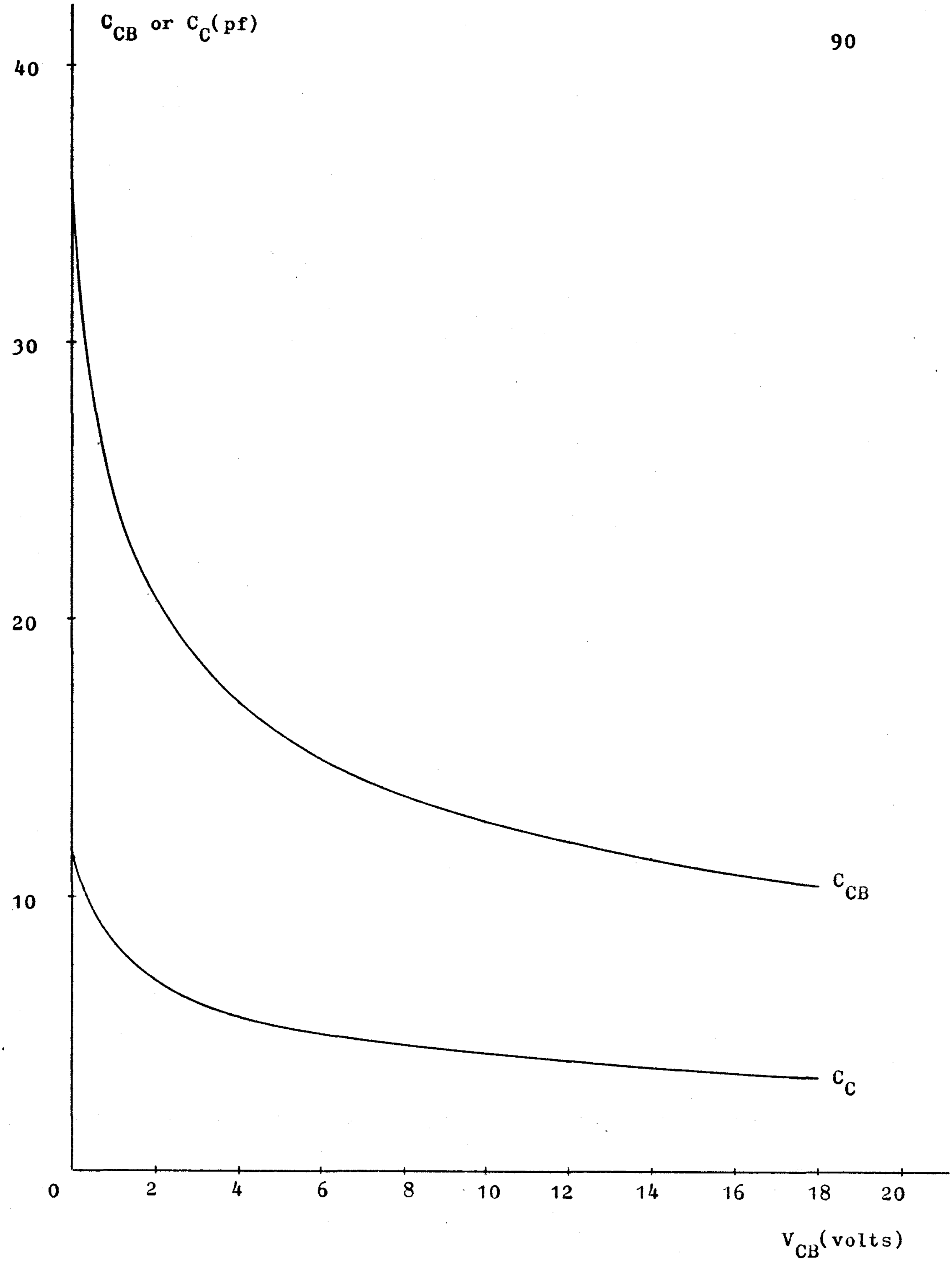

Figure 3.19 C_{CB} and C_C versus V_{CB} for $I_E = 0$

(f) The Zero-Bias Base Charge, Q_{BO}

This parameter is to be determined theoretically in an approximate way since an available experimental method does not exist so far. The detailed calculations are carried out as follows:

From Appendix A,

$$A_J = A_{JE} = \frac{\pi}{4} (d_{JE})^2 = 1.0179\text{x}10^{-3} \text{ cm}^2$$

By comparison of equation (2.74) with equation (2.75), the number of impurities per unit area in the base is,

$$N_B = \frac{qA_J D_{eo} n_i^2}{I_S} \tag{3.14}$$

Use of Einstein relation in conjunction with equations (2.73) and (3.14) gives,

$$Q_{BO} = \frac{A_J^2 qKT\mu_{eo} n_i^2}{I_S} \tag{3.15}$$

For C_{BE} = 74.2 pf (from Table 3-11) at zero-bias condition and $A_J = 1.0179\text{x}10^{-3}$ cm^2, reference (32) gives

$$\mu_{eo} = 800 \text{ cm}^2/\text{v-sec.} \qquad \text{and} \qquad \mu_h = 390 \text{ cm}^2/\text{v-sec.}$$

From reference (33), $\quad n_i = 1.3321\text{x}10^{10}$ cm^{-3}

From Section 3.2.1(a), $\quad I_S = 1.396\text{x}10^{-13}$ A.

Hence, $Q_{BO} = \underline{6.690\text{x}10^{-10}}$ Coulombs

(g) The Zero-Bias Active Base Resistance, R_{BAO}

The value of R_{BAO} is to be determined theoretically for the same reasons as stated in (f).

Repetition of equation (2.92) yields,

$$R_{BAO} = \frac{A_J}{8\pi\mu_h Q_{BO}} \tag{3.16}$$

Substitution of the values of Q_{BO}, A_J and μ_h from Section 3.2.1(f) in equation (3.16) yields

$R_{BAO} = \underline{153}$ Ohms

3.2.2 Method of Automated Model Parameter Determination (Method II)

This method can be regarded as a process of finding model parameter values which best simulate the terminal measurements made on the transistor being modelled. It is principally based on optimization theory(34) and is carried out with the aid of a digital computer. The flow chart of the procedure is illustrated in Figure 3.20 in which the specifications consist of the following.

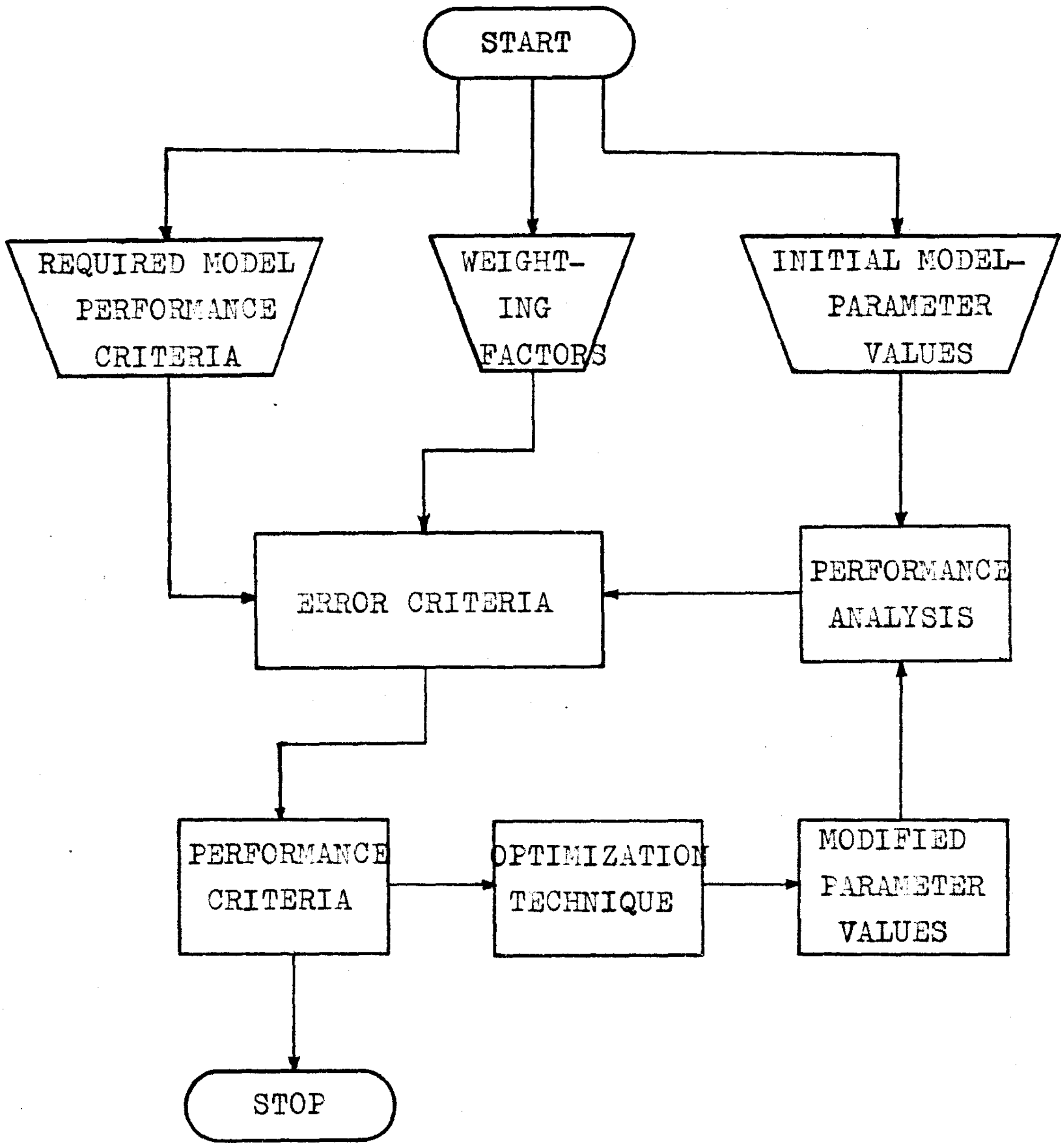

Figure 3-20 Flow Chart for Automated Model Parameters Determination

(a) <u>The Required Model Performance Criteria</u>

The transistor is considered to be in the common-emitter configuration. Moreover, it is a three-terminal device and for the static case is described by four terminal variables (i.e. V_{BE}, I_B, V_{CE} and I_C). Two criteria are therefore required to describe the device performance. By choosing I_B and V_{CE} as independent variables and regarding V_{BE} and I_C as dependent variables, two criteria, i.e. V_{BE} and $h_{FE}(=I_C/I_B)$ can be established. A set of points defining the shapes of V_{BE} and h_{FE} as functions of I_B and V_{CE} are required and shown in Table 3-14. Those points can be obtained by performing terminal measurements made on the transistor by means of a curve tracer. A suitable choice of the number of measuring points can save computer time. In this case, 128 points are measured over the active, saturation and cutoff regions of transistor operation.

(b) <u>The Initial Parameter Values</u>

Table 3-15 shows the best initial parameter values which are obtained by the experimental method (Method I). Those parameter

I_1 (A)	5.057×10^{-14}	τ_F (S)	2.650×10^{-9}
I_2 (A)	2.065×10^{-12}	τ_R (S)	2.880×10^{-6}
I_3 (A)	4.563×10^{-13}	C_C (F)	3.670×10^{-12}
I_S (A)	1.396×10^{-13}	C_E (F)	3.870×10^{-10}
N_C	1.133	Q_{BO} (C)	6.690×10^{-10}
N_{E1}	1.217	R_{BAO} (Ω)	153.0
N_{E2}	1.618		

Table 3-15 The Initial Parameter Values obtained by Method I

TABLE 3-14 MEASURED DATA FOR AUTOMATED PARAMETER DETERMINATION

VCEM(V)	IBM(A)	ICM(A)	HFEM	VBEM(V)
0.	5.0000E-08	-4.8000E-08	-9.6000E-01	3.1000E-01
0.	1.0000E-05	-9.2000E-06	-9.2000E-01	4.8600E-01
0.	4.0000E-05	-3.8300E-05	-9.5750E-01	5.3000E-01
0.	1.2000E-04	-1.0800E-04	-9.0000E-01	5.6000E-01
0.	5.0000E-04	-4.5500E-04	-9.1000E-01	6.1200E-01
3.0000E-02	5.0000E-08	-3.0000E-08	-6.0000E-01	3.3300E-01
3.0000E-02	1.0000E-05	7.8000E-06	7.8000E-01	5.1300E-01
3.0000E-02	4.0000E-05	3.5500E-05	8.8750E-01	5.5300E-01
3.0000E-02	1.2000E-04	1.2800E-04	1.0667E+00	5.8500E-01
3.0000E-02	5.0000E-04	3.6800E-04	7.3600E-01	6.4000E-01
6.0000E-02	5.0000E-08	1.0000E-08	2.0000E-01	3.6000E-01
6.0000E-02	1.0000E-05	5.5000E-05	5.5000E+00	5.4300E-01
6.0000E-02	4.0000E-05	2.7000E-04	6.7500E+00	5.8300E-01
6.0000E-02	1.2000E-04	8.0000E-04	6.6667E+00	6.1300E-01
6.0000E-02	5.0000E-04	2.3000E-03	4.6000E+00	6.6700E-01
8.0000E-02	5.0000E-08	5.8000E-08	1.1600E+00	3.7500E-01
8.0000E-02	1.0000E-05	1.1600E-04	1.1600E+01	5.5800E-01
8.0000E-02	4.0000E-05	5.5000E-04	1.3750E+01	5.9900E-01
8.0000E-02	1.2000E-04	1.5600E-03	1.3000E+01	6.2900E-01
8.0000E-02	5.0000E-04	4.4000E-03	8.8000E+00	6.7200E-01

TABLE 3-14 MEASURED DATA FOR AUTOMATED PARAMETER DETERMINATION (Cont.)

VCEM(V)	IBM(A)	ICM(A)	HFEM	VBEM(V)
1.0000E-01	5.0000E-08	1.1000E-07	2.2000E+00	3.8300E-01
1.0000E-01	1.0000E-05	2.0500E-04	2.0500E+01	5.7500E-01
1.0000E-01	4.0000E-05	9.5000E-04	2.3750E+01	6.1500E-01
1.0000E-01	1.2000E-04	2.8000E-03	2.3333E+01	6.4600E-01
1.0000E-01	5.0000E-04	7.1500E-03	1.4300E+01	6.9500E-01
3.0000E-01	5.0000E-08	4.8000E-07	9.6000E+00	4.1200E-01
3.0000E-01	1.0000E-05	5.6000E-04	5.6000E+01	6.0000E-01
3.0000E-01	4.0000E-05	2.6800E-03	6.7000E+01	6.4100E-01
3.0000E-01	1.2000E-04	8.5500E-03	7.1250E+01	6.7600E-01
3.0000E-01	5.0000E-04	3.0100E-02	6.0200E+01	7.3000E-01
5.0000E-01	5.0000E-08	4.9000E-07	9.8000E+00	4.1200E-01
5.0000E-01	1.0000E-05	5.7000E-04	5.7000E+01	6.0000E-01
5.0000E-01	4.0000E-05	2.6900E-03	6.7250E+01	6.4100E-01
5.0000E-01	1.2000E-04	8.5800E-03	7.1500E+01	6.7600E-01
5.0000E-01	5.0000E-04	3.5000E-02	7.0000E+01	7.3000E-01
1.0000E+00	5.0000E-08	4.9200E-07	9.8400E+00	4.1200E-01
1.0000E+00	1.0000E-05	5.7000E-04	5.7000E+01	6.0000E-01
1.0000E+00	4.0000E-05	2.6900E-03	6.7250E+01	6.4100E-01
1.0000E+00	1.2000E-04	8.6000E-03	7.1667E+01	6.7600E-01
1.0000E+00	5.0000E-04	3.5500E-02	7.1000E+01	7.3000E-01

TABLE 3-14 MEASURED DATA FOR AUTOMATED PARAMETER DETERMINATION (Cont.)

VCEM(V)	IBM(A)	ICM(A)	HFEM	VBEM(V)
4.0000E+00	5.0000E-08	5.0000E-07	1.0000E+01	4.1200E-01
4.0000E+00	1.0000E-05	5.7500E-04	5.7500E+01	6.0000E-01
4.0000E+00	4.0000E-05	2.7000E-03	6.7500E+01	6.4100E-01
4.0000E+00	1.2000E-04	8.7000E-03	7.2500E+01	6.7600E-01
8.0000E+00	5.0000E-08	5.0000E-07	1.0000E+01	4.1200E-01
8.0000E+00	1.0000E-05	5.8200E-04	5.8200E+01	6.0000E-01
8.0000E+00	4.0000E-05	2.7200E-03	6.8000E+01	6.4100E-01
1.0000E+01	5.0000E-08	5.0500E-07	1.0100E+01	4.1200E-01
1.0000E+01	1.0000E-05	6.0000E-04	6.0000E+01	6.0000E-01
1.0000E+01	4.0000E-05	2.8000E-03	7.0000E+01	6.4100E-01
1.5000E+01	5.0000E-08	5.1000E-07	1.0200E+01	4.1200E-01
1.5000E+01	1.0000E-05	6.2000E-04	6.2000E+01	6.0000E-01
1.5000E+01	4.0000E-05	2.8750E-03	7.1875E+01	6.4100E-01
2.0000E+01	5.0000E-08	5.2000E-07	1.0400E+01	4.1200E-01
2.0000E+01	1.0000E-05	6.2200E-04	6.2200E+01	6.0000E-01
2.5000E+01	5.0000E-08	5.2500E-07	1.0500E+01	4.1200E-01
2.5000E+01	1.0000E-05	6.4500E-04	6.4500E+01	6.0000E-01
3.0000E+01	5.0000E-08	5.3500E-07	1.0700E+01	4.1200E-01
3.0000E+01	1.0000E-05	7.0000E-04	7.0000E+01	6.0000E-01

values are not very precise since some device physics and structure are not known in detail while determining them. It is for this reason that this method is employed to re-evaluate those parameter values.

(c) Error Criteria

Based on the required model performance criteria described in part (a), two expressions for error function will be necessary. The error function that gives a measure of the deviation between the actual device performance and the simulated performance by the model can be formulated by the method of least pth approximation(35).

The least pth formulation allows two expressions for the error function as follows:

$$E_1 = \sum_{i=1}^{n} \sum_{j=1}^{m} (W_H(h_{FESij} - h_{FEMij}))^P \tag{3.17}$$

$$E_2 = \sum_{i=1}^{n} \sum_{j=1}^{m} (W_I(V_{BESij} - V_{BEMij}))^P \tag{3.18}$$

Where: W_H and W_I are weighting factors to be discussed in part (d).

h_{FEMij} is the measured d. c. common-emitter current gain at the ith data point for jth base current among a total of nxm.

V_{BEMij} is the measured base-emitter voltage at the ith data point for jth base current among a total of nxm.

h_{FESij} is the simulated d. c. common-emitter current gain corresponding to h_{FEMij}.

V_{BESij} is the simulated base-emitter voltage corresponding to V_{BEMij}.

P is a positive integer chosen to be 2 initially and 100 eventually.

The sum of E_1 and E_2 gives the error function to be considered. The final error function, termed the objective function U hereafter, is the pth root of the sum of E_1 and E_2, i.e. $U=(E_1+E_2)^{1/P}$ which will be minimized in a least pth sense during optimization process.

(d) Weighting Factors

Essentially, the task of weighting factors is to emphasize or de-emphasize the various parts of the simulated performance to suit the required model performance. The larger the weighting factor used, the more emphasis is put on that simulated performance. The weighting factors chosen for the present case are as follows:

Initially, $W_H = 1$ and $W_I = 1$

Finally, $W_H = 1$ and $W_I = 200$

(e) Performance Analysis

The model performance corresponding to a set of model parameter values is evaluated on the basis of model defining equations (2.48) and (2.87) from Chapter II, as well as the effect of extrinsic series resistances (i.e. R_E, R_C and R_{BI}). Those series resistances are kept fixed for the performance analysis and will not be modified optimally during optimization process. The computer program for the performance analysis is named SUBROUTINE OBJECT and is presented in Appendix B.

Performance analysis gives the simulated h_{FES} and V_{BES} which will be approximated to the measured h_{FEM} and V_{BEM}.

(f) Optimization Techniques

Since the bipolar junction transistor is a non-linear active device, evaluation of the partial derivatives of the objective function can not be obtained easily. Therefore the Direct Search method is appropriate. The Hooke and Jeeve's (36), (37), (38) Pattern Search is employed to minimize the objective function in a least pth sense because of its rapid convergence compared with the other multi-dimensional methods. The computer program for Pattern Search is presented in Appendix B and is named SUBROUTINE PTSH. Details of Pattern Search method can be obtained from references (36), (37) and (38).

(g) The Modified Parameter Values

The modified parameter values are the ones which have been obtained optimally by minimizing the objective function during each optimization process by means of Pattern Search. The final set of the modified parameter values can be achieved provided that any one of the performance criteria has been met.

(h) Performance Criteria

Performance criteria are based on the strategy adopted for the termination of the optimization process. The termination of the optimization process can be considered in three ways as follows:

(i) The number of iterations exceeds the pre-determined maximum number of iterations.

(ii) The number of function evaluations exceeds the pre-determined maximum number of function evaluations.

(iii) The incremental change (termed STEP SIZE in Pattern Search) in each model parameter value is smaller than the specified "tolerance" which is the required resolution to specify the objective function value at the minimum.

The above-mentioned specifications determine the frame-work of the method of automated model parameter determination.

Moreover, interpretation of Figure 3.20 is that the simulated model performance corresponding to the initial parameter values is obtained by means of model performance analysis and compared with the measured performance of the device via the pre-determined error criteria. Satisfactory simulated performance leads to the termination of the optimization process. Excessive errors lead to a reinitialization of model parameter values and the reinitialization of model parameter values is made through the minimization of the objective function value by means of Pattern Search. This process repeats itself until the simulated performance falls within the performance criteria. The final set of parameter values is the one at which the process terminates. The optimal parameter values are shown in Table 3-16 compared with those obtained by the experimental method.

	Method (I)	Method (II)
I_1 (A)	5.057×10^{-14}	6.675×10^{-14}
I_2 (A)	2.065×10^{-12}	4.832×10^{-13}
I_3 (A)	4.563×10^{-13}	4.141×10^{-13}
I_S (A)	1.396×10^{-13}	8.376×10^{-14}
N_C	1.133	1.123
N_{E1}	1.217	1.218
N_{E2}	1.618	1.636
τ_F (S)	2.650×10^{-9}	1.853×10^{-8}
τ_R (S)	2.880×10^{-6}	1.153×10^{-5}
C_C (F)	3.670×10^{-12}	5.153×10^{-12}
C_E (F)	3.870×10^{-10}	2.322×10^{-10}
Q_{BO} (C)	6.690×10^{-10}	4.683×10^{-10}
$R_{BAO}(\Omega)$	153.0	124.6

Table 3-16 Comparison of Model Parameter Values obtained by Method I and Method II

CHAPTER IV

SIMULATION RESULTS

Three conventionally-modified Ebers-Moll models used in ECAP II, SCEPTRE and NET-1 circuit analysis programs, and the abbreviated Gummel-Poon model (abbreviated with sixteen parameters including parasitic resistances) have been described in Chapter II. The basic Ebers-Moll model and the abbreviated Gummel-Poon model are systematically derived from a common mathematical origin (i.e. the basic one-dimensional carrier transport equations). In spite of the appearance of the abbreviated Gummel-Poon model, for low-bias condition and with some idealization such as assumption of low-level injection, no carrier recombination-generation effects in the space-charge regions and so forth, the model reduces to the basic Ebers-Moll model. This means that the abbreviated Gummel-Poon model is topologically equivalent to the basic Ebers-Moll model. In this chapter, models are compared on the basis of their ability to represent the common-emitter static characteristics of a silicon double-diffused transistor.

The quantitative discussions are focused on the common-emitter static characteristics which are:

(i) The output characteristics (i.e. I_C versus V_{CE} with I_B as parameter).

(ii) The dependence of common-emitter d. c. current gain on the collector current (i.e. h_{FE} versus I_C for constant V_{CE}).

(iii) The input characteristics (i.e. I_B versus V_{BE} with V_{CE} as parameter).

Figures 4.1 to 4.9 inclusive show the comparison of the measured data (dashed lines) obtained by means of a curve tracer (Tektronix type 576) for the type 2N1613 transistor at a room temperature of 25°C and the simulations by the models (the solid lines). The model parameter values used in the simulation are obtained from Chapter III.

For simplicity, the modified Ebers-Moll model in ECAP II is called EMM 1; the one in SCEPTRE, EMM 2; and the one in NET-1, EMM 3; and the abbreviated Gummel-Poon model, AGPM.

4.1 THE OUTPUT CHARACTERISTICS

It has been already shown that all three modified Ebers-Moll models employ the principle of "superposition", that is, the collector current (or the emitter current) can be expressed as the sum of a function of emitter-base voltage and a function of collector-base voltage. In order to examine the validity of the principle of "superposition", one can consider the Early effect(9), that is, the finite collector-current-dependent output conductance due to base-width modulation. For the measured output characteristics, beyond the $V_{CE} = V_{BE}$ contour, a region of bias (i.e. the active region) exists in which the collector current varies approximately linearly with the collector-emitter voltage for fixed base current in such a way that the straight line section exhibits finite incremental output conductance. In Figures 4.1 to 4.3, the simulated output characteristics (solid lines) by EMM 1, EMM 2 and EMM 3 do not exhibit finite output conductance in the active region. The deviation between the simulated and the measured output characteristics in the active region implies the violation of the principle of "superposition" for a real transistor. On the other hand, Figure 4.4, which shows the corresponding AGPM simulated output characteristics, exhibits a reasonable fit to the real transistor performance, (i.e. in the active region, the collector current varies linearly with the collector-emitter voltage). This finite output conductance results from introducing the base charge, Q_B in the denominator of equation (2.87) which through its dependence on operating junction voltages via the junction capacitances disables the "superposition" and provides a realistic description of the output conductance. However, EMM 1 to EMM 3 can be further modified to account for the Early effect by modelling the current gains α_F and α_R as functions of operating currents and junction voltages. This modification was proposed by Logan(4) recently and it is claimed that this modification can provide a realistic description of the output conductance as well.

Besides the Early effect, in the active region, it is seen that the output characteristics simulated by EMM 1, EMM 3 and AGPM but not by EMM 2 depart significantly from the corresponding measured data for low base currents (say, below 1 μA). This can be explained as follows:

(i) For EMM 1, the assumption of constant α_F and α_R is used in the

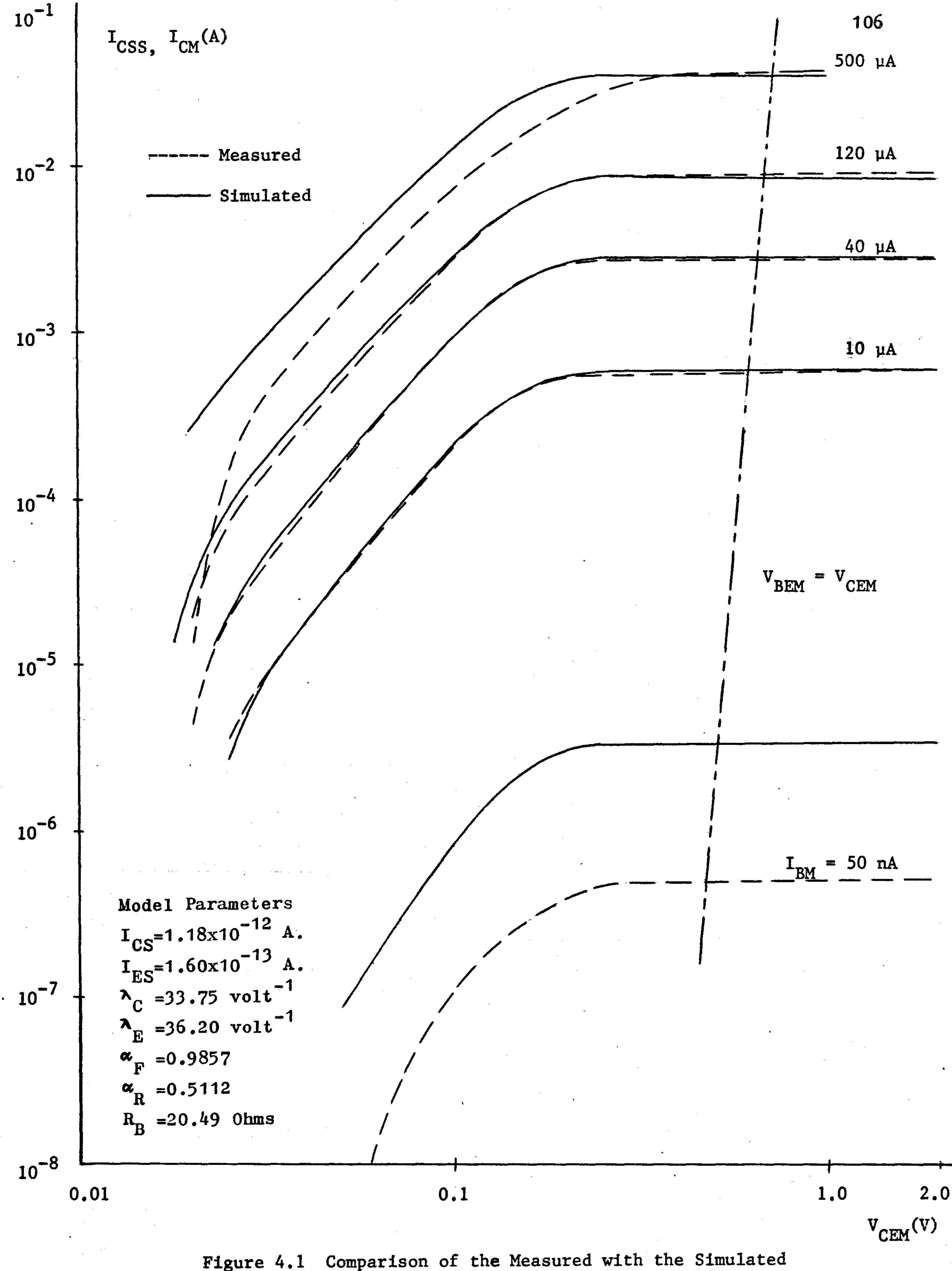

Figure 4.1 Comparison of the Measured with the Simulated Output Characteristics by Model EMM 1

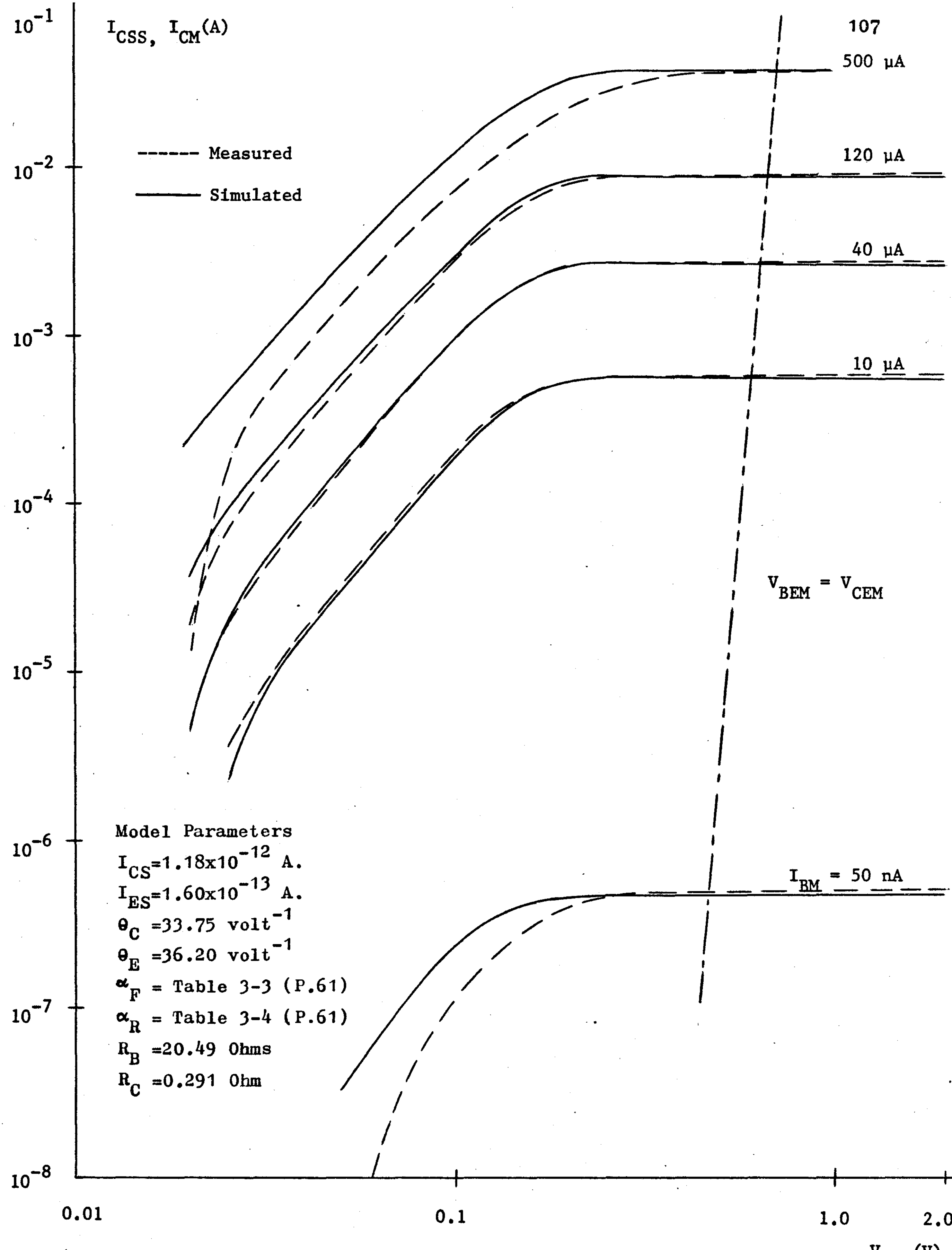

Figure 4.2 Comparison of the Measured with the Simulated Output Characteristics by Model EMM 2

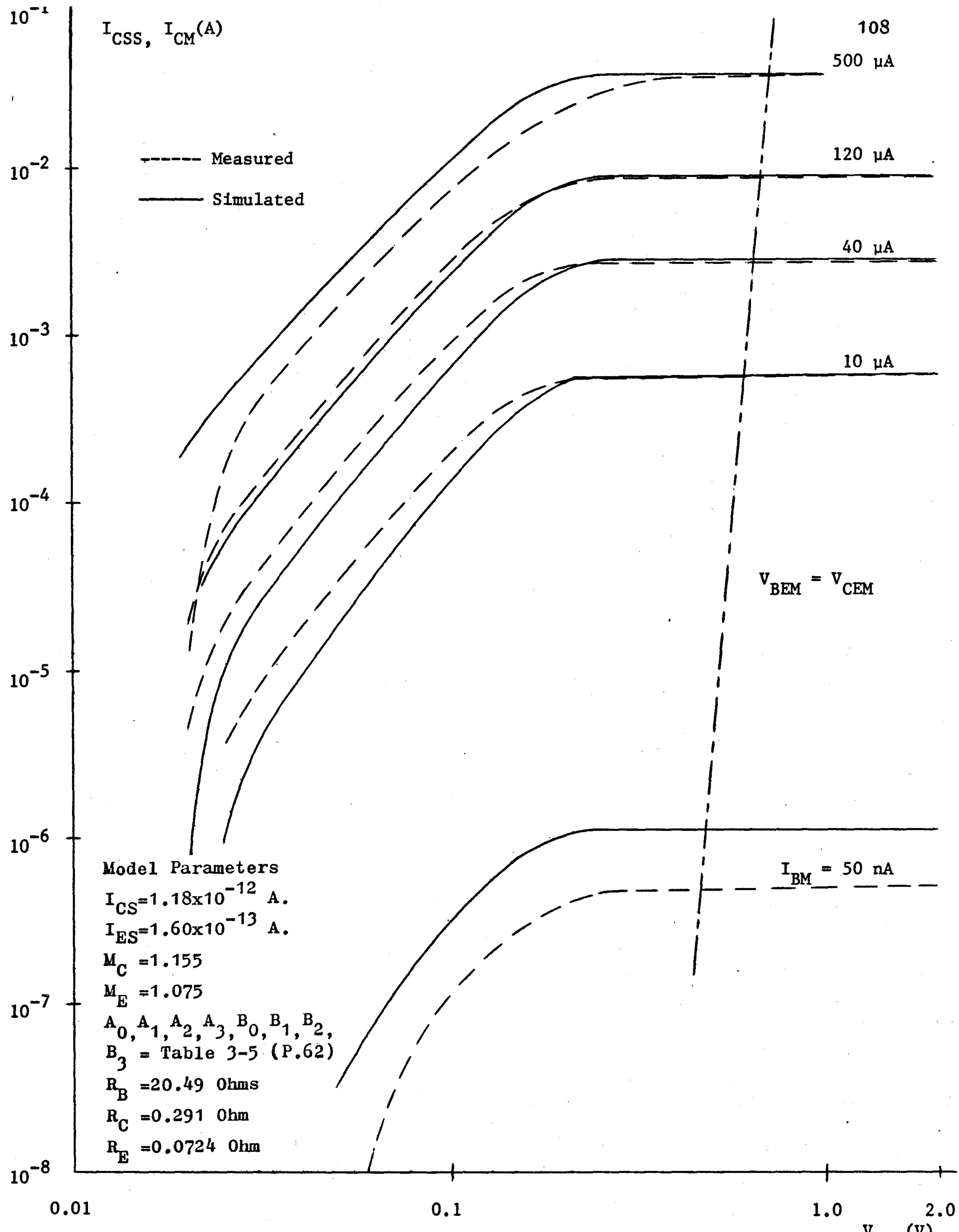

Figure 4.3 Comparison of the Measured with the Simulated Output Characteristics by Model EMM 3

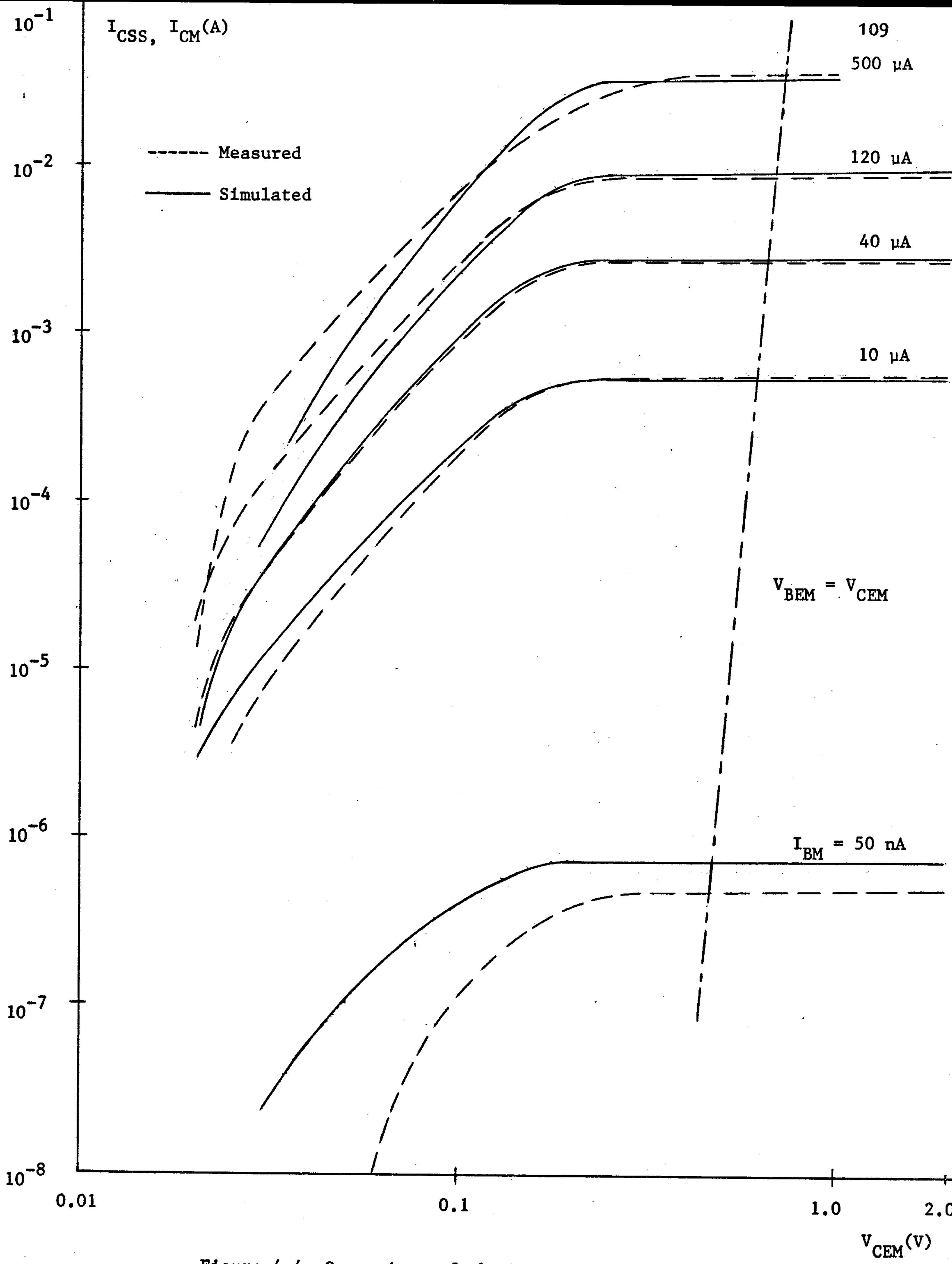

Figure 4.4 Comparison of the Measured with the Simulated Output Characteristics by Model AGPM

model and they are evaluated at the base current equal to 60 μA to meet the typical operating conditions. Hence they are over-estimated for low base currents.

(ii) For EMM 3, α_F and α_R are modelled by the third order polynomials respectively. Subject to the functional behaviour of the third order polynomial, the complete approximation of the variation in α_F (similarly in α_R) to the measured data over the wide base current range can not be achieved. For better fit over the wide base current range, a possible suggestion is to use two independent polynomials for modelling α_F (similarly for α_R), one to model α_F for low base currents and the other for high base currents.

(iii) For AGPM, one of the basic assumptions in developing this model is that the d. c. current gain, h_{FE} is very large, whereas at low base currents, h_{FE}'s are smaller and hence violation of this assumption exists.

On the other hand, Figure 4.2 shows a reasonably good fit between the measured and the simulated characteristics by EMM 2. This is because α_F and α_R, in this case, are tabulated for a range of base currents.

In the saturation region, a fairly reasonable match of the measured with the simulated characteristics of the EMM's, especially of EMM 2, is obtained as a consequence of the application of the principle of "superposition", since in the saturation region both junctions of the transistor are forward-biased and the principle of "superposition" is valid. The corresponding simulations by EMM 1 and EMM 3 respectively are a little worse than that by EMM 2. The reasons are stated above in items (i) and (ii). Figure 4.4 shows that the fit by AGPM in the saturation region is not better than that of the EMM's. The reason is that AGPM is developed on the basis of the transistor operating in the normal active mode.

Furthermore, it can be observed from Figures 4.1 to 4.4 that at extremely high base current equal to 500 μA, there are large deviations between the measured and the simulated characteristics of all models in the saturation region. All EMM's are developed on the basis of the assumption of low-level injection. At high levels of base current where high-level injection occurs, this assumption is no longer valid because the transport equations for excess carriers in the quasi-neutral regions outside the space-charge regions change; they become non-linear and the electric field has an important effect on the flow of both holes and electrons. The AGPM in which the base "push-out" effect is not considered and constant τ_F and τ_R are assumed can not provide a more accurate description of the transistor performance than the EMM's.

The numerical comparisons of the measured and the simulated output characteristics by each model are given in Table 4-1. Table 4-2 shows the measured and the simulated V_{CE} by different models at zero collector current which is one of the measures of goodness of fit in the saturation region.

TABLE 4-1 COMPARISONS OF THE MEASURED WITH THE SIMULATED OUTPUT CHARACTERISTICS BY MODELS EMM1, EMM2, EMM3 AND AGPM FOR TRANSISTOR 2N1613

			EMM1	EMM2	EMM3	AGPM
IBM(A)	VCEM(V)	ICM(A)	ICSS(A)	ICSS(A)	ICSS(A)	ICSS(A)
5.000E-08	0.	-4.800E-08	-7.048E-08	-4.209E-08	-3.603E-08	-4.564E-08
5.000E-08	3.000E-02	-3.000E-08	-7.777E-09	-1.025E-08	-8.217E-09	2.238E-08
5.000E-08	5.000E-02	-5.000E-09	8.804E-08	3.323E-08	3.280E-08	1.081E-07
5.000E-08	5.200E-02	0.	1.015E-07	3.891E-08	3.846E-08	1.188E-07
5.000E-08	6.000E-02	1.000E-08	1.649E-07	6.429E-08	6.466E-08	1.654E-07
5.000E-08	7.000E-02	3.000E-08	2.689E-07	1.019E-07	1.066E-07	2.311E-07
5.000E-08	8.000E-02	5.800E-08	4.066E-07	1.452E-07	1.603E-07	3.025E-07
5.000E-08	1.000E-01	1.100E-07	8.027E-07	2.406E-07	3.058E-07	4.471E-07
5.000E-08	1.500E-01	2.950E-07	2.254E-06	4.217E-07	7.735E-07	6.821E-07
5.000E-08	2.000E-01	4.000E-07	3.149E-06	4.797E-07	1.034E-06	7.473E-07
5.000E-08	2.500E-01	4.700E-07	3.388E-06	4.918E-07	1.101E-06	7.602E-07
5.000E-08	3.000E-01	4.800E-07	3.435E-06	4.941E-07	1.114E-06	7.628E-07
5.000E-08	3.500E-01	4.810E-07	3.444E-06	4.946E-07	1.116E-06	7.635E-07
5.000E-08	4.000E-01	4.820E-07	3.446E-06	4.947E-07	1.117E-06	7.640E-07
5.000E-08	4.500E-01	4.850E-07	3.446E-06	4.947E-07	1.117E-06	7.643E-07
5.000E-08	5.000E-01	4.900E-07	3.447E-06	4.947E-07	1.117E-06	7.647E-07
5.000E-08	1.000E+00	4.920E-07	3.447E-06	4.947E-07	1.117E-06	7.682E-07
5.000E-08	2.000E+00	4.950E-07	3.447E-06	4.947E-07	1.116E-06	7.753E-07
5.000E-08	4.000E+00	5.000E-07	3.447E-06	4.947E-07	1.113E-06	7.899E-07

TABLE 4-1 COMPARISONS OF THE MEASURED WITH THE SIMULATED OUTPUT CHARACTERISTICS BY MODELS EMM1, EMM2, EMM3 AND AGPM FOR TRANSISTOR 2N1613 (CONT.)

			EMM1	EMM2	EMM3	AGPM
IBM(A)	VCEM(V)	ICM(A)	ICSS(A)	ICSS(A)	ICSS(A)	ICSS(A)
5.000E-08	6.000E+00	5.000E-07	3.447E-06	4.947E-07	1.105E-06	8.051E-07
5.000E-08	8.000E+00	5.000E-07	3.447E-06	4.947E-07	1.091E-06	8.209E-07
5.000E-08	1.000E+01	5.050E-07	3.447E-06	4.947E-07	1.069E-06	8.373E-07
5.000E-08	1.500E+01	5.100E-07	3.447E-06	4.947E-07	9.672E-07	8.813E-07
5.000E-08	2.000E+01	5.200E-07	3.447E-06	4.947E-07	7.817E-07	9.302E-07
5.000E-08	2.500E+01	5.250E-07	3.447E-06	4.947E-07	4.959E-07	9.849E-07
5.000E-08	3.000E+01	5.350E-07	3.447E-06	4.947E-07	1.182E-07	1.046E-06
1.000E-05	0.	-9.200E-06	-1.097E-05	-1.010E-05	-6.742E-06	-9.537E-06
1.000E-05	2.100E-02	0.	-2.492E-07	-4.035E-07	-7.886E-07	3.297E-06
1.000E-05	2.500E-02	3.600E-06	2.822E-06	2.369E-06	9.149E-07	6.959E-06
1.000E-05	3.000E-02	7.800E-06	7.291E-06	6.399E-06	3.393E-06	1.227E-05
1.000E-05	3.500E-02	1.200E-05	1.257E-05	1.115E-05	6.319E-06	1.849E-05
1.000E-05	4.000E-02	1.800E-05	1.877E-05	1.673E-05	9.765E-06	2.577E-05
1.000E-05	5.000E-02	3.400E-05	3.457E-05	3.088E-05	1.855E-05	4.397E-05
1.000E-05	6.000E-02	5.500E-05	5.591E-05	4.991E-05	3.052E-05	6.788E-05
1.000E-05	7.000E-02	7.800E-05	8.410E-05	7.486E-05	4.654E-05	9.827E-05
1.000E-05	8.000E-02	1.160E-04	1.202E-04	1.065E-04	6.750E-05	1.353E-04
1.000E-05	1.000E-01	2.050E-04	2.173E-04	1.902E-04	1.272E-04	2.260E-04

TABLE 4-1 COMPARISONS OF THE MEASURED WITH THE SIMULATED OUTPUT CHARACTERISTICS BY MODELS EMM1, EMM2, EMM3 AND AGPM FOR TRANSISTOR 2N1613 (CONT.)

IBM(A)	VCEM(V)	ICM(A)	EMM1 ICSS(A)	EMM2 ICSS(A)	EMM3 ICSS(A)	AGPM ICSS(A)
1.000E-05	1.500E-01	4.300E-04	5.061E-04	4.279E-04	3.534E-04	4.392E-04
1.000E-05	2.000E-01	5.300E-04	6.470E-04	5.387E-04	5.134E-04	5.193E-04
1.000E-05	2.500E-01	5.500E-04	6.811E-04	5.651E-04	5.623E-04	5.362E-04
1.000E-05	3.000E-01	5.600E-04	6.878E-04	5.702E-04	5.728E-04	5.394E-04
1.000E-05	3.500E-01	5.600E-04	6.890E-04	5.712E-04	5.749E-04	5.401E-04
1.000E-05	4.000E-01	5.650E-04	6.892E-04	5.714E-04	5.753E-04	5.405E-04
1.000E-05	4.500E-01	5.680E-04	6.893E-04	5.714E-04	5.753E-04	5.407E-04
1.000E-05	5.000E-01	5.700E-04	6.893E-04	5.714E-04	5.754E-04	5.409E-04
1.000E-05	1.000E+00	5.700E-04	6.893E-04	5.714E-04	5.754E-04	5.432E-04
1.000E-05	2.000E+00	5.750E-04	6.893E-04	5.714E-04	5.754E-04	5.477E-04
1.000E-05	4.000E+00	5.750E-04	6.893E-04	5.714E-04	5.753E-04	5.570E-04
1.000E-05	6.000E+00	5.750E-04	6.893E-04	5.714E-04	5.753E-04	5.666E-04
1.000E-05	8.000E+00	5.820E-04	6.893E-04	5.714E-04	5.753E-04	5.765E-04
1.000E-05	1.000E+01	6.000E-04	6.893E-04	5.714E-04	5.752E-04	5.868E-04
1.000E-05	1.500E+01	6.200E-04	6.893E-04	5.714E-04	5.750E-04	6.142E-04
1.000E-05	2.000E+01	6.220E-04	6.893E-04	5.714E-04	5.745E-04	6.442E-04
1.000E-05	2.500E+01	6.450E-04	6.893E-04	5.714E-04	5.737E-04	6.771E-04
1.000E-05	3.000E+01	7.000E-04	6.893E-04	5.714E-04	5.726E-04	7.136E-04

TABLE 4-1 COMPARISONS OF THE MEASURED WITH THE SIMULATED OUTPUT CHARACTERISTICS BY MODELS EMM1, EMM2, EMM3 AND AGPM FOR TRANSISTOR 2N1613 (CONT.)

IBM(A)	VCEM(V)	ICM(A)	EMM1 ICSS(A)	EMM2 ICSS(A)	EMM3 ICSS(A)	AGPM ICSS(A)
4.000E-05	0.	-3.830E-05	-3.972E-05	-3.937E-05	-2.690E-05	-3.837E-05
4.000E-05	1.850E-02	0.	4.063E-09	-7.953E-08	-2.183E-06	-1.568E-06
4.000E-05	2.000E-02	4.500E-06	4.470E-06	4.335E-06	5.963E-07	2.608E-06
4.000E-05	2.500E-02	1.950E-05	2.110E-05	2.077E-05	1.095E-05	1.821E-05
4.000E-05	3.000E-02	3.550E-05	4.075E-05	4.018E-05	2.320E-05	3.673E-05
4.000E-05	3.500E-02	6.500E-05	6.391E-05	6.304E-05	3.765E-05	5.863E-05
4.000E-05	4.000E-02	9.100E-05	9.112E-05	8.988E-05	5.468E-05	8.445E-05
4.000E-05	5.000E-02	1.700E-04	1.601E-04	1.578E-04	9.807E-05	1.501E-04
4.000E-05	6.000E-02	2.700E-04	2.528E-04	2.489E-04	1.571E-04	2.387E-04
4.000E-05	7.000E-02	3.800E-04	3.742E-04	3.680E-04	2.360E-04	3.551E-04
4.000E-05	8.000E-02	5.500E-04	5.282E-04	5.185E-04	3.390E-04	5.028E-04
4.000E-05	1.000E-01	9.500E-04	9.337E-04	9.134E-04	6.306E-04	8.947E-04
4.000E-05	1.500E-01	2.030E-03	2.076E-03	2.024E-03	1.711E-03	2.049E-03
4.000E-05	2.000E-01	2.530E-03	2.603E-03	2.541E-03	2.453E-03	2.604E-03
4.000E-05	2.500E-01	2.630E-03	2.727E-03	2.665E-03	2.679E-03	2.728E-03
4.000E-05	3.000E-01	2.680E-03	2.752E-03	2.689E-03	2.729E-03	2.751E-03
4.000E-05	3.500E-01	2.680E-03	2.756E-03	2.693E-03	2.738E-03	2.755E-03
4.000E-05	4.000E-01	2.680E-03	2.757E-03	2.694E-03	2.740E-03	2.757E-03
4.000E-05	4.500E-01	2.685E-03	2.757E-03	2.694E-03	2.741E-03	2.758E-03

TABLE 4-1 COMPARISONS OF THE MEASURED WITH THE SIMULATED OUTPUT CHARACTERISTICS BY MODELS EMM1, EMM2, EMM3 AND AGPM FOR TRANSISTOR 2N1613 (CONT.)

			EMM1	EMM2	EMM3	AGPM
IBM(A)	VCEM(V)	ICM(A)	ICSS(A)	ICSS(A)	ICSS(A)	ICSS(A)
4.000E-05	5.000E-01	2.690E-03	2.757E-03	2.694E-03	2.741E-03	2.759E-03
4.000E-05	1.000E+00	2.690E-03	2.757E-03	2.694E-03	2.741E-03	2.769E-03
4.000E-05	2.000E+00	2.695E-03	2.757E-03	2.694E-03	2.741E-03	2.789E-03
4.000E-05	4.000E+00	2.700E-03	2.757E-03	2.694E-03	2.741E-03	2.830E-03
4.000E-05	6.000E+00	2.715E-03	2.757E-03	2.694E-03	2.741E-03	2.872E-03
4.000E-05	8.000E+00	2.720E-03	2.757E-03	2.694E-03	2.741E-03	2.915E-03
4.000E-05	1.000E+01	2.800E-03	2.757E-03	2.694E-03	2.741E-03	2.960E-03
4.000E-05	1.500E+01	2.875E-03	2.757E-03	2.694E-03	2.740E-03	3.077E-03
4.000E-05	2.000E+01	2.960E-03	2.757E-03	2.694E-03	2.740E-03	3.202E-03
4.000E-05	2.500E+01	3.080E-03	2.757E-03	2.694E-03	2.739E-03	3.337E-03
4.000E-05	3.000E+01	3.340E-03	2.757E-03	2.694E-03	2.738E-03	3.483E-03
6.000E-05	0.	-5.650E-05	-5.764E-05	-5.761E-05	-4.037E-05	-5.764E-05
6.000E-05	1.800E-02	0.	1.463E-06	1.463E-06	-2.116E-06	-8.847E-06
6.000E-05	2.000E-02	8.000E-06	1.057E-05	1.056E-05	3.783E-06	-1.232E-06
6.000E-05	2.500E-02	3.200E-05	3.623E-05	3.617E-05	2.040E-05	2.031E-05
6.000E-05	3.000E-02	6.200E-05	6.653E-05	6.641E-05	4.005E-05	4.591E-05
6.000E-05	3.500E-02	9.700E-05	1.022E-04	1.020E-04	6.324E-05	7.624E-05
6.000E-05	4.000E-02	1.380E-04	1.441E-04	1.438E-04	9.053E-05	1.121E-04

TABLE 4-1 COMPARISONS OF THE MEASURED WITH THE SIMULATED OUTPUT CHARACTERISTICS BY MODELS EMM1, EMM2, EMM3 AND AGPM FOR TRANSISTOR 2N1613 (CONT.)

IBM(A)	VCEM(V)	ICM(A)	EMM1 ICSS(A)	EMM2 ICSS(A)	EMM3 ICSS(A)	AGPM ICSS(A)
6.000E-05	5.000E-02	2.600E-04	2.502E-04	2.493E-04	1.600E-04	2.035E-04
6.000E-05	6.000E-02	3.900E-04	3.925E-04	3.907E-04	2.545E-04	3.277E-04
6.000E-05	7.000E-02	5.900E-04	5.786E-04	5.750E-04	3.803E-04	4.918E-04
6.000E-05	8.000E-02	8.000E-04	8.139E-04	8.078E-04	5.445E-04	7.028E-04
6.000E-05	1.000E-01	1.440E-03	1.429E-03	1.415E-03	1.005E-03	1.273E-03
6.000E-05	1.500E-01	3.070E-03	3.136E-03	3.113E-03	2.680E-03	3.086E-03
6.000E-05	2.000E-01	3.850E-03	3.910E-03	3.902E-03	3.806E-03	4.055E-03
6.000E-05	2.500E-01	4.080E-03	4.092E-03	4.091E-03	4.148E-03	4.280E-03
6.000E-05	3.000E-01	4.120E-03	4.128E-03	4.127E-03	4.223E-03	4.320E-03
6.000E-05	3.500E-01	4.125E-03	4.134E-03	4.134E-03	4.238E-03	4.328E-03
6.000E-05	4.000E-01	4.125E-03	4.136E-03	4.136E-03	4.241E-03	4.331E-03
6.000E-05	4.500E-01	4.125E-03	4.136E-03	4.136E-03	4.242E-03	4.332E-03
6.000E-05	5.000E-01	4.125E-03	4.136E-03	4.136E-03	4.242E-03	4.334E-03
6.000E-05	1.000E+00	4.125E-03	4.136E-03	4.136E-03	4.242E-03	4.348E-03
6.000E-05	2.000E+00	4.150E-03	4.136E-03	4.136E-03	4.242E-03	4.377E-03
6.000E-05	4.000E+00	4.180E-03	4.136E-03	4.136E-03	4.242E-03	4.436E-03
6.000E-05	6.000E+00	4.250E-03	4.136E-03	4.136E-03	4.242E-03	4.497E-03
6.000E-05	8.000E+00	4.300E-03	4.136E-03	4.136E-03	4.242E-03	4.559E-03

TABLE 4-1 COMPARISONS OF THE MEASURED WITH THE SIMULATED OUTPUT CHARACTERISTICS BY MODELS EMM1, EMM2, EMM3 AND AGPM FOR TRANSISTOR 2N1613 (CONT.)

			EMM1	EMM2	EMM3	AGPM
IBM(A)	VCEM(V)	ICM(A)	ICSS(A)	ICSS(A)	ICSS(A)	ICSS(A)
6.000E-05	1.000E+01	4.350E-03	4.136E-03	4.136E-03	4.242E-03	4.622E-03
6.000E-05	1.500E+01	4.450E-03	4.136E-03	4.136E-03	4.241E-03	4.788E-03
6.000E-05	2.000E+01	4.580E-03	4.136E-03	4.136E-03	4.241E-03	4.965E-03
6.000E-05	2.500E+01	4.750E-03	4.136E-03	4.136E-03	4.240E-03	5.153E-03
6.000E-05	3.000E+01	5.050E-03	4.136E-03	4.136E-03	4.239E-03	5.354E-03
1.200E-04	0.	-1.080E-04	-1.084E-04	-1.102E-04	-8.088E-05	-1.155E-04
1.200E-04	1.780E-02	0.	1.392E-05	1.477E-05	4.440E-06	-3.538E-05
1.200E-04	2.000E-02	1.900E-05	3.489E-05	3.617E-05	1.906E-05	-2.142E-05
1.200E-04	2.500E-02	7.200E-05	8.870E-05	9.104E-05	5.660E-05	1.462E-05
1.200E-04	3.000E-02	1.280E-04	1.522E-04	1.558E-04	1.010E-04	5.755E-05
1.200E-04	3.500E-02	1.960E-04	2.270E-04	2.319E-04	1.532E-04	1.085E-04
1.200E-04	4.000E-02	2.850E-04	3.146E-04	3.211E-04	2.147E-04	1.688E-04
1.200E-04	5.000E-02	5.000E-04	5.362E-04	5.460E-04	3.707E-04	3.235E-04
1.200E-04	6.000E-02	8.000E-04	8.324E-04	8.459E-04	5.814E-04	5.346E-04
1.200E-04	7.000E-02	1.160E-03	1.218E-03	1.236E-03	8.609E-04	8.167E-04
1.200E-04	8.000E-02	1.560E-03	1.703E-03	1.726E-03	1.223E-03	1.164E-03
1.200E-04	1.000E-01	2.800E-03	2.959E-03	2.991E-03	2.218E-03	2.205E-03
1.200E-04	1.500E-01	5.900E-03	6.347E-03	6.504E-03	5.668E-03	5.864E-03
1.200E-04	2.000E-01	7.750E-03	7.841E-03	8.146E-03	7.883E-03	8.234E-03

TABLE 4-1 COMPARISONS OF THE MEASURED WITH THE SIMULATED OUTPUT CHARACTERISTICS BY MODELS EMM1, EMM2, EMM3 AND AGPM FOR TRANSISTOR 2N1613 (CONT.)

IBM(A)	VCEM(V)	ICM(A)	EMM1 ICSS(A)	EMM2 ICSS(A)	EMM3 ICSS(A)	AGPM ICSS(A)
1.200E-04	2.500E-01	8.420E-03	8.183E-03	8.543E-03	8.553E-03	8.843E-03
1.200E-04	3.000E-01	8.550E-03	8.256E-03	8.621E-03	8.702E-03	8.952E-03
1.200E-04	3.500E-01	8.570E-03	8.269E-03	8.636E-03	8.732E-03	8.972E-03
1.200E-04	4.000E-01	8.580E-03	8.271E-03	8.639E-03	8.737E-03	8.977E-03
1.200E-04	4.500E-01	8.580E-03	8.272E-03	8.639E-03	8.739E-03	8.980E-03
1.200E-04	5.000E-01	8.580E-03	8.272E-03	8.639E-03	8.739E-03	8.982E-03
1.200E-04	1.000E+00	8.600E-03	8.272E-03	8.639E-03	8.739E-03	9.007E-03
1.200E-04	2.000E+00	8.650E-03	8.272E-03	8.639E-03	8.739E-03	9.055E-03
1.200E-04	4.000E+00	8.700E-03	8.272E-03	8.639E-03	8.739E-03	9.154E-03
1.200E-04	6.000E+00	8.800E-03	8.272E-03	8.639E-03	8.739E-03	9.255E-03
1.200E-04	8.000E+00	8.900E-03	8.272E-03	8.639E-03	8.739E-03	9.358E-03
1.200E-04	1.000E+01	8.980E-03	8.272E-03	8.639E-03	8.739E-03	9.462E-03
1.200E-04	1.500E+01	9.200E-03	8.272E-03	8.639E-03	8.738E-03	9.732E-03
1.200E-04	2.000E+01	9.400E-03	8.272E-03	8.639E-03	8.738E-03	1.001E-02
1.200E-04	2.500E+01	9.800E-03	8.272E-03	8.639E-03	8.737E-03	1.031E-02
1.200E-04	3.000E+01	1.100E-02	8.272E-03	8.639E-03	8.736E-03	1.062E-02
5.000E-04	0.	-4.550E-04	-3.877E-04	-3.745E-04	-3.386E-04	-4.829E-04
5.000E-04	1.930E-02	0.	2.403E-04	2.321E-04	1.924E-04	-2.495E-04

TABLE 4-1 COMPARISONS OF THE MEASURED WITH THE SIMULATED OUTPUT CHARACTERISTICS BY MODELS EMM1, EMM2, EMM3 AND AGPM FOR TRANSISTOR 2N1613 (CONT.)

			EMM1	EMM2	EMM3	AGPM
IBM(A)	VCEM(V)	ICM(A)	ICSS(A)	ICSS(A)	ICSS(A)	ICSS(A)
5.000E-04	2.000E-02	1.350E-05	2.722E-04	2.625E-04	2.189E-04	-2.376E-04
5.000E-04	2.500E-02	1.800E-04	5.194E-04	5.001E-04	4.266E-04	-1.437E-04
5.000E-04	3.000E-02	3.680E-04	8.107E-04	7.796E-04	6.707E-04	-3.173E-05
5.000E-04	3.500E-02	5.880E-04	1.153E-03	1.107E-03	9.567E-04	1.012E-04
5.000E-04	4.000E-02	8.350E-04	1.553E-03	1.490E-03	1.291E-03	2.587E-04
5.000E-04	5.000E-02	1.530E-03	2.561E-03	2.445E-03	2.125E-03	6.616E-04
5.000E-04	6.000E-02	2.300E-03	3.898E-03	3.710E-03	3.232E-03	1.216E-03
5.000E-04	7.000E-02	3.360E-03	5.623E-03	5.330E-03	4.652E-03	1.957E-03
5.000E-04	8.000E-02	4.400E-03	7.768E-03	7.354E-03	6.439E-03	2.940E-03
5.000E-04	1.000E-01	7.150E-03	1.320E-02	1.251E-02	1.105E-02	5.761E-03
5.000E-04	1.500E-01	1.540E-02	2.705E-02	2.665E-02	2.454E-02	1.764E-02
5.000E-04	2.000E-01	2.220E-02	3.283E-02	3.352E-02	3.223E-02	2.838E-02
5.000E-04	2.500E-01	2.690E-02	3.415E-02	3.528E-02	3.460E-02	3.200E-02
5.000E-04	3.000E-01	3.010E-02	3.441E-02	3.565E-02	3.516E-02	3.270E-02
5.000E-04	3.500E-01	3.300E-02	3.445E-02	3.572E-02	3.529E-02	3.282E-02
5.000E-04	4.000E-01	3.430E-02	3.446E-02	3.573E-02	3.531E-02	3.284E-02
5.000E-04	4.500E-01	3.500E-02	3.446E-02	3.573E-02	3.531E-02	3.285E-02
5.000E-04	5.000E-01	3.500E-02	3.446E-02	3.573E-02	3.532E-02	3.285E-02
5.000E-04	1.000E+00	3.550E-02	3.447E-02	3.573E-02	3.532E-02	3.290E-02

TABLE 4-2 COMPARISONS OF THE MEASURED WITH THE SIMULATED COLLECTOR-EMITTER TERMINAL VOLTAGES, AT COLLECTOR CURRENT EQUAL TO ZERO, BY MODELS EMM1, EMM2, EMM3 AND AGPM FOR TRANSISTOR 2N1613

IBM(A)	ICM(A)	VCEM(V)	EMM1 VCES(V)	EMM2 VCES(V)	EMM3 VCES(V)	AGPM VCES(V)
5.000E-08	0.	5.200E-02	3.223E-02	3.578E-02	3.514E-02	2.266E-02
1.000E-05	0.	2.100E-02	2.135E-02	2.162E-02	2.292E-02	1.688E-02
4.000E-05	0.	1.850E-02	1.850E-02	1.853E-02	1.968E-02	1.907E-02
6.000E-05	0.	1.800E-02	1.767E-02	1.767E-02	1.873E-02	2.031E-02
1.200E-04	0.	1.780E-02	1.624E-02	1.618E-02	1.710E-02	2.306E-02
5.000E-04	0.	1.930E-02	1.331E-02	1.336E-02	1.371E-02	3.112E-02

4.2 THE DEPENDENCE OF COMMON-EMITTER D. C. CURRENT GAIN ON THE COLLECTOR CURRENT

Figure 4.5 shows the measured d. c. current gains, h_{FE}'s (dashed lines) as a function of collector current at collector-emitter voltage equal to one volt and the simulations (solid lines) by different models.

For different values of base currents, the simulated h_{FE}'s of EMM 1 are constant throughout because of the assumption of constant α_F and α_R evaluated at base current equal to 60 µA to meet the typical operating conditions. Hence h_{FE}'s are over-estimated for any base current less than 60 µA and under-estimated for any base current greater than 60 µA.

There is an excellent match between the measured and the simulated h_{FE}'s by EMM 2 for a range of base currents. This excellence is achieved by tabulating α_F and α_R as a function of base currents. Since α_F and α_R are derived solely from the measurements made at the device terminals, no attempt is made to relate the device performance to the structural and physical parameters. The accuracy can be increased by increasing the number of measured data points used in constructing this model. This approach, however, has serious drawbacks in that the resulting model based on the large tables becomes complex.

The simulated h_{FE}'s by EMM 3 well match the measured h_{FE}'s for base currents above 1 µA to 500 µA but not for base currents below 1 µA to 50 nA. α_F and α_R are modelled by the third order poly-

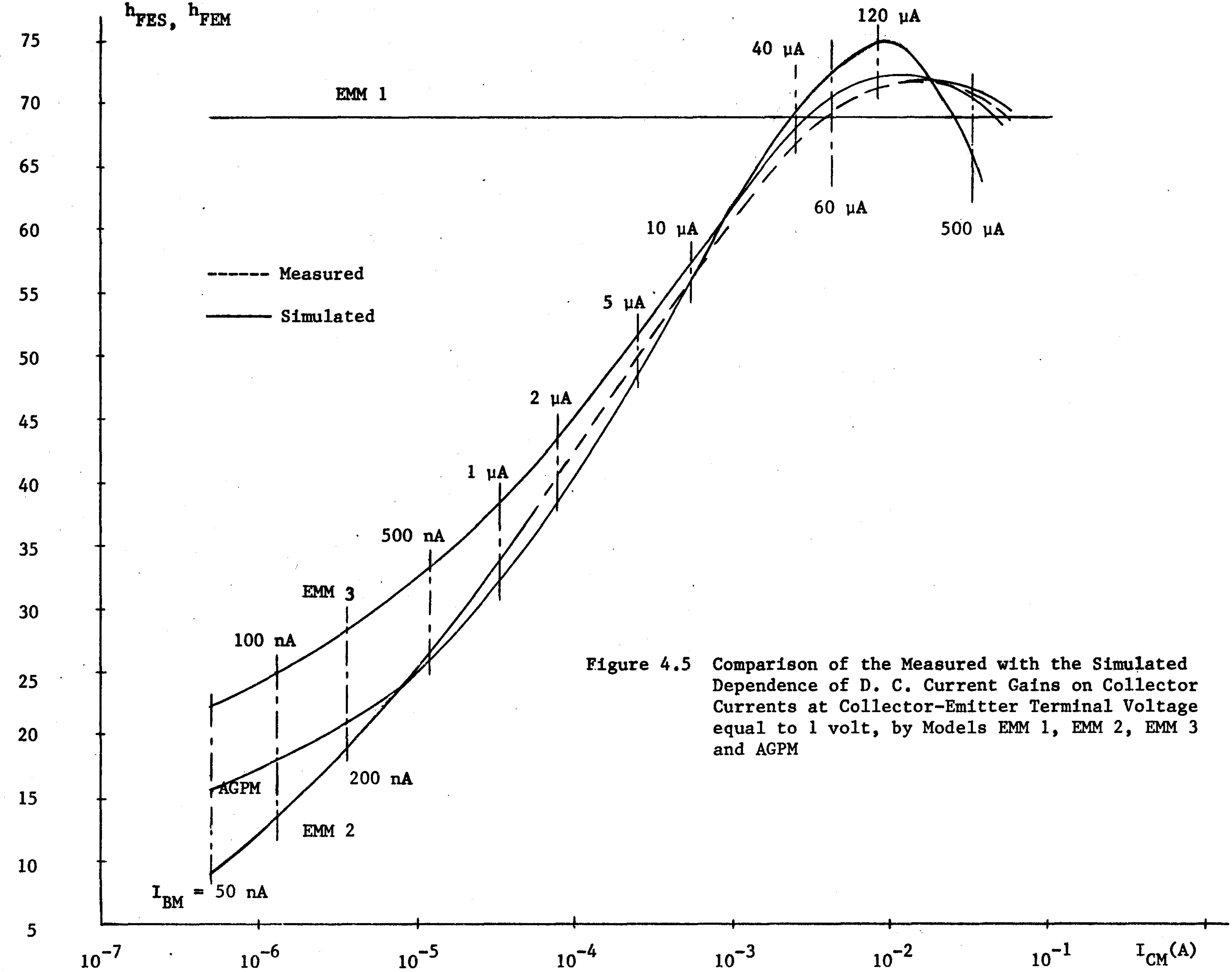

Figure 4.5 Comparison of the Measured with the Simulated Dependence of D. C. Current Gains on Collector Currents at Collector-Emitter Terminal Voltage equal to 1 volt, by Models EMM 1, EMM 2, EMM 3 and AGPM

nomials which have no direct connection with the device physics hence, being subject to the functional behaviour of the polynomials, a complete match of h_{FE}'s over this wide range of base currents is not possible. For complete match, two polynomials for α_F (likewise, for α_R) are required: one used to model α_F for base currents larger than 1 μA; other used to model α_F for base currents less than 1 μA. However, this would increase the number of model parameters.

The simulation of h_{FE}'s by AGPM is more of interest and although the match between the measured and the simulated h_{FE}'s is not so good as that of EMM 2 and EMM 3, the AGPM can give a realistic simulation. A good match at base currents ranging from 200 nA to 40 μA can be observed in Figure 4.5. The large discrepancy which appears at base currents below 200 nA is mainly due to the assumption of large h_{FE} made in the development of this model, as the simulated h_{FE}'s at base currents equal to 50 nA and 100 nA are larger than the corresponding measured values. At base currents above 40 μA, a discrepancy between the measured and the simulated h_{FE}'s results because the base "push-out" effect (one of the high level-injection effects) is not considered completely in the derivation of the model defining equations. For more accurate model performance, it is recommended that the base "push-out" effect should be included by introducing a base "push-out" factor (which can be treated as a model parameter) in the equation for base charge, Q_B which has a functional dependence on the operating conditions of the transistor.

Table 4-3 gives the numerical comparisons of the measured and the simulated h_{FE}'s by different models.

4.3 <u>THE INPUT CHARACTERISTICS</u>

Figures 4.6 through 4.9 show fairly good match between the measured input characteristics and those simulated by each models. The numerical data are given in Table 4-4.

In Figure 4.6, the deviation between the measured and the simulated input characteristics of EMM 1 is pronounced compared with that of other models. This is because of the assumption of constant α_F and α_R and the neglect of the effect of R_E.

Figure 4.7 shows that the simulated input characteristics of EMM 2 are a little better than that of EMM 1 since all the values of α_F and α_R are evaluated on the basis of device terminal measurements for different values of base current at a fixed collector-emitter voltage. However, the effect of emitter neutral region resistivity is still not considered in this model. Consequently, the simulated base-emitter voltages are higher than the measured base-emitter voltages at high levels of base current.

The simulation of input characteristics of EMM 3 exhibits much better match with the measured characteristics than do the EMM 1 and EMM 2. This improvement is mainly due to the fact that α_F and α_R are modelled as functions of junction voltages as well as base currents. The effect of resistivity of the neutral region of the emitter is accounted for in this model. The significant effect of R_E can be observed while the transistor is operated at high levels

TABLE 4-3 COMPARISONS OF THE MEASURED WITH THE SIMULATED DEPENDENCE OF D. C. CURRENT GAINS ON COLLECTOR CURRENTS AT COLLECTOR-EMITTER TERMINAL VOLTAGE EQUAL TO 1.0 VOLT, BY MODELS EMM1, EMM2, EMM3 AND AGPM FOR TRANSISTOR 2N1613

			EMM1	EMM2	EMM3	AGPM
IBM(A)	ICM(A)	HFEM	HFES	HFES	HFES	HFES
5.000E-08	4.920E-07	9.840E+00	6.893E+01	9.893E+00	2.233E+01	1.536E+01
1.000E-07	1.360E-06	1.360E+01	6.893E+01	1.360E+01	2.505E+01	1.844E+01
2.000E-07	3.750E-06	1.875E+01	6.893E+01	1.876E+01	2.826E+01	2.200E+01
5.000E-07	1.350E-05	2.700E+01	6.893E+01	2.717E+01	3.338E+01	2.757E+01
1.000E-06	3.400E-05	3.400E+01	6.893E+01	3.421E+01	3.801E+01	3.252E+01
2.000E-06	8.190E-05	4.095E+01	6.893E+01	4.119E+01	4.332E+01	3.820E+01
5.000E-06	2.500E-04	5.000E+01	6.893E+01	5.028E+01	5.123E+01	4.690E+01
1.000E-05	5.700E-04	5.700E+01	6.893E+01	5.714E+01	5.754E+01	5.432E+01
4.000E-05	2.690E-03	6.725E+01	6.893E+01	6.735E+01	6.852E+01	6.922E+01
6.000E-05	4.125E-03	6.875E+01	6.893E+01	6.893E+01	7.070E+01	7.247E+01
1.200E-04	8.600E-03	7.167E+01	6.893E+01	7.199E+01	7.282E+01	7.506E+01
5.000E-04	3.550E-02	7.100E+01	6.893E+01	7.146E+01	7.063E+01	6.580E+01

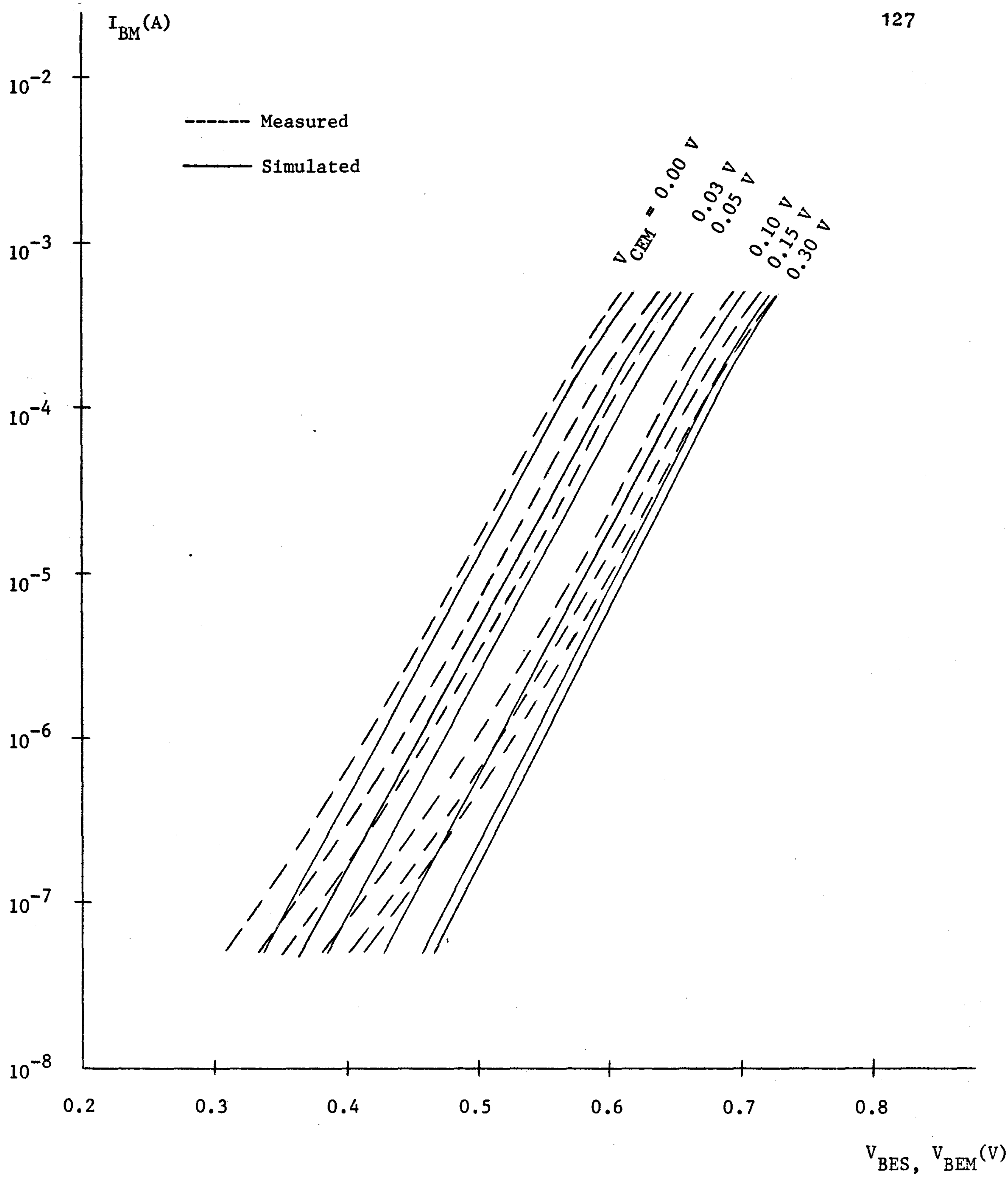

Figure 4.6 Comparison of the Measured with the Simulated Input Characteristics by Model EMM 1

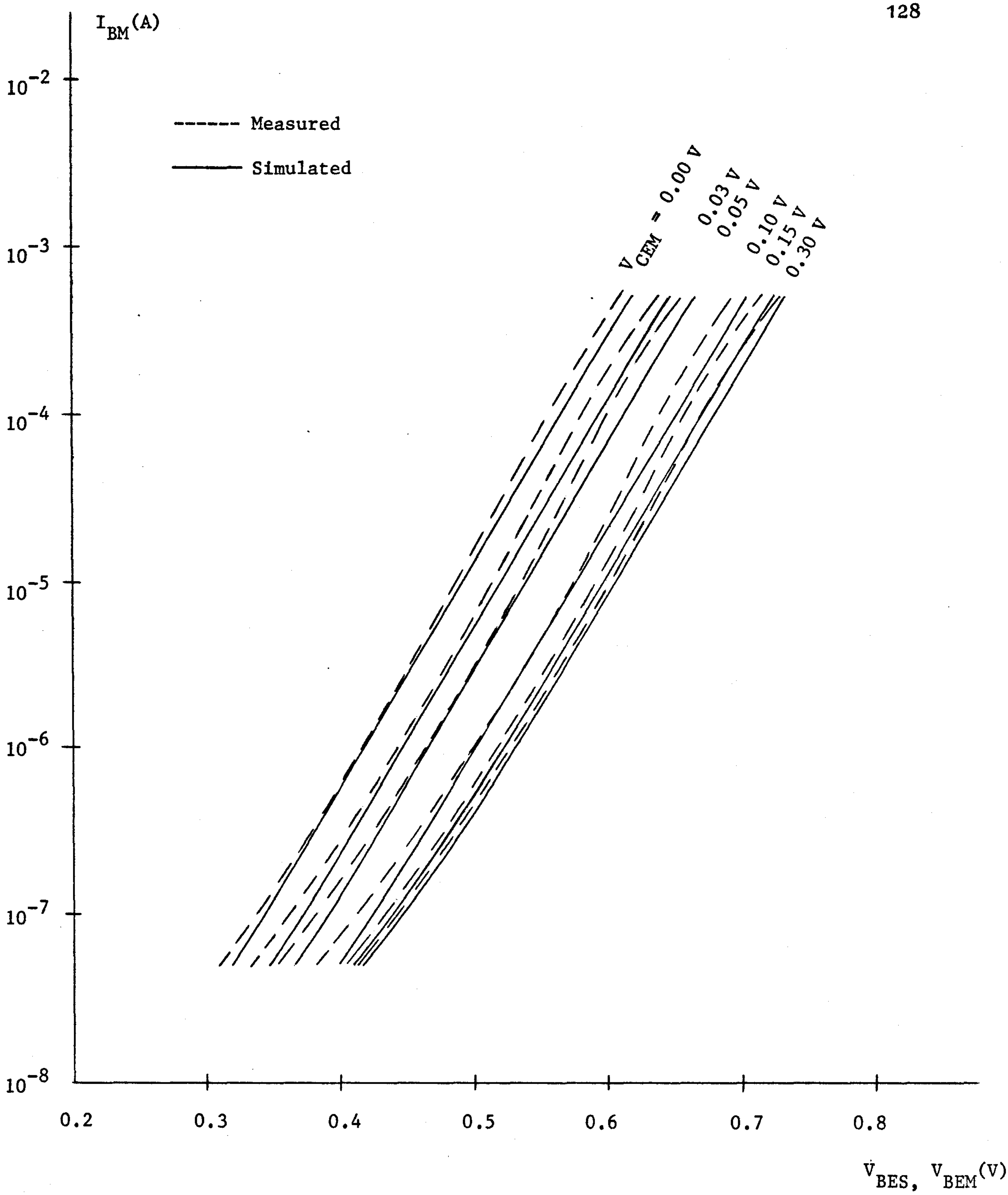

Figure 4.7 Comparison of the Measured with the Simulated Input Characteristics by Model EMM 2

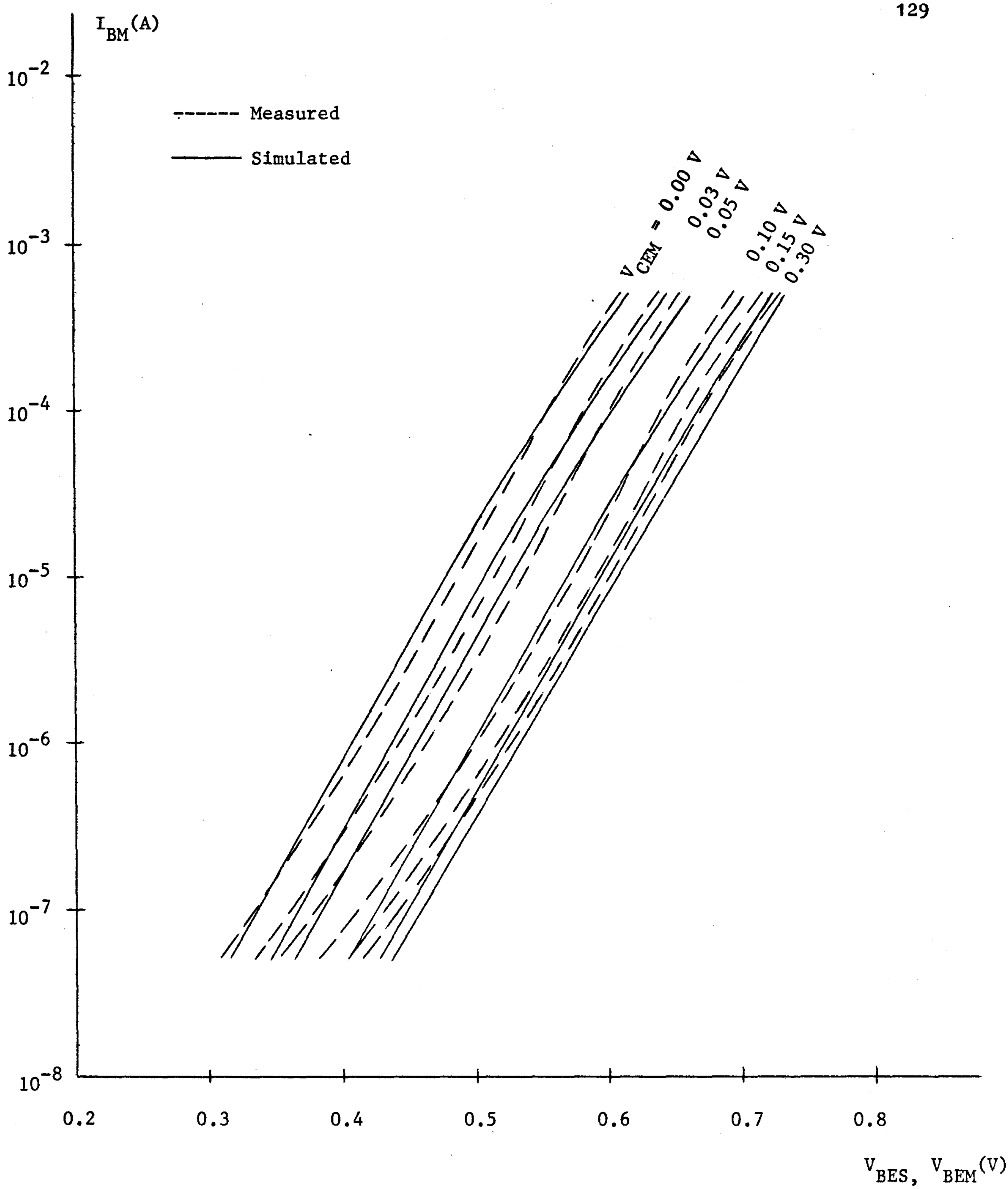

Figure 4.8 Comparison of the Measured with the Simulated Input Characteristics by Model EMM 3

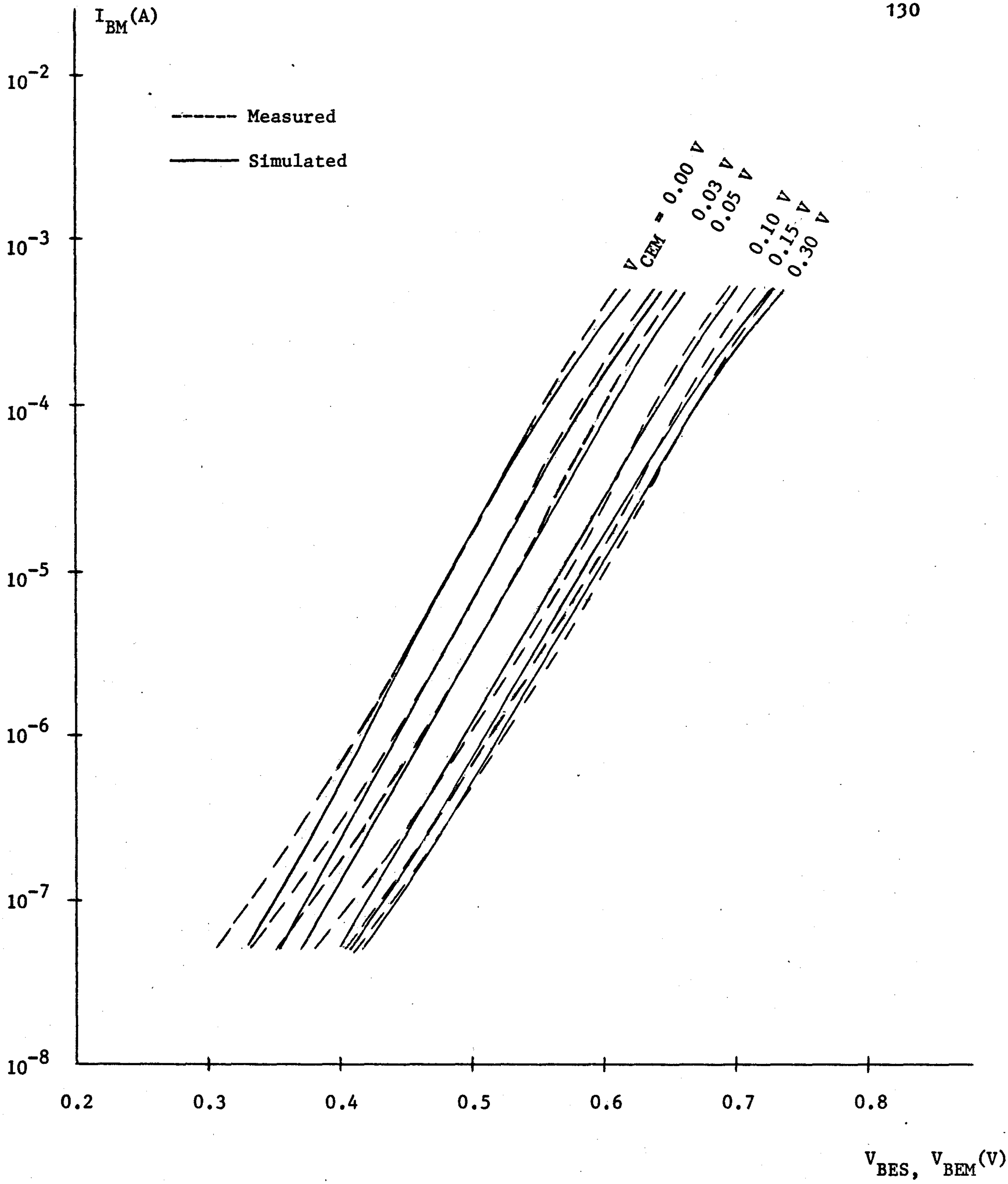

Figure 4.9 Comparison of the Measured with the Simulated Input Characteristics by Model AGPM

TABLE 4-4 COMPARISONS OF THE MEASURED WITH THE SIMULATED INPUT CHARACTERISTICS BY MODELS EMM1, EMM2, EMM3 AND AGPM FOR TRANSISTOR 2N1613

VCEM(V)	IBM(A)	VBEM(V)	EMM1 VBES(V)	EMM2 VBES(V)	EMM3 VBES(V)	AGPM VBES(V)
0.	5.000E-08	3.100E-01	3.371E-01	3.203E-01	3.158E-01	3.346E-01
0.	1.000E-07	3.350E-01	3.577E-01	3.434E-01	3.367E-01	3.549E-01
0.	2.000E-07	3.600E-01	3.782E-01	3.652E-01	3.576E-01	3.751E-01
0.	5.000E-07	3.930E-01	4.054E-01	3.952E-01	3.855E-01	4.018E-01
0.	1.000E-06	4.150E-01	4.259E-01	4.176E-01	4.067E-01	4.220E-01
0.	2.000E-06	4.375E-01	4.465E-01	4.400E-01	4.281E-01	4.422E-01
0.	5.000E-06	4.650E-01	4.737E-01	4.693E-01	4.566E-01	4.691E-01
0.	1.000E-05	4.860E-01	4.943E-01	4.916E-01	4.784E-01	4.896E-01
0.	4.000E-05	5.300E-01	5.360E-01	5.357E-01	5.231E-01	5.319E-01
0.	6.000E-05	5.400E-01	5.484E-01	5.484E-01	5.366E-01	5.448E-01
0.	1.200E-04	5.600E-01	5.701E-01	5.708E-01	5.604E-01	5.676E-01
0.	5.000E-04	6.120E-01	6.202E-01	6.194E-01	6.159E-01	6.220E-01
3.000E-02	5.000E-08	3.330E-01	3.666E-01	3.485E-01	3.448E-01	3.612E-01
3.000E-02	1.000E-07	3.600E-01	3.871E-01	3.718E-01	3.656E-01	3.817E-01
3.000E-02	2.000E-07	3.875E-01	4.076E-01	3.939E-01	3.866E-01	4.021E-01
3.000E-02	5.000E-07	4.200E-01	4.347E-01	4.242E-01	4.145E-01	4.291E-01
3.000E-02	1.000E-06	4.430E-01	4.552E-01	4.466E-01	4.357E-01	4.495E-01

TABLE 4-4 COMPARISONS OF THE MEASURED WITH THE SIMULATED INPUT CHARACTERISTICS BY MODELS EMM1, EMM2, EMM3 AND AGPM FOR TRANSISTOR 2N1613 (CONT.)

VCEM(V)	IBM(A)	VBEM(V)	EMM1 VBES(V)	EMM2 VBES(V)	EMM3 VBES(V)	AGPM VBES(V)
3.000E-02	2.000E-06	4.650E-01	4.758E-01	4.691E-01	4.571E-01	4.698E-01
3.000E-02	5.000E-06	4.940E-01	5.029E-01	4.985E-01	4.857E-01	4.969E-01
3.000E-02	1.000E-05	5.130E-01	5.235E-01	5.208E-01	5.075E-01	5.176E-01
3.000E-02	4.000E-05	5.530E-01	5.651E-01	5.648E-01	5.522E-01	5.601E-01
3.000E-02	6.000E-05	5.650E-01	5.775E-01	5.775E-01	5.657E-01	5.731E-01
3.000E-02	1.200E-04	5.850E-01	5.992E-01	5.998E-01	5.894E-01	5.960E-01
3.000E-02	5.000E-04	6.400E-01	6.432E-01	6.482E-01	6.447E-01	6.506E-01
5.000E-02	5.000E-08	3.530E-01	3.858E-01	3.658E-01	3.634E-01	3.768E-01
5.000E-02	1.000E-07	3.800E-01	4.062E-01	3.895E-01	3.842E-01	3.976E-01
5.000E-02	2.000E-07	4.050E-01	4.267E-01	4.120E-01	4.052E-01	4.183E-01
5.000E-02	5.000E-07	4.375E-01	4.538E-01	4.425E-01	4.332E-01	4.456E-01
5.000E-02	1.000E-06	4.625E-01	4.742E-01	4.652E-01	4.544E-01	4.662E-01
5.000E-02	2.000E-06	4.850E-01	4.947E-01	4.877E-01	4.759E-01	4.868E-01
5.000E-02	5.000E-06	5.150E-01	5.218E-01	5.171E-01	5.045E-01	5.141E-01
5.000E-02	1.000E-05	5.350E-01	5.423E-01	5.394E-01	5.263E-01	5.349E-01
5.000E-02	4.000E-05	5.750E-01	5.838E-01	5.834E-01	5.710E-01	5.778E-01
5.000E-02	6.000E-05	5.850E-01	5.951E-01	5.961E-01	5.844E-01	5.908E-01
5.000E-02	1.200E-04	6.050E-01	6.178E-01	6.183E-01	6.081E-01	6.139E-01
5.000E-02	5.000E-04	6.580E-01	6.676E-01	6.665E-01	6.629E-01	6.686E-01

TABLE 4-4 COMPARISONS OF THE MEASURED WITH THE SIMULATED INPUT CHARACTERISTICS BY MODELS EMM1, EMM2, EMM3 AND AGPM FOR TRANSISTOR 2N1613 (CONT.)

VCEM(V)	IBM(A)	VBEM(V)	EMM1 VBES(V)	EMM2 VBES(V)	EMM3 VBES(V)	AGPM VBES(V)
1.000E-01	5.000E-08	3.830E-01	4.287E-01	3.982E-01	4.033E-01	4.038E-01
1.000E-01	1.000E-07	4.100E-01	4.488E-01	4.234E-01	4.245E-01	4.256E-01
1.000E-01	2.000E-07	4.370E-01	4.690E-01	4.480E-01	4.457E-01	4.473E-01
1.000E-01	5.000E-07	4.725E-01	4.956E-01	4.802E-01	4.740E-01	4.758E-01
1.000E-01	1.000E-06	5.000E-01	5.157E-01	5.037E-01	4.956E-01	4.972E-01
1.000E-01	2.000E-06	5.225E-01	5.358E-01	5.268E-01	5.173E-01	5.186E-01
1.000E-01	5.000E-06	5.550E-01	5.624E-01	5.566E-01	5.461E-01	5.469E-01
1.000E-01	1.000E-05	5.750E-01	5.826E-01	5.790E-01	5.681E-01	5.685E-01
1.000E-01	4.000E-05	6.150E-01	6.233E-01	6.227E-01	6.126E-01	6.128E-01
1.000E-01	6.000E-05	6.260E-01	6.354E-01	6.352E-01	6.259E-01	6.263E-01
1.000E-01	1.200E-04	6.460E-01	6.566E-01	6.570E-01	6.490E-01	6.503E-01
1.000E-01	5.000E-04	6.950E-01	7.055E-01	7.042E-01	7.016E-01	7.069E-01
1.500E-01	5.000E-08	4.050E-01	4.551E-01	4.112E-01	4.265E-01	4.136E-01
1.500E-01	1.000E-07	4.300E-01	4.746E-01	4.378E-01	4.481E-01	4.361E-01
1.500E-01	2.000E-07	4.575E-01	4.942E-01	4.644E-01	4.700E-01	4.584E-01
1.500E-01	5.000E-07	4.925E-01	5.201E-01	4.986E-01	4.990E-01	4.878E-01
1.500E-01	1.000E-06	5.175E-01	5.396E-01	5.233E-01	5.211E-01	5.098E-01
1.500E-01	2.000E-06	5.400E-01	5.591E-01	5.470E-01	5.432E-01	5.319E-01

TABLE 4-4 COMPARISONS OF THE MEASURED WITH THE SIMULATED INPUT CHARACTERISTICS BY MODELS EMM1, EMM2, EMM3 AND AGPM FOR TRANSISTOR 2N1613 (CONT.)

VCEM(V)	IBM(A)	VBEM(V)	EMM1 VBES(V)	EMM2 VBES(V)	EMM3 VBES(V)	AGPM VBES(V)
1.500E-01	5.000E-06	5.700E-01	5.850E-01	5.774E-01	5.726E-01	5.611E-01
1.500E-01	1.000E-05	5.930E-01	6.045E-01	6.000E-01	5.948E-01	5.834E-01
1.500E-01	4.000E-05	6.350E-01	6.441E-01	6.434E-01	6.389E-01	6.296E-01
1.500E-01	6.000E-05	6.460E-01	6.559E-01	6.557E-01	6.517E-01	6.439E-01
1.500E-01	1.200E-04	6.650E-01	6.765E-01	6.772E-01	6.738E-01	6.696E-01
1.500E-01	5.000E-04	7.170E-01	7.243E-01	7.239E-01	7.235E-01	7.314E-01
3.000E-01	5.000E-08	4.120E-01	4.663E-01	4.150E-01	4.360E-01	4.162E-01
3.000E-01	1.000E-07	4.425E-01	4.854E-01	4.422E-01	4.582E-01	4.389E-01
3.000E-01	2.000E-07	4.675E-01	5.045E-01	4.697E-01	4.805E-01	4.615E-01
3.000E-01	5.000E-07	5.025E-01	5.298E-01	5.048E-01	5.102E-01	4.912E-01
3.000E-01	1.000E-06	5.250E-01	5.490E-01	5.301E-01	5.328E-01	5.135E-01
3.000E-01	2.000E-06	5.500E-01	5.681E-01	5.542E-01	5.555E-01	5.358E-01
3.000E-01	5.000E-06	5.795E-01	5.935E-01	5.849E-01	5.854E-01	5.654E-01
3.000E-01	1.000E-05	6.000E-01	6.127E-01	6.076E-01	6.078E-01	5.880E-01
3.000E-01	4.000E-05	6.410E-01	6.516E-01	6.510E-01	6.516E-01	6.352E-01
3.000E-01	6.000E-05	6.540E-01	6.632E-01	6.632E-01	6.641E-01	6.501E-01
3.000E-01	1.200E-04	6.760E-01	6.836E-01	6.847E-01	6.856E-01	6.773E-01
3.000E-01	5.000E-04	7.300E-01	7.307E-01	7.317E-01	7.339E-01	7.463E-01

of base current.

Contrary to the above-mentioned discrepancy appearing in Figures 4.6 to 4.8, the simulated base-emitter voltages of AGPM are lower than the measured base-emitter voltages for different base currents as shown in Figure 4.9. This discrepancy is probably due to one of the high-level injection effects called "emitter crowding" which is illustrated in Figure 4.10. For the diffused planar transistor, the base current causes the emitter bias voltage at the edge of the emitter, $V_{BE\ edge}$ to be higher than that at the centre, $V_{BE\ centre}$. At low current levels, $V_{BE\ edge} - V_{BE\ centre} \ll KT/q$, and the current is distributed uniformly as shown in Figure 4.10(a). At high current levels, the difference in biasing voltages becomes so pronounced that virtually all of the injection takes places at the edges of the emitter as shown in Figure 4.10(b). This effect is known as "emitter crowding" and causes the measured base-emitter voltages to be higher than that predicted by the model. Transistors are often used at high current levels and the "emitter crowding" is a two-dimensional effect, whereas unfortunately, AGPM is based on a one-dimensional approach. Hence a true or complete physical model of the transistor calls for a two-dimensional approach.

In general, the relatively large discrepancy between the measured and the simulated input characteristics by different models appears at the very low current levels because of the effect of generation and recombination at surfaces and in the inversion layers at the surfaces which are significant at low bias voltages. This effect is known as "surface effect" (39). The "surface effect" in modern diffused transistors actually has been minimized but however not eliminated.

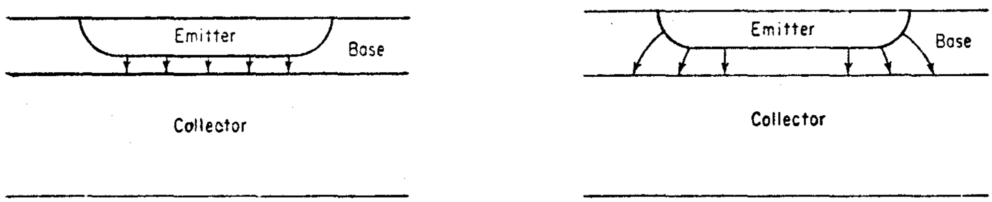

(a) At Low Current Levels (b) At High Current Levels

Figure 4.10 Current Distribution below the Emitter

CHAPTER V

CONCLUSIONS

This thesis has described and compared several large-signal transistor models, which are of different degrees of accuracy and and simplicity.

The accuracy of the basic Ebers-Moll model is limited by so many assumptions mentioned earlier in Chapter II, to a restricted range of currents and voltages; whereas the modified Ebers-Moll models can offer significant improvement in accuracy. The modifications of the basic Ebers-Moll model consist of retaining the form of the equations but increasing the accuracy by allowing the parameters of the model to vary with currents and voltages or by curve-fitting the parameters' functional dependence to measured data. The advantage of these modifications lies on the side of accuracy. On the other hand, these also produce disadvantages, such as limitations on computer memory, on numerical accuracy and consequently, on the size of the circuit being simulated. As an additional disadvantage, the parameters for the model derive solely from measurements made at the device terminals. No attempt is normally made to relate the device behaviour to the structural and material parameters. Nevertheless, the Ebers-Moll models or modifications thereof, have found relatively wide spread use as models for bipolar junction transistors because of the relative ease of obtaining the model parameters.

The abbreviated Gummel-Poon model is an alternative approach (i.e. the charge control approach) which offers significant advantages. Its novel feature is that the high level injection and the Early effects are incorporated into the model through the use of Gummel's new charge control relation. This makes the performance of the model substantially exceed that of the modified Ebers-Moll models of comparable complexity, and, thereby, the model enables trading between simplicity and accuracy. Moreover, in addition to the constant inactive base resistance, the inclusion of a base-charge-dependent active base resistance into the model gives the more accurate description of a diffused planar transistor whereas, in the modified Ebers-Moll model, the active base resistance is not included but the constant inactive base resistance used to account for the finite resistivity of the semiconductor material of the base region.

The disadvantage of this model is the difficulty in obtaining its model parameters, especially the charge-control parameters; some of which are not obtainable with the existing measurement techniques.

The most important approximations limiting the validity of this model are the assumption of the one-dimensional current flow which however is not the case in a practical transistor, and the assumption of large current gains even at low current levels. The latter assumption would cause considerable departure from a real transistor while operating in the cutoff region.

For future investigations, there are several possible areas or topics which are as follows:

(i) Inclusion of temperature effect which can be accounted for by considering the temperature dependence of parameters and the actual operating temperature of the transistor junctions.

(ii) Inclusion of the multidimensional effects which can be accounted for by formulating the multidimensional carrier transport equations and applying their solutions to develop a more precise model.

(iii) Extensions to full Gummel-Poon model to include the base "push-out" effect and the modelling of base-emitter junction capacitance.

(iv) Extension to fully automated parameter determination methods to eliminate the difficulties in parameter evaluation.

(v) Inclusion of modelling the Early effect in the Ebers-Moll model, as proposed by John Logan(4).

(vi) Application of models to circuit analysis and system design.

APPENDIX A

Microscopic Measurement of Device Geometry

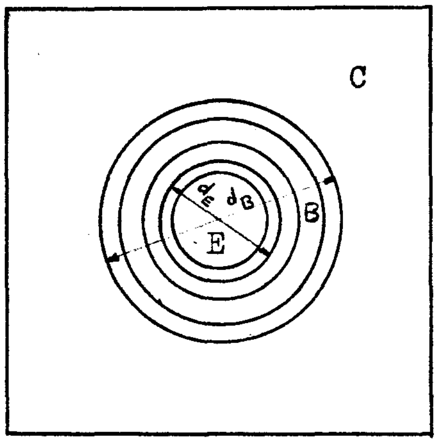

Fig. A-1(a) Top View

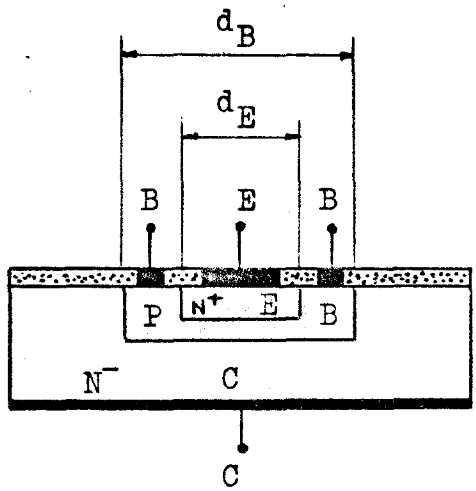

Fig. A-1(b) Cross-Section

Figure A-1 Internal Structure of 2N1613

Measured Data:

(1) Diameter of the Emitter = d_E = 0.36 mm.

(2) Diameter of the Base = d_B = 0.62 mm.

APPENDIX B

COMPUTER PROGRAMMES

```
RUN(S)
SETINDF.
REDUCE.
LGO.
'        6400 END OF RECORD
      PROGRA MAPD (INPUT,OUTPUT,TAPE5=INPUT,TAPE6=OUTPUT)
C
C MAIN PROGRAMME FOR AUTOMATED PARAMETER DETERMINATION
C
      DIMENSION OO(13), DELTA(13), TOLER(13)
C
      COMMON/AAA/ AICM(15, 5),AIBM( 5),VCEM(15),VBEM(15, 5),M1
      COMMON/BBB/ RE, RC, RB, BP
C
C TO READ IN MEASURED DATA EXPRESSED IN M.K.S. UNITS.
C
      M1=15
      DO 300 M=1,M1
      IF( M .LT. 9 ) J1=5
      IF( M .EQ. 9 ) J1=4
      IF( M .GT.  9 ) J1=3
      IF( M .GE. 13 ) J1=2
300   READ(5,97) (AICM(M,J), J=1,J1)
 97   FORMAT(8E10.3)
C
      DO 400 M=1,M1
      IF( M .LT. 9 ) J1=5
      IF( M .EQ. 9 ) J1=4
      IF( M .GT.  9 ) J1=3
      IF( M .GE. 13 ) J1=2
400   READ(5,98) ( VBEM(M,J), J=1,J1)
98    FORMAT(8F10.3)
C
      AIBM(1)=5.E-8
      AIBM(2)=1.0E-5
      AIBM(3)=4.0E-5
      AIBM(4)=1.2E-4
      AIBM(5)=5.E-4
C
      VCEM( 1)=0.
      VCEM( 2)=0.03
      VCEM( 3)=0.06
      VCEM( 4)=0.08
      VCEM( 5)=0.1
      VCEM( 6)=0.3
      VCEM( 7)=0.5
      VCEM( 8)=1.
```

```
      VCEM( 9)=4.
      VCEM(10)=8.
      VCEM(11)=10.
      VCEM(12)=15.
      VCEM(13)=20.
      VCEM(14)=25.
      VCEM(15)=30.
C
C TO READ IN THE STARTING VALUES OF PARAMETERS OF THE MODEL.
C
      IMAX=13
C
      BP=1.
      RE=0.0724
      RB=20.49
      RC=0.291
C
      AI1=5.057E-14
      AI2=2.065E-12
      AI3=4.563E-13
      AIS=2.374E-12
      ANC=1.133
      ANE1=1.217
      ANE2=1.618
      QB0=7.782E-11
      CC=3.67E-12
      CE=3.87E-10
      TAUF=2.650E-9
      TAUR=2.880E-6
      RBA0=867.
C
      DELTA(1)=0.1*AI1
      DELTA(2)=0.1*AI2
      DELTA(3)=0.1*AI3
      DELTA(4)=0.1*AIS
      DELTA(5)=0.01*ANC
      DELTA(6)=0.01*ANE1
      DELTA(7)=0.01*ANE2
      DELTA(8)=0.1*QB0
      DELTA(9)=0.1*CC
      DELTA(10)=0.1*CE
      DELTA(11)=0.1*TAUF
      DELTA(12)=0.1*TAUR
      DELTA(13)=0.01*RBA0
C
      OO(1)=ABS(AI1)
      OO(2)=ABS(AI2)
      OO(3)=ABS(AI3)
      OO(4)=ABS(AIS)
      OO(5)=ABS(ANC)
      OO(6)=ABS(ANE1)
      OO(7)=ABS(ANE2)
      OO(8)=ABS(QB0)
      OO(9)=ABS(CC)
      OO(10)=ABS(CE)
      OO(12)=ABS(TAUF)
      OO(12)=ABS(TAUR)
```

```
      OO(13)=ABS(RBAO)
C
      MOBJ=5000
      MITER=9000
      INTDATA=1
      ALPHA=3.0
      BETA=0.5
      DO 100 I=1,IMAX
100   TOLER(I)=OO(I)/20000.
      CALL PTSH(IMAX,MOBJ,MITER,INTDATA,ALPHA,BETA,DELTA,TOLER,OO)
      STOP
      END
C
C
'        6400 END OF RECORD
-4.800E-08-9.200E-06-3.830E-05-1.080E-04-4.550E-04
-3.000E-08 7.800E-06 3.550E-05 1.280E-04 3.680E-04
 1.000E-08 5.500E-05 2.700E-04 8.000E-04 2.300E-03
 5.800E-08 1.160E-04 5.500E-04 1.560E-03 4.400E-03
 1.100E-07 2.050E-04 9.500E-04 2.800E-03 7.150E-03
 4.800E-07 5.600E-04 2.680E-03 8.550E-03 3.010E-02
 4.900E-07 5.700E-04 2.690E-03 8.580E-03 3.500E-02
 4.920E-07 5.700E-04 2.690E-03 8.600E-03 3.550E-02
 5.000E-07 5.750E-04 2.700E-03 8.700E-03
 5.000E-07 5.820E-04 2.720E-03
 5.050E-07 6.000E-04 2.800E-03
 5.100E-07 6.200E-04 2.875E-03
 5.200E-07 6.220E-04
 5.250E-07 6.450E-04
 5.350E-07 7.000E-04
     0.310     0.486     0.530     0.560     0.602
     0.333     0.513     0.553     0.585     0.630
     0.360     0.543     0.583     0.613     0.657
     0.375     0.558     0.599     0.629     0.672
     0.383     0.575     0.615     0.646     0.685
     0.412     0.600     0.641     0.676     0.720
     0.412     0.600     0.641     0.676     0.720
     0.412     0.600     0.641     0.676     0.720
     0.412     0.600     0.641     0.676
     0.412     0.600     0.641
     0.412     0.600     0.641
     0.412     0.600     0.641
     0.412     0.600
     0.412     0.600
     0.412     0.600
'            END OF FILE
```

```
      SUBROUTINE OBJECT (O,U)
      REAL O(16), U
      DIMENSION Q(15, 5), QB(15, 5), VCE(15, 5), VBE(15, 5), VBC(15, 5),
     1          VBES(15, 5),AICSS(15, 5),AIES(15, 5),AIEM(15, 5),
     2          AUX1(15, 5), AUX2(15, 5), AUX3(15, 5), AUX4(15, 5),
     3          AUX5(15, 5),HFES(15, 5),HFEM(15, 5),AIBS(15, 5)
      DIMENSION AUX6(15,5), RBT(15,5), E1(15,5), E2(15,5)
      COMMON/AAA/ AICM(15, 5),AIBM( 5),VCEM(15),VBEM(15, 5),M1
      COMMON/BBB/ RE, RC, RB, BP
C
      AI1=ABS(O(1))
      AI2=ABS(O(2))
      AI3=ABS(O(3))
      AIS=ABS(O(4))
      ANC=ABS(O(5))
      ANE1=ABS(O(6))
      ANE2=ABS(O(7))
      QB0=ABS(O(8))
      CC=ABS(O(9))
      CE=ABS(O(10))
      TAUF=ABS(O(11))
      TAUR=ABS(O(12))
      RBA0=ABS(O(13))
C
C     B=Q/KT  Q=1.602E-19 C.  K=1.38E-23 J/DEGREE K  T=298 DEGREES K
C
      B=160.2/(1.38*2.98)
C
C TO CALCULATE VBES, AICSS BY TREATING VCEM AND AIBM AS INDEPENDENT VARIABLES
C
      DO 10 M=1,M1
      IF( M .LT. 9 ) J1=5
      IF( M .EQ. 9 ) J1=4
      IF( M .GT.  9 ) J1=3
      IF( M .GE. 13 ) J1=2
      DO 20 J=2,J1
      AIEM(M,J)=-AIBM(J)-AICM(M,J)
      VCE(M,J)=VCEM(M )-AICM(M,J)*RC+AIEM(M,J)*RE
      VBEHI=0.8
      VBELO=0.2
11    VBE(M,J)=0.5*(VBEHI+VBELO)
      VBC(M,J)=VBE(M,J)-VCE(M,J)
      AUX1(M,J)=EXP(B*VBE(M,J)/ANE1)
      AUX2(M,J)=EXP(B*VBE(M,J)/ANE2)
      AUX4(M,J)=EXP(B*VBC(M,J)/ANC)
      AIBS(M,J)=AI1*(AUX1(M,J)-1.)
     1          +AI2*(AUX2(M,J)-1.)
     2          +AI3*(AUX4(M,J)-1.)
      IF(AIBM(J) .GT. AIBS(M,J))  VBELO=VBE(M,J)
      IF(AIBM(J) .LT. AIBS(M,J))  VBEHI=VBE(M,J)
      IF( ABS(VBEHI-VBELO) .LT. 1.0E-8   ) GO TO 12
      GO TO 11
12    CONTINUE
      AUX3(M,J)=EXP(B*VBC(M,J))
      AUX6(M,J)=EXP(B*VBE(M,J))
      Q(M,J)=0.5*(QB0+CE*VBE(M,J)+CC*VBC(M,J))
```

```
      AUX5(M,J)=SQRT(Q(M,J)**2+QBO*AIS*(BP*TAUF*(AUX6(M,J)-1.0)
     1          +TAUR*(AUX3(M,J)-1.0)))
      QB(M,J)=A(M,J)+AUX5(M,J)
      AICSS(M,J)=AIS*(AUX6(M,J)-AUX3(M,J))*QBO/QB(M,J)-AI3*(AUX4(M,J)-1.)
      AIES(M,J)=-AICSS(M,J)-AIBS(M,J)
      RBT(M,J)=RB+(RBAO*QBO)/QB(M,J)
      VBES(M,J)=VBE(M,J)+AIBS(M,J)*RBT(M,J)-AIES(M,J)*RE
      HFES(M,J)=AICSS(M,J)/AIBS(M,J)
      HFEM(M,J)=AICM(M,J)/AIBM(J)
C
C TO FORMULATE OBJECTIVE FUNCTION BY METHOD OF LEAST PTH APPROXIMATION
C
      P=100.
      LP=P
      WI=100.
      WH=1.
      E1(M,J)=(WI*ABS(VBES(M,J)-VBEM(M,J)))**LP
      E2(M,J)=(WH*ABS(HFES(M,J)-HFEM(M,J)))**LP
20    CONTINUE
10    CONTINUE
      ERROR=0.0
      DO 40 M=1,M1
      IF( M .LT. 9 ) J1=5
      IF( M .EQ. 9 ) J1=4
      IF( M .GT.  9 ) J1=3
      IF( M .GE. 13 ) J1=2
      DO 50 J=2,J1
      ERROR=ERROR+E1(M,J)+E2(M,J)
50    CONTINUE
40    CONTINUE
C
C TO FIND THE NORM OF THE ERROR FUNCTION AND  U =NORM WHICH IS THE OBJECTIVE
C FUNCTION TO BE MINIMIZED.
C
      PTH=1.0/P
      U=ABS(ERROR)**PTH
      RETURN
      END
```

```
      SUBROUTINE DATA (OO,UO,DELTA,NOBJ,NITER)
      REAL OO(13), DELTA(13)
      WRITE(6,998) OO
      WRITE(6,999) UO, NOBJ, NITER
  998 FORMAT(1X, 7(5X, E12.5),/1H0, 7(5X, E12.5)/)
  999 FORMAT(6X, E12.5, 2(5X, I4)//)
      RETURN
      END
```

```
      SUBROUTINE PTSH(IMAX,MOBJ,MITER,INTDATA,ALPHA,BETA,DELTA,TOLER,OO)
C
C            PATTERN  SEARCH
C     **************************
C     **************************
C
C
C      PURPOSE
C    ***********
C
C      TO LOCATE  A  LOCAL  MINIMUM  OF  THE  SCALAR  FUNCTION  U.   WHERE  U
C      IS  A  FUNCTION  OF  IMAX  CONTROLABLE  VARIABLES  (VECTOR  O)
C      THIS  PROGRAM  USES  A  DIRECT  SEARCH  METHOD,  IT  ONLY  REQUIRES  THE
C      USER  TO  SPECIFY   THE  FN  U,  NO  INFORMATION  ABOUT  ITS  PARTIAL  D
C      -RIVATIVES  WITH  RESPECT  TO  THE  CONTROLABLE  VARIABLES  IS  REQUIRED
C      THE  USER  IS  REMINDED  THAT  THE  SEARCH  WILL  LOCATE  A  MINIMUM  OF
C      THE  FN.  U  BUT  IT  CANT  QUARANTEE  A  GLOBAL  MINIMUM
C      A  PROVISION  HAS  BEEN  MADE  TO  KEEP  TRACK  OF  THE  MUMBER  OF  FUNC
C      -ION  EVALUATIONS  (NOBJ).  SHOULD  A  SPECIFIED  NUMBER  (MOBJ)  BE  EX
C      -EEDED  THE  SEARCH  WILL  BE  STOPPED  AT  THIS  POINT.
C      A  CHECK  IS  ALSO  KEPT  ON  THE  NUMBER  OF  ITERATIONS.    IF  THIS
C      SHOULD   EXCEED  A  PREDETERMINED  AMOUNT  THE  PROGRAM  WILL  BE  STOPP
C      -D  AUTOMATICALLY
C      DESCRIPTION  OF  PARAMETERS
C    *********************************
C
C      INTEGER
C      I             SUBSCRIPT  TO  DENOTE  VARIABLE
C      IMAX          TOTAL  NO.  OF  VARIABLES  TO  BE  OPTIMIZED  ( LESS  THAN  2
C      NOBJ          INDEX  TO  RECORD  THE  NO.  OF  FUNCTION  EVALUATIONS
C      MOBJ          MAX  NO.  OF  FUNCTION  EVALUATIONS
C      NITER         INDEX  TO  RECORD  THE  NO.  OF  ITERATIONS
C      MITER         MAX  NO.  OF  ITERATIONS
C      INTDATA       USED  TO  SIGNIFY  IF  INTERMEDIATE  DATA  IS  REQUIRED
C
C      REAL
C      U             OBJECTIVE  FN.  WHICH  IS  TO  BE  MINIMIZED  (SCALAR )
C      UO            VALUE  OF  OBJECTIVE  AT  A  BASE  POINT
C      TEMPU         CURRENT  BEST  VALUE  OF  U  ( USED  IN  SUBROUTINE  EXPLOR )
C      ALPHA         ACCELERATION  FACTOR  FOR  THE  PATTERN-MOVE
C      BETA          REDUCTION  FACTOR  TO  INCREASE  RESOLUTION  AS  MIN.  IS
C                    APPROCHED
C      O(I)          VECTOR  IN  N-DIMENSIONAL  SPACE
C      OO(I)         VECTOR  LOCATION  OF  A  BASE-POINT
C      DELTA(I)      INCREMENTAL  CHANGE  INVARIABLE  O(I)  ( USED  IN  EXPLOR )
C      TOLER(I)      REQUIRED  RESOLUTION  TO  SPECIFY  THE  O(I)  VALUE  AT  THE
C                    MINIMUM
C      STEPO(I)      INTERMEDIATE  PARAMETER  USED  TO  CALC.  A  PATTERN-MOVE
C
C      PARAMETERS  SPECIFIED  BY  THE  USER
C      ********************************
C
C      IMAX          (LESS  THAN  20     )
C      MOBJ          (TYPICALLY  100-500)
C      MITER         (TYPICALLY  MOBJ/(2*IMAX)  )
```

```
C     INTDATA       (=0  NO  INTERMEDIATE  RESULTS  REQUIRED  )
C                   (=1  IMTERMEDIATE  RESULTS  ARE  REQUIRED  )
C     ALPHA         (USUALLY  1.00   )
C     BETA          (USUALLY  0.10   )
C     DELTA(I)      (DEPENDS  ON  THE  SCALING  OF  THE  PROBLEM  )
C     TOLER(I)      (DEPENDS  ON  THE  REQUIRMENTS  OF  THE  USER  )
C     ST(I)         (LOCATION  OF  THE  STARTING  POINT  FOR  THE  SEARCH  )
C
C     SUBROUTINES  SUPPLIED  BY  THE  USER
C    ********************************
C
C     SUBROUTINE  OBJECT (O,U)
C     THIS  SUBROUTINE  SPECIFIES  THE  SCALAR  FUNCTIONTO  BE  MINIMIZED.
C     U  IS  A  FUNCTION  OF  THE  CONTROLLABLE  VARIABLES  VECTOR  O.
C
C     SUBROUTINE  DATA (OO,UO,DELTA,NOBJ,NITER )
C     THIS  PROGRAM  SHOULD  CONSIST  OF  ONE  WRITE  STATEMENT  WITH  ITS  AS
C     -CIATED  FORMAT  DESCRIPTION.  IT  INSTRUCTS  THE  COMPUTER  TO  PRINT  C
C     -T  RESULTS.  NOTE  THE  SAME  FORMAT  IS  USED  FOR  INTERMEDIATE  DATA
C     AND  THE  FINAL  RESULTS.   ANY  OF  THE  PARAMETERS  DECLARED  IN  THE
C     -RGUEMENT  LIST  MAY  BE  SPECIFIED  IN  THE  WRITE  STATEMENT
C
C

      INTEGER  I,IMAX
      REAL  DELTA(20),TOLER(20),O(20),OO(20),STEPO(20)
C
C     SET  THE  ITERATION  AND  FUNCTION  EVALUATION  COUNTERS  TO  ZERO
C
      NOBJ=0
      NITER=0
C
C     A  BASE  POINT  HAS  BEEN  DEFINED  OO.   IN  ORDER  TO  EVALUATE  U(O)
C     THE  OO  INFORMATION  MUST  BE  TRANSFERED  TO  O
C
    1 DO  2  I=1,IMAX
    2 O(I)=OO(I)
C
C     EVALUATE  THE  OBJECTIVE  FUNCTION  AT  THIS  LOCATION
C
      CALL  OBJECT  ( O,U )
      UO = U
C
C     PRINT  OUT  BASE  POINT  DATA
C
      IF(INTDATA .EQ. 1)  CALL  DATA (OO,UO,DELTA,NOBJ,NITER )
C
C     CHECK  THE  NO.  OF  FUNCTION  EVALUATIONS  AND  ITERATIONS
C
      NOBJ=NOBJ+1
      IF(NOBJ .GT. MOBJ)  GO  TO  85
      NITER=NITER+1
      IF(NITER .GT. MITER)  GO  TO  80
C
C     EXPLOR  U  TO  FIND  THE  MIN  IN  THE  ENVIRONS  OF  O
C
      CALL  EXPLOR  (IMAX,MOBJ,NOBJ,DELTA,O,U,TEMPU)
      IF(NOBJ .GT. MOBJ)  GO  TO  85
```

```
C
C     CHECK TO SEE IF THERE HAS BEEN A REDUCTION IN THE OBJ. FN. U
C
      IF(TEMPU .LT. UO) GO TO 20
C
C     NO IMPROVEMENT SO CHECK IF STEP SIZE IS SMALLER THAN SPECIFIED
C     TOLERANCE     IF SO STOP       IF NOT REDUCE INCREMENT SIZE
C
      L=0
   13 DO 14  I=1,IMAX
   14 IF( ABS(DELTA(I))  .LT.  TOLER(I) )  L=L+1
      IF(L .EQ. IMAX)  GO TO 70
C
C     REDUCE THE STEP SIZE TO IMPROVE THE RESOLUTION
C
      DO 15  I=1,IMAX
   15 DELTA(I)=DELTA(I)*BETA
      GO  TO  1
C
C
C     IF THERE HAS BEEN A REDUCTION IN U TRY TO EXPLOIT THIS SUCES
C     BY UP-DATING THE DIRECTION INFORMATION (SIGN OF DELTA )
C     HOPEFULLY THIS WILL REDUCE NO. OF FALSE MOVES (FUNCTION EVALUAT
C
C     -N EVALUATIONS )
C
   20 DO  23  I=1,IMAX
      IF(O(I) .GT. OO(I)   .AND.   DELTA(I) .LT. 0.0 )  GO  TO  22
      IF(O(I) .LE. OO(I)   .AND.   DELTA(I) .GT. 0.0 )  GO  TO  22
      GO  TO  23
   22 DELTA(I)=-DELTA(I)
   23 CONTINUE
C
C     UP DATE THE VALUE OF BASE POINT OO AND THE ASSOCIATED VALUE
C     THE OBJECTIVE FUNCTION    THEN MAKE A PATTERN MOVE
C
   30 UO=TEMPU
      DO 31  I=1,IMAX
      STEPO(I)=O(I)-OO(I)
      OO(I)=O(I)
   31 O(I)=OO(I)+ALPHA*STEPO(I)
      NITER=NITER+1
      IF(INTDATA .EQ.1)  CALL  DATA (OO,UO,DELTA,NOBJ,NITER )
      IF(NITER .GT. MITER)  GO  TO  80
C
C     FIND THE VALUE OF THE OBJECTIVE FUNCTION AT THIS NEW POINT
C
      CALL  OBJECT (O,U)
      NOBJ=NOBJ+1
      IF(NOBJ .GT. MOBJ)  GO  TO  85
C
C     BEFORE COMPARING U WITH UO EXPLOR O TO GET BEST VALUE IN THE
C     REGION OF O
C
      CALL  EXPLOR  (IMAX,MOBJ,NOBJ,DELTA,O,U,TEMPU)
      IF(NOBJ .GT. MOBJ)  GO  TO  85
C
```

```
C       IS  U  LESS  THAN  THE  VALUE  AT  THE  LAST  BASE  POINT
C       IF  NOT  THE  PATTERN  MOVE  HAS  FAILED    GO  TO  1  AND  START  AGAI
C
        IF(TEMPU .LT. UO)  GO  TO  37
        GO  TO  1
C
C       THERE  HAS  BEEN  AN  IMPROVEMENT     CHECK  PATTERN  ISNT  CHASING  IT
C       TAIL         IS  THE  NEW  PT.  INSIDE  THE  REGION   OO+ OR -DELTA/2
C
     37 DO  40  I=1,IMAX
        IF(  DIM(O(I),OO(I)) .GT. ABS(DELTA(I)/2.0)  )  GO  TO  20
     40 CONTINUE
        GO  TO  1
     70 WRITE(6,71)
     71 FORMAT(1H1,10X,*MIN.  LOCATED  TO  THE  SPECIFIED  ACCURACY*//
       18X,45H*********************************************//)
        GO  TO  90
     80 WRITE(6,81)  NITER
     81 FORMAT(//,10X,*PROGRAM  STOPED   MAX.  NO.  OF  ITERATIONS  EXCEEDED
       1ED     NITER=*,I4  )
        GO  TO  90
     85 WRITE(6,86)  NOBJ
     86 FORMAT(///,10X,*PROGRAM  STOPPED  MAX.  NO.  OF  FN.  EVALUATIONS  EXCEE
       1EXCEEDED    NOBJ =*,I4)
     90 CALL DATA (OO,UO,DELTA,NOBJ,NITER )
        RETURN
        END
        SUBROUTINE  EXPLOR  (IMAX,MOBJ,NOBJ,DELTA,O,U,TEMPU)
C       ******************************************
C       ******************************************
C       PURPOSE
C      **************
C
C
C       TO  FIND  THE  MINIMUM  IN  THE  REGION  OF  O      THE  SUBROUTINE  TA
C       -S  EACH  CO-ORDINATE  AT  A  TIME  AND  INCREMENTS  IT  WITH  A  PVE  S
C       -P  IF  NO  GOOD  IT  TRIES  A  -VE  STEP  IF  STILL  NO  IMPROVEMENT  I
C       RESETS  THE  CO-ORDINATE  TO  ITS  INITIAL  VALUE   AND  REPEATS  THE  P
C       -OCEEDURE  EACH  OF  THE  REMAINING  CO-ORDINATES  IN  TURN
C
C
C
        REAL  O(20),DELTA(20),U,TEMPU
        TEMPU=U
        DO  6  I=1,IMAX
      2 O(I)=ABS(O(I)+DELTA(I))
        CALL  OBJECT (O,U)
        NOBJ = NOBJ + 1
        IF(NOBJ .GT. MOBJ)  GO  TO  10
        IF(U .LT. TEMPU)  GO  TO  5
        O(I)=ABS(O(I)-2.0*DELTA(I))
        CALL  OBJECT (O,U)
        NOBJ = NOBJ + 1
        IF(NOBJ .GT. MOBJ)  GO  TO  10
        IF(U .LT. TEMPU)  GO  TO  5
        O(I)=ABS(O(I)+DELTA(I))
        GO  TO  6
      5 TEMPU = U
      6 CONTINUE
     10 RETURN
        END
```

APPENDIX C

Comparison of the Measured with the Simulated α_F and α_R versus I_{BM}

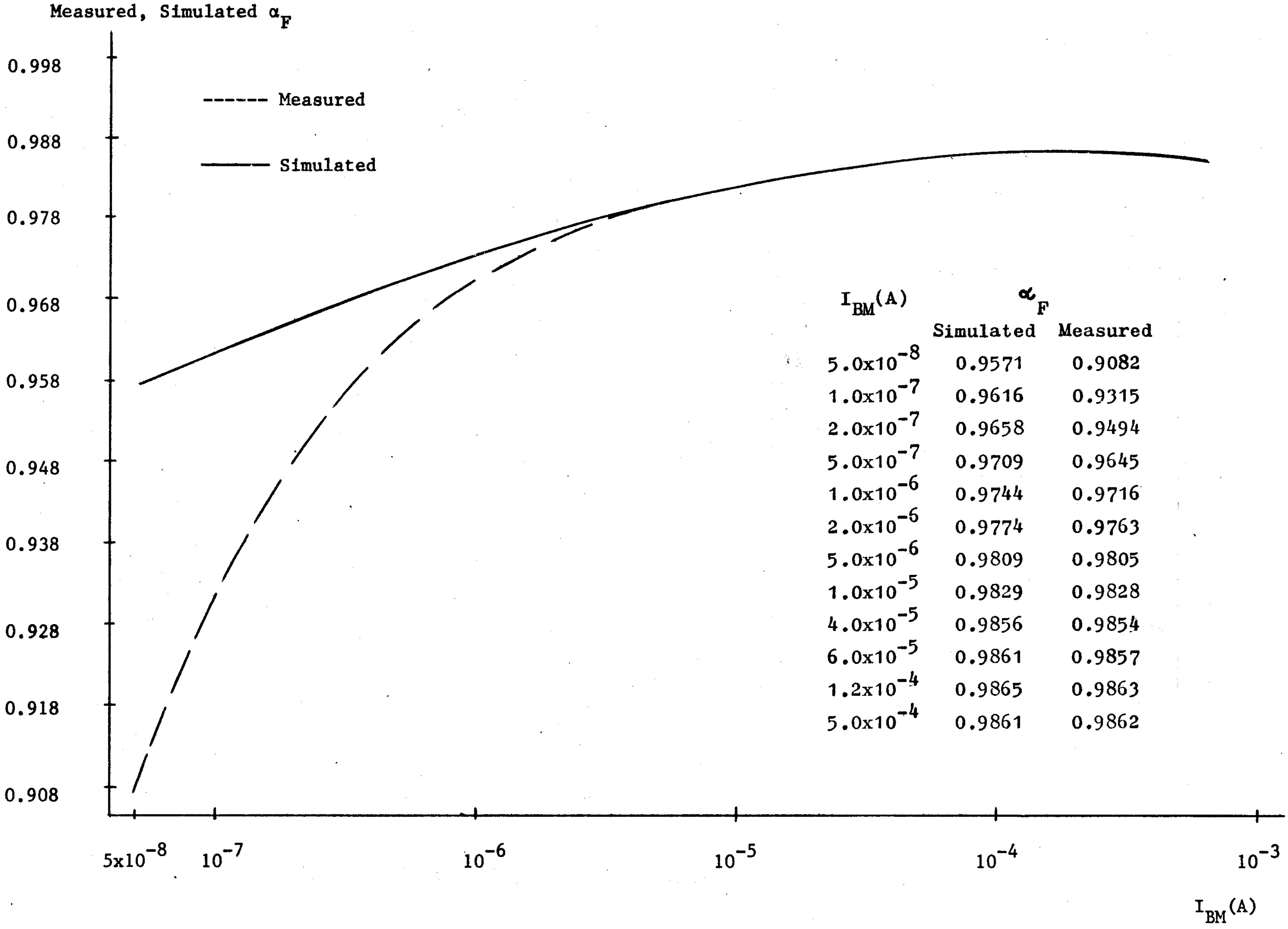

$I_{BM}(A)$	α_F Simulated	α_F Measured
$5.0x10^{-8}$	0.9571	0.9082
$1.0x10^{-7}$	0.9616	0.9315
$2.0x10^{-7}$	0.9658	0.9494
$5.0x10^{-7}$	0.9709	0.9645
$1.0x10^{-6}$	0.9744	0.9716
$2.0x10^{-6}$	0.9774	0.9763
$5.0x10^{-6}$	0.9809	0.9805
$1.0x10^{-5}$	0.9829	0.9828
$4.0x10^{-5}$	0.9856	0.9854
$6.0x10^{-5}$	0.9861	0.9857
$1.2x10^{-4}$	0.9865	0.9863
$5.0x10^{-4}$	0.9861	0.9862

Figure C-1 Comparison of the Measured with the Simulated α_F versus I_{BM} at V_{CE} = 2 V.

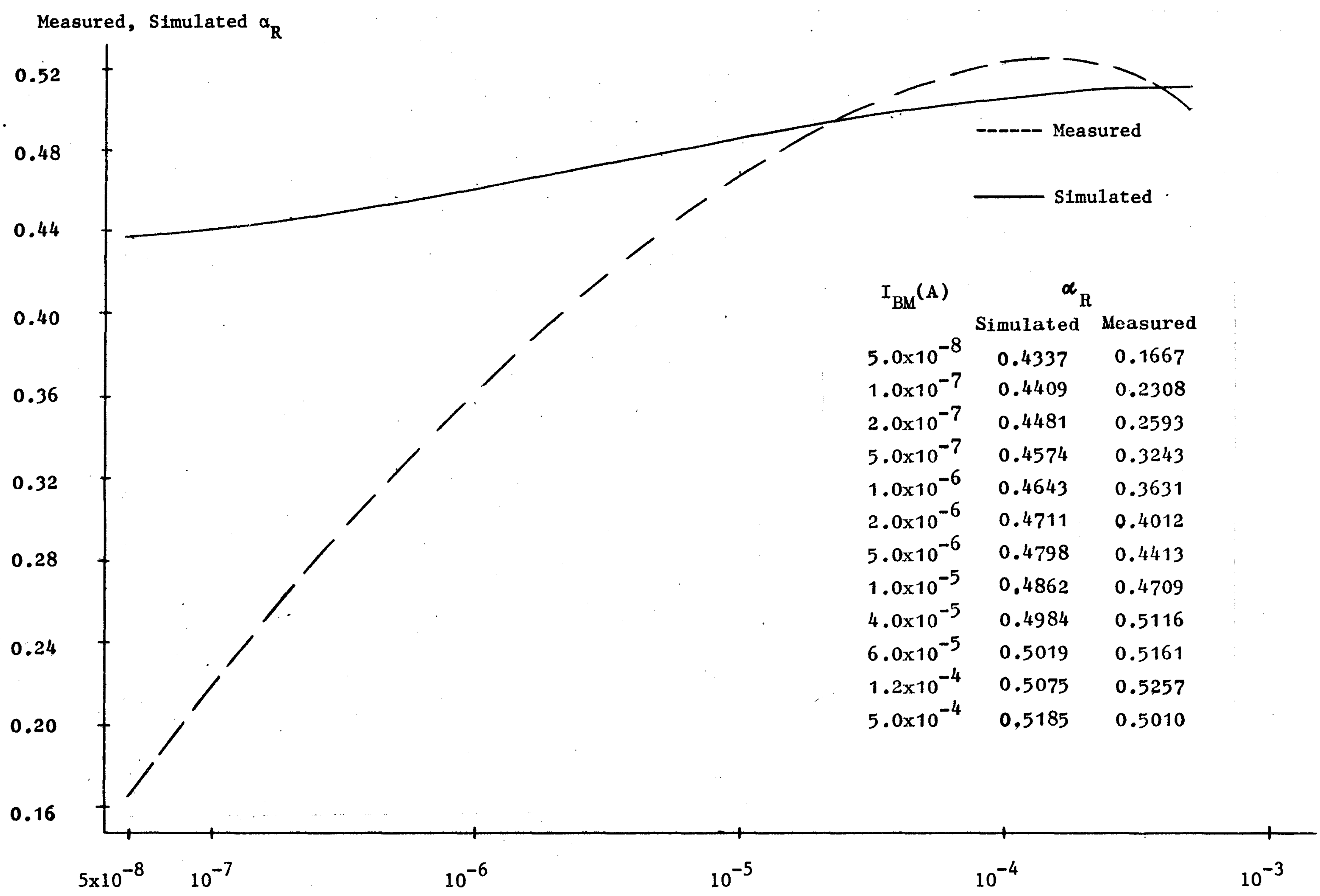

I_{BM}(A)	α_R Simulated	α_R Measured
5.0×10^{-8}	0.4337	0.1667
1.0×10^{-7}	0.4409	0.2308
2.0×10^{-7}	0.4481	0.2593
5.0×10^{-7}	0.4574	0.3243
1.0×10^{-6}	0.4643	0.3631
2.0×10^{-6}	0.4711	0.4012
5.0×10^{-6}	0.4798	0.4413
1.0×10^{-5}	0.4862	0.4709
4.0×10^{-5}	0.4984	0.5116
6.0×10^{-5}	0.5019	0.5161
1.2×10^{-4}	0.5075	0.5257
5.0×10^{-4}	0.5185	0.5010

Figure C-2 Comparison of the Measured with the Simulated α_R versus I_{BM} at $V_{CE} = -2$ V.

REFERENCES

(1) 1620 Electronic Circuit Analysis Program (1620-EE-02X), Users Manual, IBM Corporation, H20-0170-1, 1965.

(2) H. W. Mathers, S. S. Sedore and J. R. Sents, "Revised SCEPTRE Users Manual, Volume 1", IBM Electronics System Center, Owego, New York, Technical Report No. AFWL-TR-67-124, April, 1968.

(3) A. F. Malmberg, et al, "NET-1 Network Analysis Program 7090/94 Verson", University of California, Los Almaos, Calif., 1964.

(4) J. Logan, "Modeling for Circuit and System Design", Proc. I.E.E.E., January, 1972, P.P. 78-85.

(5) R. Beaufoy and J. Sparkes, "The Junction Transistor as a Charge-Controlled Devices", A.T.E.J.(London), 13, No. 4. October, 1957, P.P. 310-324.

(6) H. K. Gummel and H. C. Poon, "An Integral Charge Control Model of Bipolar Transistor", B.S.T.J., P.P. 827-852, May-June, 1970.

(7) D. Hamilton, et al, "Comparison of Large-Signal Models for Junction Transistors", Proc. I.E.E.E., Vol. 52, March, 1964, P.P. 239-248.

(8) F. A. Lindholm, et al, "Assessing Model Adequacy and Selecting Model Complexity in Integrated-Circuit Simulation", I.E.E.E. Journal of Solid-State Circuits, Vol. SC-6, No.4, August, 1971, P.P. 213-222.

(9) J. Early, "Effects of Space-Charge Layer Widening in Junction Transistors", Proc. I.R.E., 40, No.11, November, 1952, P.P.1401-1406.

(10) C. T. Sah, et al," Carrier Generation and Recombination in p-n

Junctions and p-n Junction Characteristics", Proc. I.R.E., 45, No.9, September, 1957, P.P. 1228-1243.

(11) W. Webster, "On the Variation of Junction Transistor Current Gain Amplification Factor with Emitter Current", Proc. I.R.E., 42, No.6, June, 1954, P.P. 914-920.

(12) C. Kirk, "A Theory of Transistor Cutoff Frequency Falloff at High Current Densities", I.R.E. Trans. on Electron Devices, ED-9, No.2, March, 1962, P.P. 164-174.

(13) R. L. Pritchard, et al, "Small Signal Parameters of Grown Junction Transistors at High Frequencies", 1954 I.R.E. Conventional Record, Pt. 3, P.P. 89-98.

(14) N. H. Fletcher, "Self-Bias Cutoff Effect in Power Transistors", Proc. I.R.E., 43, No. 11, November, 1955, P. 1669.

(15) A. S. Grove, "Physics and Technology of Semiconductor Devices", New York, Wiley, 1967.

(16) P. E. Gray, et al, "Physical Electronics and Circuit Models of Transistors", New York, Wiley, 1964.

(17) J. Early, "Effects of Space-Charge Layer Widening in Junction Transistors", Proc.I.R.E., 40, No.11, November, 1952, P.P.1401-1406.

(18) W. Shockley, "The Theory of p-n Junction in Semiconductors and p-n Junction Transistors", B.S.T.J., Vol. 28, P.P.435-489, July, 1949.

(19) J. Ebers and J. Moll, "Large-Signal Behavor of Junction Transistor", Proc. I.R.E., December, 1954, P.P. 1761-1772.

(20) D. Koehler, "The Charge Control Concept in the form of Equivalent Circuits, Representing a Link between the Classic Large-Signal Diodes and Transistor Models", B.S.T.J., 46, No. 3, March, 1967, P.P. 523-576.

(21) H. Gummel, "A Charge Control Relation for Bipolar Transistor", B.S.T.J., 49, No. 1, January, 1970, P.P. 115-120.

(22) H. C. Poon and H. K. Gummel, "An Integral Charge Control Model of Bipolar Transistor", B.S.T.J., May-June, 1970, P.P. 827-853. H. C. Poon and H. K. Gummel, "A Compact Bipolar Transistor Model", 1970 I.S.S.C.C. Digest of Tech. Papers, Vol. 13, Feb., 1970, P.P. 78-80.

(23) W. Shockley and W. Read Jr., "Statistics of Recombination of Holes and Electrons", Phys. Rev., Vol. 87, September, 1952, P.P. 835-852.

(24) R. Hall, "Germanium Rectifier Characteristics", Phys. Rev., Vol. 83, July, 1951, P.228.

(25) R. Hall, "Electron-hole Recombination in Germanium", Phys. Rev., Vol. 87, July, 1952, P. 837.

(26) R. Noyce, et al, "Carrier Generation and Recombination in the Space Charge Region of a p-n Junction", Bull. Amer. Phys. Soc. II, Vol. 1, H9, P.382, December 27, 1956.

(27) S. Sze, "Physics of Semiconductor Devices", Chapter 3, P.P. 647-651, John Wiley, New York, 1969.

(28) Chapter of (27), P.P. 65-70.

(29) J. Moll and J. Ross, "The Dependence of Transistor Parameters on the Distribution of Base Layer Resistivity", Proc. I.R.E., Vol. 44, January, 1956, P.P. 72-78.

(30) R. Thornton, et al, "Handbook of Basic Transistor Circuits and Measurement", SEEC Series, Vol. 7, John Wiley, New York, 1966.

(31) B. Chawla and H. Gummel, "Transition Region Capacitance of Diffused p-n Junction", I.E.E.E. Trans., Electron Device, ED-18, March, 1971, P.P.178-195.

(32) Chapter 1 of (27), P. 40 and P. 89.

(33) Chapter of (27), P. 28.

(34) D. A. Pierre, "Optimization Theory with Applications", John Wiley, New York, 1969.

(35) G. Temes and D. Zai, "Least pth Approximation", I.E.E.E. Trans. on Circuit Theory, Vol.CT-16, P.P. 235-237, May, 1969.

(36) R. Hooke and T. Jeeves, "Direct Search Solution of Numerical and Statistical Problems", J. ACM, Vol. 8, P.P. 212-229, April, 1961.

(37) D. Wilde, "Optimum Seeking Methods", Chapter 5, Engelwood Cliffs N. J. Printice Hall, 1964.

(38) J. Kowalik and M. Osborne, "Methods for Unconstrained Optimization Problems", Chapter 2, Elsevier, 1968.

(39) J. Mitchell and D. Wilson, "Surface Effects of Radiation on Semiconductor Devices", B.S.T.J., January, 1967, P.P. 1-80.